Bayesian Optimization for Lightweight Design of Variable Stiffness Composite Cylinders

Aravind Ashok

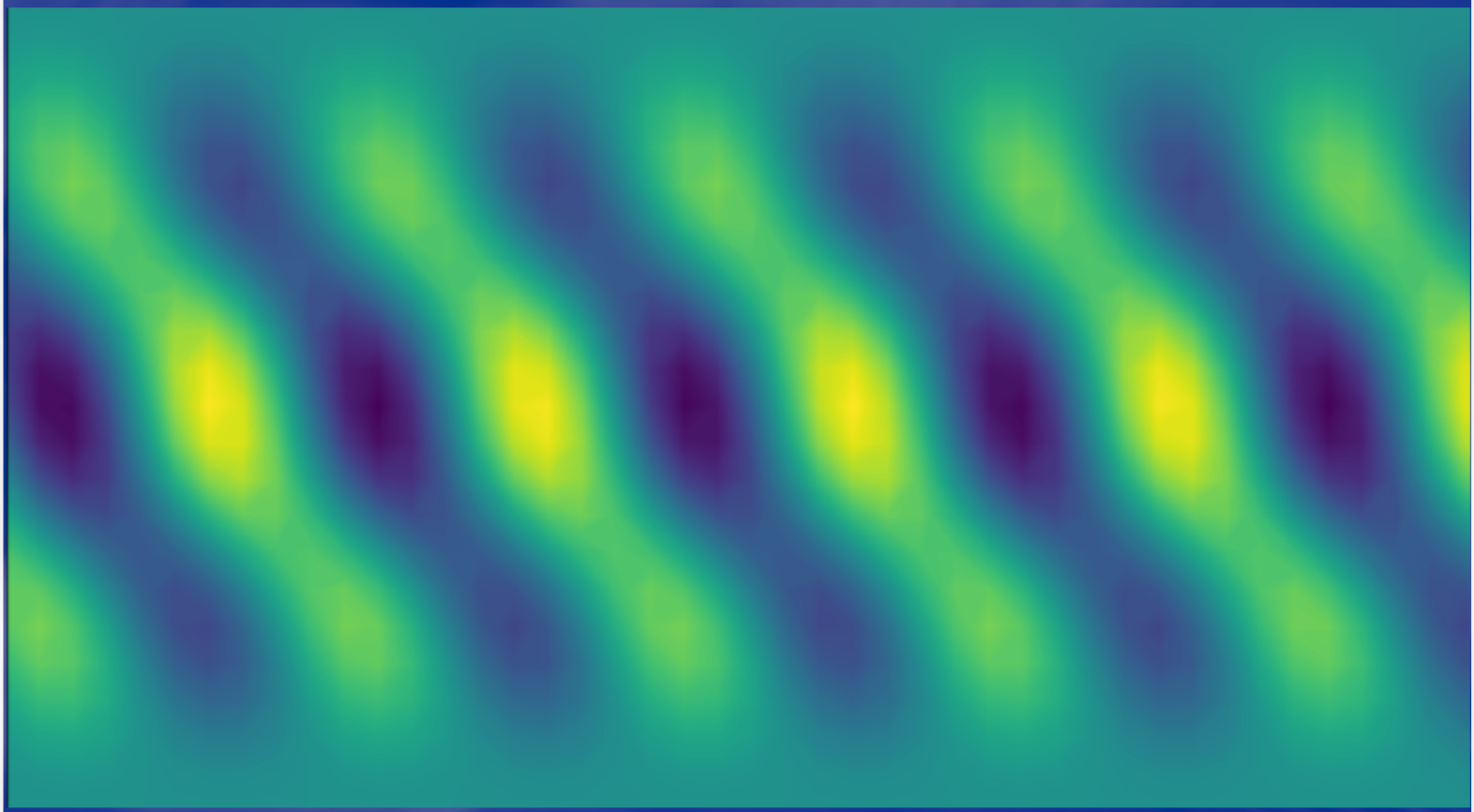

Masters Thesis

Aerospace Structures and Materials
Faculty of Aerospace Department

TU Delft

Bayesian Optimization for Lightweight Design of Variable Stiffness Composite Cylinders

by

Aravind. Ashok

to obtain the degree of Master of Science
at the Delft University of Technology,
to be defended publicly on Friday October 22, 2021 at 09:30 AM.

Student number:	4921739	
Project duration:	January 23, 2020 – October 22, 2021	
Thesis committee:	Dr. Ing. S. G. P. Castro,	TU Delft, supervisor
	Prof. Dr. C. Bisagni,	TU Delft
	Dr. Ir. O. K. Bergesma ,	TU Delft

An electronic version of this thesis is available at http://repository.tudelft.nl/.

Abstract

The advancement in the steering capabilities of fibre placement machines has improved the tailoring potential and therefore the design possibilities for composite structures. However, the larger design freedom leads to complex and non-convex design spaces. Finding the optimum solution thus becomes costly and challenging, specifically considering the non-linear coupling of thickness with the steering of the filaments or tows. Additionally, an accurate representation of the variable stiffness adds complexity to the modeling strategies, requiring additional refinement relative to constant-stiffness counterpart designs. Surrogate modeling and more exploratory optimization techniques make it possible to circumvent the higher execution time by using a limited set of high-fidelity model evaluations. This enables efficient and accurate exploration of the design space. Bayesian optimization techniques applies the surrogate model to offer strategic and probabilistic exploration of the design space and have demonstrated success in various fields. However, the application of Bayesian optimization schemes in structural optimization is in its nascent stage. The present thesis is a successful attempt that further pushes the application of Bayesian optimization for the lightweight design of variable stiffness cylinders.

A novel finite element SC-BFSC is proposed for modeling and the computational efficiency for linear buckling analysis is investigated. The results showcase an enhanced computational efficiency with retained accuracy. Prior to optimization, a comprehensive Design of Experiment study is conducted, wherein different parameters and kernels were investigated for optimum performance. An optimization framework for the problem is proposed, utilizing the Gaussian process with Matern32 Kernel for regression model and a set of acquisition functions.

The proposed optimization framework is implemented successfully and verified against a Genetic Algorithm(GA) based solution, which is an optimization method of proven success and robustness. The result obtained showcase the Bayesian optimization strategy's ability to identify comparable solutions at a fraction of the computation time required for the GA optimization in most cases. This study successfully demonstrates the Bayesian optimization's ability for designing lightweight variable stiffness cylinders, while providing a framework that is generally applicable in lightweight design of composite structures.

Preface

This thesis is a story of two models. One model deals with the buckling of fibre steered composite cylinders and the other is concerned with employing the results from the previous model to provide an optimum solution. Although, initially I dreamt a little more grander assuming to manufacture the optimal solution. The direction shifted with complications from the project and even more complicated 2020. However, this enabled me to explore deeper into the simulation and optimization realm that enlightened me on various aspects of the subject. All in all, I am extremely grateful for this opportunity to work on this stimulating topic.

This story that ends in the form of a degree attained from TU Delft would not have been possible without the support I received through many kind hearted people that I was fortunate to have encountered through the process. In the sense that, I see this achievement as a team effort that deserves to be shared with many. Hence, I want to extend this gratitude in words.

Firstly, I would like to thank my supervisor Dr Ing Saullo Castro for all his support and out-of-office hour replies to my doubts during my long thesis, the weekly discussions which sometimes resulted in interesting detours helped me a lot to cope with the bizarre nature of early 2020. I would also like to thank Zhihua, Fredreik and Sebastian who helped a lot in understanding my optimization problem. Bouncing ideas back and forth with them has helped me understand the subject better and has brought me closer to the optimization goal.

Aside from the academic support I received during this time, I am grateful for the unexpected friendships I made in this journey. Honourable mentions go to Harsha, Rahul, Srikanth and Yasir, who constantly who invited me into their clan. They helped me feel home in a foreign country and always kept my spirits high. The classmates from ASM never failed to add humour and fun to my day. Be it frantically discussing the assignments or passionately debating about TV series, movies, even global politics. Although, we could only enjoy working on our thesis from our office desks for a few months, it was nice to have a coffee break to lift the heavy weight of our day to day problems. Ranting about the relatable hiccups of our life helped me feel like I was not alone in this be it frantically discussing the assignments or having a debate about TV series, movies to global politics.

It is an undisputed fact that this section will not be complete without thanking my family. I want to thank my parents, Ashok and Preetha, who have supported me wholeheartedly from the start. They were always there when I needed them. Every call with them ended with encouragement. The love and support in their eyes were almost palpable through the video calls. And I probably will not be able to get back in one piece if I don't mention my sister, Lakshmi. Although jokes apart, Thank you sis for keeping me in mind and sharing your stories with me. Your constant bickering with me and your funny stories always transported me back to our happy childhood days. Your active participation in moots and the passionate anecdotes thereafter were a source of motivation and entertainment.

Life in Delft was not always a piece of cake, it came with its own hurdles and I only got through it with a few people who stood by me during the difficult times. John, thank you for

your advice when I came to Delft and your kind offer to let me stay in your place. Thanks to Kammath, AJ and Manu who gave a lot of advice and help. Thanks to the football and gym buddies that helped me keep fit and agile even though it was short-lived. Thanks to KSA in 1st year with our weekly dinner fun that took me back to the jolly dinners from back home. Thank you Jeroen for giving me the opportunity to work with you, it was an enriching and yet fun internship.

To put it shortly, I thoroughly enjoyed this journey and I am grateful to everyone who made this happen. I can definitely say that I only intended to come back with a degree but now I also have strangers who turned into family and a bundle of cherished memories.

Aravind. Ashok
Delft, October 19, 2021

List of Figures

List of Tables

Nomenclature

]	[
AFP	Automated Fibre Placement
BO	Bayesian Optimization
BFS	Bögner-Fox-Schmit Element
BFSS	Bögner-Fox-Schmit-Castro Element
P_{cr}	Calculated Buckling Load
CLT	Classical laminate theory
R^2	Coefficient of Determination/ Variance Score
$\mathbf{K}$	Constitutive Stiffness Matrix
CTS	Continuous Tow Shearing
CP	Control Points
DOF	Degree of Freedom
$\boldsymbol{DL}$	Design Load
DoE	Design of Experiment
u, v, w	displacements of the element
EI	Expected Improvement
ξ	Exploration-Expoitation Weight
ϵ	Extensional Strain
FSDT	First-order shear deformation theory
GP	Gaussian Process
$\mathbf{K_{G0}}$	Geometric Stiffness Matrix
S_i	Hermite Shape Function
LHS	Latin Hypercube Sampling
LCB	Lower Confidence Bound

Q	Material Stiffness Matrix
MSE	Mean Squared Error
$\mu(x)$	Mean
ξ and η	Natural Coordinates
n_y	Number of nodes along Circumference
θ	Orientation Angle
PF	Penalty Function
Φ	Potential Energy
PI	Probability of Improvement
RBF	Radial Basis Function
$\mathbf{N}, \mathbf{M}$	Resultant Membrane Force and Distributed Moments
κ	ROtational Strain
SC-BFSC	Single-Curvature Bögner-Fox-Schmit-Castro Element
VS	Variable Stiffness
$\sigma^2()$	variance

Contents

1

Introduction

A wise man proportions his beliefs to the evidence

David Hume,1748

Modern composite manufacturing has come a long way since its inception and its application is spread throughout various industry and cutting edge fields. However, the true potential of composites have always been limited by technological and manufacturing constraints. As new technologies emerged, superior designs followed and costs reduced. Early research in variable stiffness(VS) composite has shown that by locally varying steering angles in lamina, the laminate properties such as the buckling loads can be significantly enhanced[13]. Along with advancements in robotics and automated manufacturing techniques such as automated fibre placement(AFP) and continuous tow shearing(CTS) there has been renewed interest in variable stiffness composite. Continuously varying angle of the tow allows for tailored load redistribution, which is a potential untapped with straight fibre panels. However, with the ability of varying fibre angles, the number of variables increases and hence, design space become exponentially larger[4], therefore increasing the computational complexity.

The weight reduction and knockdown factors are the evergreen subjects of interest in aerospace industry and can be considered polar opposites of each other as increase of one reduces the other. An everpresent motivation exists to realise lightweight structures through the reduction of the knockdown factors and therefore enhancing confidence in the structural integrity. This thesis focuses on one such problem, optimizing cylinders to minimize weight for given design buckling load. Of the wide expanse of optimization algorithms available, designers typically choose the tested and proven methods such as gradient based methods and genetic algorithm strategies. Stochastic based methods are a type which have not gained much traction in the structural optimization field even though they have a proven track record in other fields. Bayesian optimization is in the lead of such stochastic methods due to its straightforward formulation and easy implementation. With past studies, VS composites highlighted its ability to steer the loads away from the critical junctions on the structure thus allowing the structure to carry more load. This indicates that there is a lot of potential with VS composites and improvements of varying range can be obtained depending on the structures and loading conditions[51, 81, 111].

The large design space and potential of VS makes it an ideal playing field to study the Bayesian optimization(BO). BO is stochastic based optimization strategy which utilizes the predictions from the surrogate model to find the optimum solution. This falls under the family of surrogate based optimization. With other surrogate based optimizations like neural network and other heuristic methods[10, 14, 105] being used in structural optimization, the aplicability of BO and its potency is yet to be revealed. With this interest, the thesis focuses on the efficient implementation and modelling of VS composite cylinder and understanding the capability of this optimization for the lightweight design for given buckling load. Additionally, a novel SC-BFSC, element is investigated and benchmarked for its applicability for eigen value estimations.

The thesis structure is as follows. The thesis begins with the literature study which covers the basic principles and reviews of the recent research of composites and buckling formulation(**Chapter 2**) which gives an understanding for the modeling of the VS cylinder. This is followed by **Chapter 3** which reviews the optimization process and its literature. Literature review helped create a roadmap for the objectives and methodology. **Chapter 4** gives the research goals and objective that are aimed in this thesis. Methodology begins with **Chapter 5** where the novel SC-BFSC element definition and buckling formulation is explained. **Chapter 6** implements the VS cylindrical model and is verified against 2 reference cases. The optimization problem and its objective, constraint and design space are discussed and finalized in **Chapter 7**. The optimization process and its design of experiments are reported in **Chapter 8**. **Chapter 9** shows the results and observations from the VS model verification and optimization results. The conclusions from the drawn from the results in **Chapter 10** and based on the conclusions, recommendations for future are presented.

I

Literature Study

2

Variable Stiffness Composites

Literature Study

From wood to metal to composites, the aerospace sector has been at the forefront of material development for improving strength to weight ratio. The composite structure development began gearing up in the 1960s with more integrated composites main structures[77]. Until recent advancements in the automated manufacturing of composites, layup of the composite was mostly constant. By changing the tow slits in the newer techniques like automated fibre placement(AFP) and continuous tow shearing(CTS), the angle of the tow can be varied. The research into variable stiffness(VS) composites began in the late 1980s to further improve strength and buckling performance [49, 50].

AFP deposits strips of composite material called tows through a gantry system. It has the ability to curve, cut and restart. Typically, multiple tows are present at the machine head to produce a course[108]. Heat and pressure are applied to merge with the previous layers and produce the structure. There are some defects that may occur from varying the angle. Overlaps and gaps are created when two adjacent course have different paths. This might induce stress concentrations due to the uneven distribution of fibres and resin. Waviness is another defect that gets introduced from gaps and overlaps. Other manufacturing defects are wrinkles, tow twists and spliced tows.

CTS is a process developed by Kim et al. to improve over AFP. The tows are steered through in-plane shear deformation instead of bending(AFP). This allows the tow to align well with the reference curve which will reduce the number of overlaps and gaps formed. CTS also allows for tighter curvature which increases the design bounds. One thing to note is that steering by shear deformation causes the width of tow to be effectively reduced. This induces local thickness variations which must be accounted for. The differences in the manufacturing techniques can be seen in Figure 2.1.

2.1. Variable Stiffness Design

It is observed that the optimum design distributes the load away from the critical points like cutouts. Variable-stiffness design is a pivotal step as this would define how the problem is defined and solved. VS designing can be categorized mainly into two: using interpolation

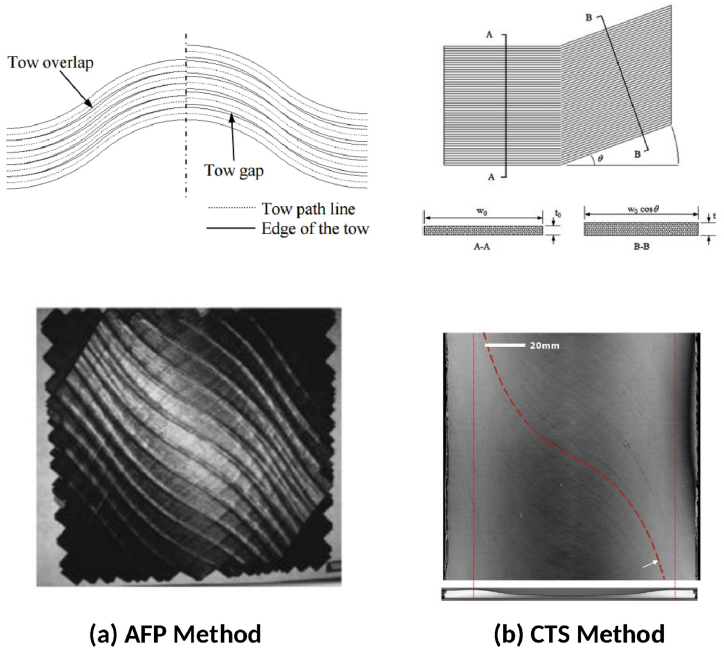

Figure 2.1: AFP(a) and CTS(b) thickness variation depiction[57, 68, 112]

function as the basis to define the fibre orientation of each lamina or; using Lamination parameters as design variables which defines the mechanical properties of the laminate as a whole and then converting it into stacking sequence and fibre orientation.

2.1.1. Interpolation Function

The varying fibre orientation can be defined in many manners with the simplest being linear variation where the angle changes linearly along an axis as proposed by Gürdal et al.. The formulation in Equation **2.1** where a is the length along the x-axis with its origin lying at $a/2$. T_0 is the angle at the centre and T_1 is the angle at either end.

$$\theta(x) = \frac{2(T_1 - T_0)}{a}|x| + T_0 \tag{2.1}$$

The points where angles are defined(T_i) are known as the control points. Linear variation reduces the flexibility and potential of the VS composites. Fibre Orientation based on Lagrange polynomial was introduced in the study by Wu et.al[111]. This introduces non-linearity into the function which allows for bigger variations. Equation **6.4** represents the Lagrange function where T_{mn} are the angles at control points in the X and Y-plane with M and N being the total number of control points at corresponding axes. Figure 2.2 shows the path definition using Lagrange polynomial[40]. Choosing the control points will define the freedom of fibre orientation the user will have and increase the complexity of the problem. Right choices will help reach optima faster and avoid getting trapped in local optima[111].

$$\theta(x,y) = \sum_{m=0}^{M-1}\sum_{n=0}^{N-1} T_{mn} \cdot \prod_{m\neq i}\left(\frac{x - x_i}{x_m - x_i}\right) \cdot \prod_{n\neq j}\left(\frac{y - y_j}{y_n - y_j}\right) \tag{2.2}$$

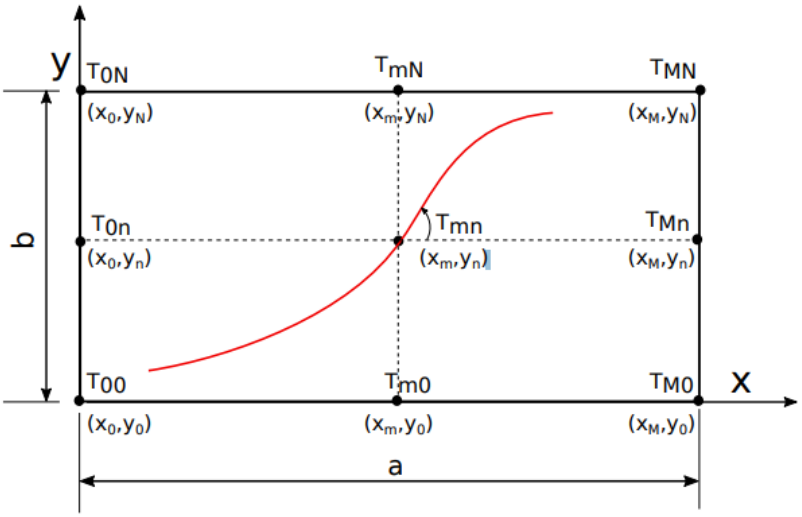

Figure 2.2: Lagrange Interpolation for fibre orientation[40]

2.1.2. Lamination Parameter

Gürdal et.al used lamination parameters as the basis to design the variable stiffness[43, 91]. Lamination parameters are non-dimensional functions based on the ABD matrix and are trigonometric bound . It can be calculated using integration along the thickness of trigonometric combinations of laminates' orientation angle as shown in Equation **2.3**. They reduce the design space to convex space due to the presence of trigonometric functions. The ABD matrix are calculated with Equation **2.4** where $\mathbf{\Gamma}$ are the material invariants matrices[44, 100]. The formula along with its derivation is shown in the work of Van Campen. Since the variables do not depend on the number of laminates, they are the superior alternative when the number of layers is high. However, in optimization, lamination parameters provides the stiffness properties which may not give a unique solution for orientation. This requires the use of two-stage optimization. For example, J.Van Campen et.al uses lamination parameters to optimize the stacking sequence of VS composite laminate for structural performance[101, 102]. The lamination parameters are solved with gradient-descent optimization and the orientation angles are in-turn solved with genetic algorithm.

$$
\begin{aligned}
\left(V_1^{\mathrm{A}}, V_2^{\mathrm{A}}, V_3^{\mathrm{A}}, V_4^{\mathbf{A}}\right) &= \int_{-\frac{1}{2}}^{\frac{1}{2}} (\cos 2\theta, \sin 2\theta, \cos 4\theta, \sin 4\theta)\, d\bar{z} \\
\left(V_1^{\mathrm{B}}, V_2^{\mathrm{B}}, V_3^{\mathrm{B}}, V_4^{\mathrm{B}}\right) &= 4\int_{-\frac{1}{2}}^{\frac{1}{2}} \bar{z}(\cos 2\theta, \sin 2\theta, \cos 4\theta, \sin 4\theta)\, d\bar{z} \\
\left(V_1^{\mathrm{D}}, V_2^{\mathrm{D}}, V_3^{\mathrm{D}}, V_4^{\mathrm{D}}\right) &= 12\int_{-\frac{1}{2}}^{\frac{1}{2}} \bar{z}^2(\cos 2\theta, \sin 2\theta, \cos 4\theta, \sin 4\theta)\, d\bar{z}
\end{aligned}
\tag{2.3}
$$

$$
\begin{aligned}
\mathbf{A} &= h\left(\mathbf{\Gamma}_0 + \mathbf{\Gamma}_1 V_1^{\mathbf{A}} + \mathbf{\Gamma}_2 V_2^{\mathbf{A}} + \Gamma_3 V_3^{\mathbf{A}} + \mathbf{\Gamma}_4 V_4^{\mathbf{A}}\right) \\
\mathbf{B} &= \frac{h^2}{4}\left(\mathbf{\Gamma}_1 V_1^{\mathbf{B}} + \mathbf{\Gamma}_2 V_2^{\mathbf{B}} + \mathbf{\Gamma}_3 V_3^{\mathbf{B}} + \mathbf{\Gamma}_4 V_4^{\mathbf{B}}\right) \\
\mathbf{D} &= \frac{h^3}{12}\left(\mathbf{\Gamma}_0 + \mathbf{\Gamma}_1 V_1^{\mathbf{D}} + \mathbf{\Gamma}_2 V_2^{\mathbf{D}} + \mathbf{\Gamma}_3 V_3^{\mathbf{D}} + \Gamma_4 V_4^{\mathbf{D}}\right)
\end{aligned}
\tag{2.4}
$$

Fibre steering will induce change in the effective width and thickness of lamina due to shearing and bending. This change must be accounted for in mass calculations and geometric imperfections of the surface. Adriana W. Blom and Gürdal provides an approximation function for the effective width of the steered tow. The change in thickness must be calculated locally. The manufacturing of laminate is carried out normally from the inside layer to the outermost. Therefore, the thickness variations will accumulate to the outer surface whereas the inner surface is smooth. Castro et al. in the study of edge-based smoothened Point Interpolation(ES-PIM) for VS laminate buckling used the effective width relation from Blom to calculate local thickness. This relation is used (Equation **2.5**) in their study which compares ES-PIM model with discrete thickness FEM model which is believed to be a good approximation with the discrete thickness FEM work. $\Delta\theta$ is the change in angle along the path.

$$h_x = \frac{h}{cos(\Delta\theta)} \tag{2.5}$$

This is applicable for filament winding and AFP processes. This means that thickness varies with the orientation and cannot be assumed to be constant. Figure 2.3 represents the correct ply thickness distribution as shown in paper by Wang et al.. In Figure 2.3(b), the blue line shows the mid-plane shift due to thickness variation.

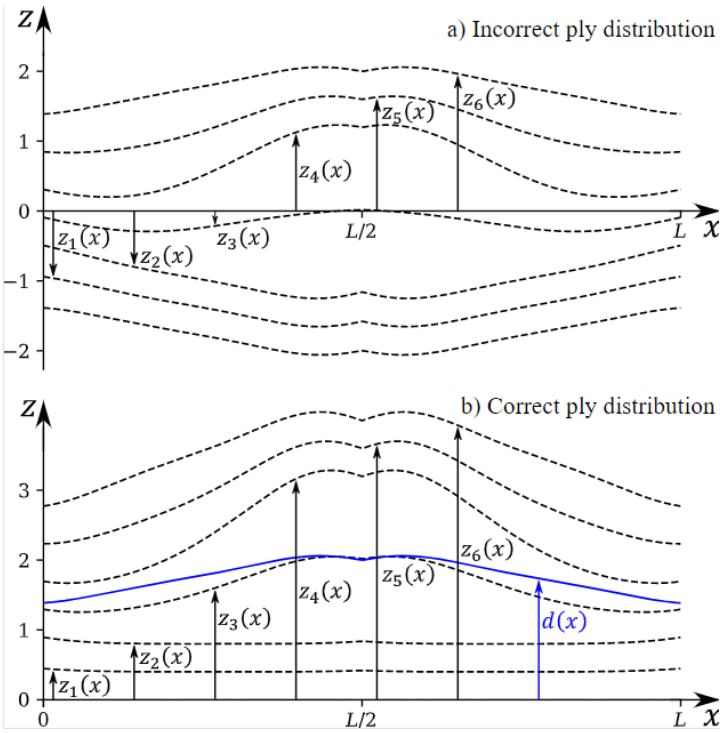

Figure 2.3: Ply thickness representation[107]

Last few decades, research on VS composites have exploded as technology started catching up to the creativity of composite researchers. In the work of Olmedo and Gurdal, buckling analysis of VS composite plate is studied. The fibre orientation is varied with respect to one axis and compared. Results show that critical loads can be increased upto 80% than straight fibres with similar weights. Nagendra et al. gave a design methodology for tow steering to improve performance using Non-Uniform Rational B-Splines(NURBS) to define

path independent of FE meshes. The work demonstrated by testing this method on plate with a hole and an engine fan blade. Various loading cases were observed and the results showed considerable improvement over the conventional laminates.

Gürdal et al. studied the effect of VS on the in-plane and buckling response of composite panels. Using linear interpolation of angles for fibre path, a comparison study between the straight/ constant stiffness and VS composites are done on in-plane loading and buckling response. Results showed improvements from Constant stiffness and note that trend between in-plane stiffness and buckling load vary inversely. Ijsselmuiden used lamination parameters to optimize the VS composite plates to maximize buckling load. Although using lamination parameters make the design space convex, it requires 2nd solver to find the stacking sequence. The studies presented showed that buckling load improved up to 189% with respect to quasi-isotropic laminates.

Research on variable stiffness cylindrical shells are small when compared to the small-scaled VS laminates and plates. Thin shelled cylinders mainly fail due to local buckling. The main characteristics related to this are the radial displacement caused by the sudden initialization of global buckling and the difficult prediction of failure loads[109]. Adriana W. Blom and Gürdal designed a cylinder with circumferential varying fibre orientation and results showed about 17% improvement in critical bending moment relative to quasi-isotropic. Güldü and Kayran numerically modelled VS cylindrical shells and optimized the shells for different load conditions where particle swarm optimization was used with angle parameters per laminate. Both axial and circumferential path definitions were studied. For an eight-ply symmetric-balanced shell, results show that for compressive loading, axial and circumferential path variation showed improvement over constant stiffness with axial being superior(37% to 7%). Similarly, for pure torsional load, 15% and bending load 17% improvement can be seen. From the above studies, it is evident that VS composite can bring in good improvement. It is also seen that the difference is more noticeable when we focus on improving one aspect of structure. In **Section 2.2**, the buckling of cylindrical shells and its finite element formulation are reviewed.

2.1.3. Classical Laminate Theory

With Composite shells, Classical laminate theory(CLT) has been used often for calculating the stress and strain elements which is a extension of the classical plate theory for laminated plates. CLT is based on plane stress conditions and Kirchoff's hypothesis which gives the following assumptions: straight lines normal to the reference remains straight after deformation; there is no thickness variation from the load; normal stress is negligible when compared to in-plane stresses and; shells are thin i.e. thickness is small compared to other dimensions. With this, the in-plane displacements are assumed to vary linearly along the thickness and the transverse displacement is constant, i.e. the transverse normal strain is zero[79]. CLT's formulation is simple and easy to implement. However, the laminate is prone to thickness failure due to its relatively small transverse shear moduli(G_{13}, G_{23}). Therefore, it is avoided for designs that are likely to fail from transverse shear or delamination. The strain is calculated from the strain-displacement calculations where the displacements are found from above assumptions. The force and moment resultants are calculated from the strain and ABD matrix which can be given in Equation **2.6** where $\epsilon^{\mathbf{0}}, \epsilon^{\mathbf{1}}$ are the membrane strains and curvature respectively, **A** is the membrane stiffness matrix, **B** bending-extensional coupling matrix and **D** bending stiffness matrix. The ABD stiffness

matrix is calculated from material stiffness Q_{ij} of each layer(1 to N) as shown in Equation **2.7** which is the stiffness in accordance to the fibre orientation.

$$\begin{Bmatrix} \mathbf{N} \\ \mathbf{M} \end{Bmatrix} = \begin{bmatrix} \mathbf{A} & \mathbf{B} \\ \mathbf{B} & \mathbf{D} \end{bmatrix} \begin{Bmatrix} \epsilon^{\mathbf{0}} \\ \epsilon^{\mathbf{1}} \end{Bmatrix} \tag{2.6}$$

$$\left(\mathbf{A_{ij}}, \mathbf{B_{ij}}, \mathbf{D_{ij}}\right) = \sum_{k=1}^{N} \int_{z_k}^{z_{k+1}} Q_{ij}^{k} \left(1, z.z^2\right) \tag{2.7}$$

CLT equates different layers into statistically equal stiffness layers which is termed as equivalent layer theory. Since CLT does not take into account shear deformations it is applicable for thin shell cases. To combat this, First-order shear deformation theory(FSDT) takes transverse shear stress into account which results in more accurate results than CLT and Higher-Order Shear Deformation theory(HSDT) goes further to add higher-oreder variations of the in-plane deformations which will remove the need for shear correction factor. Although this makes it more accurate, it adds additional degree of freedoms into the shell formulae which can make it costlier to compute.

2.2. Buckling Formulation

Along with the strength, buckling analysis of thin shells are very important. It forms many structures in the aerospace sector including fuselage panels and space launch vehicle structures. The compressive strength of a cylindrical shell can be calculated with maximum load it is able to carry when axially loaded before failure. Therefore, it is limited by the material property and the geometric cross-section. Usually, the cylinder buckles before it fails as reaching the critical stress is not the bottleneck. Buckling can be said to be the critical point of juncture when the structure shifts from stable to unstable. Thin shells can carry a great deal of load in the form of membrane compression[22]. If the compression energy transforms into bending, it can lead to catastrophic failure.

Figure 2.4 shows the load-deformation curve on an axially compressed thick cylinder presented by Sobel and Newman[22, 96]. From origin(O) to point A, the cylinder compresses axisymmetrically. At A denotes the load at which the cylinder buckles(perfect condition). B is the bifurcation point where it can continue deforming axisymmetrically (OABC) or deform more towards one side(OABD). The curve can vary depending on the cylinder dimensions and boundary conditions. But usually, we can spot the critical buckling load, the bifurcation point and sometimes failure load. More general load-deflection curve is shown in Figure 2.5. Eigenvalue analysis calculates the bifurcation load(Point A). This solves for a perfect cylinder with no imperfections on its surface, boundary conditions or loads. Realistically, the buckling load is much lower that is caused from the non-linearity of material properties and the aforementioned imperfections. Therefore, for a more accurate load and design calculation, non-linear analysis should be considered. Nevertheless, eigenvalue analysis is relatively inexpensive(faster) to solve, its buckling shape is quite similar to the non-linear results and the shape information can be used on geometric imperfection for the non-linear analysis. Post-buckling requires non-linear solvers which solve the post-buckling deformation iteratively.

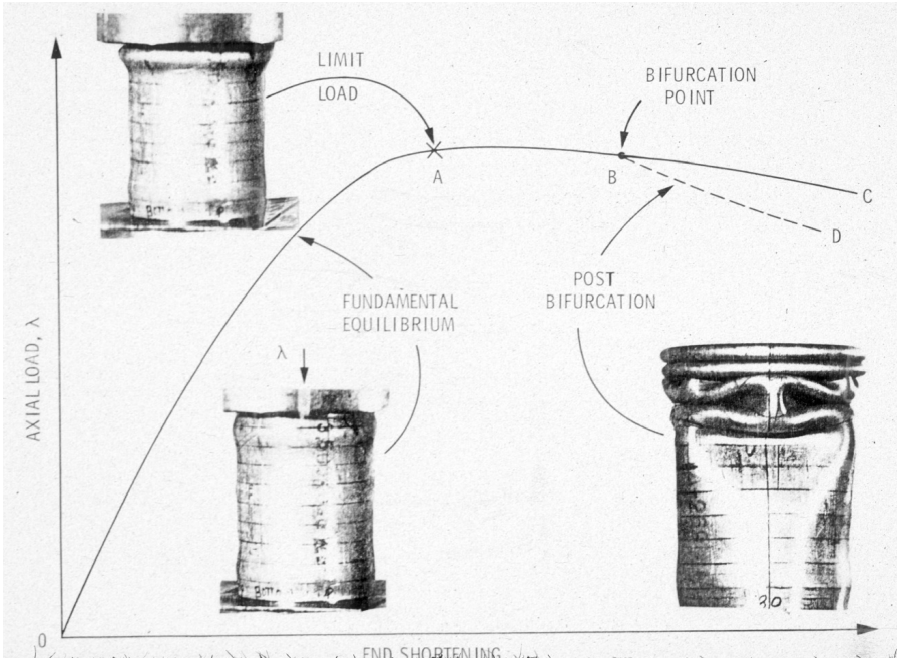

Figure 2.4: Cylinder Buckling Example[22, 96]

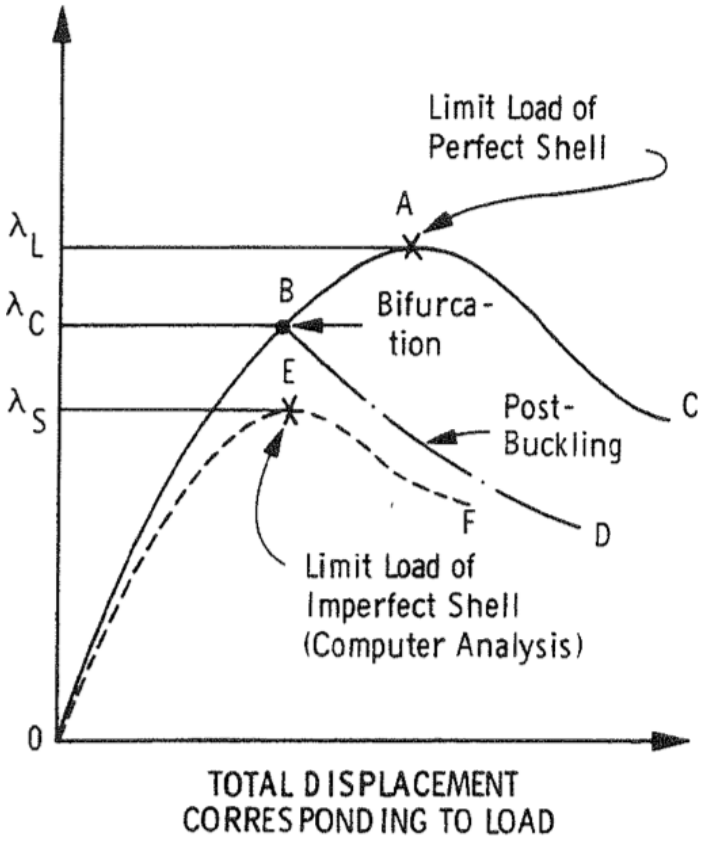

Figure 2.5: Typical Buckling Load-displacement Diagram[22]

The buckling of plates and shells can be solved using the principle of minimum potential energy and the neutral equilibrium method[54]. Π is the total potential energy which can be split into strain energy U and external work V. Equation **2.8** shows the second variation of the total potential energy and Equation **2.9** shows the eigenvalue equation for linear buckling where λ is the eigenvalue and Φ is the eigen function. λ gives the buckling loads and corresponding Φ gives its buckling shape function.

$$\delta^2\Pi = \delta^2 (U + V) = 0 \tag{2.8}$$

$$(\mathbf{K_0} - \lambda \mathbf{K_{G0}}) \{\Phi\} = \mathbf{0} \tag{2.9}$$

Buckling of variable stiffness composites can be solved through finite element analysis(FEA) or semi-analytically. And the stress and strain elements calculation for composite elements are calculated generally calculated from classical laminate theory(CLT) or first-order shear deformation theory(FSDT)[73, 88, 89, 110]. Methods used to solve vary depending on the problem definition and authors choice. For example, Castro et al. used CLT and FSDT to solve the linear buckling conical cylindrical shells semi-analytically. Results show a good correlation and the importance of shear correction factor for thicker shells is observed. Wu et al. studied buckling and optimization of VS composite plate using CLT and FEA, where buckling is solved using rayleigh-ritz method. Gürdal et al. studied the stiffness variation effects on Variable stiffness(VS) plates using CLT and custom solver ELLPACK. Oliveri and Milazzo formulated a raleigh-ritz approach for the post-buckling of VS stiffness stiffened panels using FSDT and FEA. Meshless based methods are also an emerging field in FEA. Castro et al. studied the use of Edge-based Smoothed Point Interpolation Method (ES-PIM) on buckling of variable stiffness composite. It shows that the smoothing can improve the convergence rate for linear buckling. Vertonghen and Castro compares the discrete thickness model and smoothed with continuous thickness distribution. They are modelled semi-analytically using Ritz-method and the smoothened results showed good correlation whereas the discrete thickness model experienced convergence issues. Labans and Bisagni compared the experimental cylindrical buckling results and an FEA model using ABAQUS and were able to correlate the load and mode shapes.

2.2.1. BFS Element

Using Finite Element Analysis(FEA), the properties are assigned to each mesh element, allowing the problem to be discretized into small meshed elements where the properties are defined individually. The use of finite elements is advantageous when complex designs and boundary conditions are present. The element formulation can be approached in different ways. Yang et al. reviews the different approaches and reviews diffrent modelling techniques for composite elements. Hyer and Lee studied buckling performance of VS composite using FEA. For linear buckling, FEA solves the eigenvalue problem of the structure with prescribed boundary conditions. Bucalem and Bathe states that the development of shell elements should be guided by the following requirements:

1. Element should be reliable: no spurious zero-energy mode, no shear/membrane lock and insensitive to geometric distortions.

2. Computationally Effective.

3. Element formulation should be generic: non-linear application, thick/thin shells.

4. Element formulation must be clear and simple to be used in engineering analysis.

Bögner-Fox-Schmit(BFS) element is formulated by taking the tensor product of cubic Hermite interpolation functions with continuous derivative and bilinear lagrange polynomials which are used to interpolate the membrane and bending degree of freedoms(DOFs)[16, 82]. According to Zhang's study on rectangular elements, BFS element is widely used for rectangular elements due to its simple and effective formulation. There are 6 DOFs per node which are $u, v, w, \theta_x, \theta_y$ and Γ where u, v, w are the displacements along X, Y and Z directions, $\theta_x = \frac{\delta w}{\delta x}$, $\theta_y = \frac{\delta w}{\delta y}$, and $\Gamma = \frac{\delta w}{\delta y \delta y}$. This amounts to 24 DOFs per element as represented in Figure 2.6.

Standard BFS element is limited by the fact that it can only solve out-of-plane deflection and cannot solve in-plane stress, even a linear interpolation is not possible. Castro and Jansen modified the BFS element to enable the 3^{rd} order interpolation of in-plane displacement, termed BFSC element. This is accomplished by adding in-plane displacement first derivatives which allow for calculating large displacement gradients. This is particularly useful in cylindrical shell application due to the 'elephant-foot' effect and possible complex mode shapes[24]. They perform a multi-model post-buckling analysis of a plate using the BFSC element and it is observed that the 3^{rd} order interpolation of out-of-plane displacement helps for faster eigenvalue analysis and additional in-plane displacement derivatives improve the convergence rate for the second-order fields used in the initial post-buckling analysis.

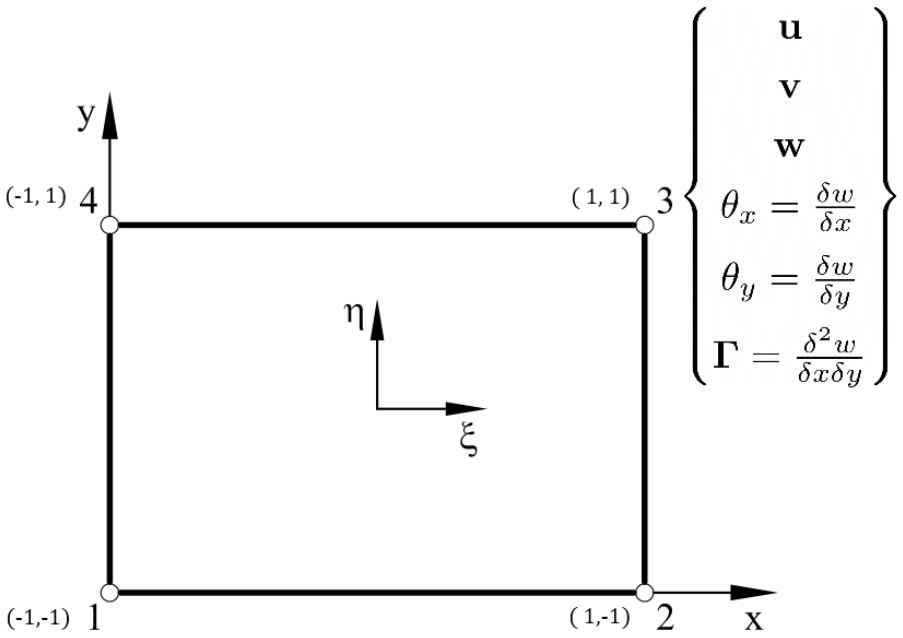

Figure 2.6: BFS element representation

The buckling behaviour of plates and shells have been studied extensively in this section. Even though VS composites are relatively younger, there is plenty of work on how buckling responds with the design changes in variable stiffness[1, 42, 61, 81, 109, 111]. It is learnt that even though eigenvalue analysis may be limited by the fact that material nonlinearity and geometric imperfections are not considered, it can still act as initial design

parameters as they provide a good comparison for mode shape and are much faster than non-linear buckling analysis. In VS composites, optimization is an essential step as it is hard to comprehend all of the design space. **Chapter 3** looks into the optimization of VS composites and gives an overview of the processes planned to be used in this thesis.

3

Optimization

Literature Study

Optimization can be classified into deterministic and non-deterministic methods[15]. Deterministic based algorithms use gradient and/or hessian information in addition to the objective function to predict the global solution. Continuous design variables are desirable for these algorithms. If the model is highly complex and non-linear, it may take longer to converge and may not even find the global optimum. On the other hand, non-deterministic algorithms work with only the function information. As it only uses function values, they take longer to solve. However, if the model has many local optima, with enough time the global optimum can be found which is not always the case with deterministic based methods. Evolutionary strategies, particle swarm optimization, stochastic based optimization, simulated annealing etc. fall under this category. The selection process of optimization is dependent on the problem and the parameters available. In this section, previous research on the optimization of variable stiffness composite is briefly touched upon. Genetic Algorithm and Bayesian Optimization is delved deep as the thesis compares the two.

Ghiasi et.al. has studied the optimization algorithms and their efficiency with respect to CS composites[34] and VS composites[35]. For CS, it is found that gradient methods are the faster methods. But being forced to use continuous design variables, the need for first and second derivatives and their tendency to get stuck in the local optima are its drawbacks. The direct search methods are found to be a good match as well. Genetic algorithm is the popular choice followed by simulated annealing. Stochastic methods are also discussed. The disadvantages noticed from them are the slow convergence rate and their heuristic nature makes it difficult to compare. The paper concludes that hybrid methods which use a combination of optimization algorithms has seen favourable results but they are usually problem-specific. With respect to VS composites, different parameterizations for the spatial variations of properties are reviewed. The author describes gradient-based methods to have the same advantages as had in constant stiffness but the increased design space combined with computer intensive first and/or second-order derivatives make it hard to advocate. In Direct methods, Nelder-Mead, Box's complex method and Genetic Algorithms are discussed. Nelder-Mead and Box's complex methods are relatively fast to solve but they may not find global optimum and cannot take a large number of design variables. Genetic

Algorithms take longer to solve and have a slower convergence rate but are more robust and have a higher success rate to get to the global optimum. The authors conclude the paper with their ranking. The optimality criterion methods(Strain energy, Fiber steering relative to principal stress, Fully stressed design etc.) and topology optimization should be used when applicable, as these break the problem into simple formulations which can easily be updated. Multi-level optimization should be looked into next as it decomposes the problem into sub-problems which generally work well in composite optimizations. Genetic Algorithm or gradient-based optimization or a combination should be used when the problem cannot be broken down into sub-problems.

The thesis of Ijsselmuiden describes that the composite optimization philosophy can be approached from 2 directions: bottom-up and top-down. Bottom-up, where the definition starts from the tow path and number of laminates which will later determine the stiffness and in turn failure loads. Top-down, starts from the global stiffness which meets the loading requirements which is used to calculate the tow path and number of laminates needed. Depending on the design strategy and other factors like cost and manufacturing constraints, either of the philosophy is chosen. The bottom-up approach is favoured in the variable stiffness calculation because of its ability to include the manufacturing constraint. Also, variations induced from the tow path makes it difficult to reverse-engineer from the global design.

3.1. Genetic Algorithm

Genetic Algorithm(GA)]GAGenettic Algorithm is a type of evolutionary optimization inspired by the Darwinian principle of evolution. The earliest research into evolutionary strategies was proposed in 1964 by Rechenberg[87] which did not include populations. This was later established by Schewefel[86]. GA was first proposed by Holland and De Jong in 1975 and was popularized by Goldberg[36] who explained the mathematical, theoretical and conceptual basics for implementation and provided research results and applications. The algorithm exchanges information between the populations of a generation. The exchange is based on the selection and recombination conditions. The information is encoded into the chromosomes and genetic operators are applied to obtain the population for the next generation. The main components are chromosome encoding, fitness function, selection, recombination and evolution scheme. GA can work with discrete and/or continuous variables. Fitness function is the value produced from the input candidate which shows how "fit" or good the solution is. In most optimization cases, this is the objective function. Basic guidelines for the fitness function is the requirement of clear definition that is quantifiable (i.e. maximum and minimum is easily identifiable) and can be implemented efficiently[69]. In Figure 3.1, basic steps in the GA optimization are shown as a flowchart. Each loop is a generation run that evaluates a set of population($P(i)$). Here the fitness of the parent population are evaluated and the best ones are paired for the next generation($P(i+1)$) through the selection process and mutation. The process is repeated till the upper limit of the number of generations is reached or if the solution has converged and the solver is confident of not getting a better one. Even though GA is expected to give the global optimum, there are cases of GA prematurely converging.

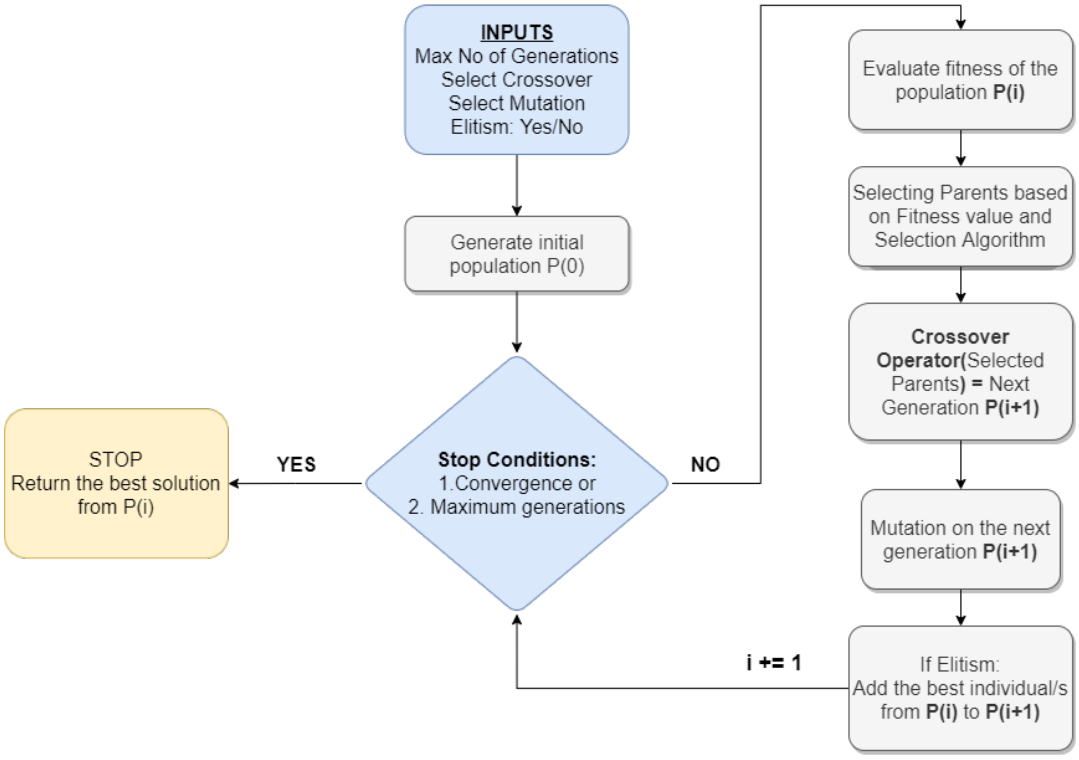

Figure 3.1: GA framework

3.1.1. Encoding

The first operation in GA is encoding. The variables are represented as bit-string. These can be binary, Octal, Hexadecimal, Permutation, Value or Tree[55]. In Binary encoding, each chromosome is represented by a binary string. Similarly, octal and hexadecimal use octals and hexadecimal numbers respectively to represent the chromosome. Generally, binary encoding is implemented in the algorithm as it is easy and faster to execute. In Permutation encoding, the chromosome is represented by a string of numbers that represents the position in a sequence. The travelling salesman problem can be represented through permutation encoding as the sequence can represent the order of cities. Value encoding uses the real value as it is. They can be real numbers, integers or characters. Value encoding is used when there are complicated values where binary encoding fails. It is also helpful for finding weights in a neural network. Tree encoding is used for evolving problems or expressions in genetic programming. The chromosome is represented by a tree of objects/functions. It can be considered as 2D encoding where former ones are 1D. In the review of GA by Katoch et al., a comparison table(Table **3.1**) for the operators is provided which show the pros and cons.

3.1.2. Selection

The selection process determines which parent chromosomes are chosen to create the next generation. The convergence rate depends on the selection technique. The selection of the point for generating children are based on the fitness function, i.e. fitter individuals have a higher probability of selection.

Roulette Wheel Selection

Roulette wheel takes all the individuals and puts them on a wheel. The area allocated for each is dependent on the fitness value. For a population of n with their corresponding fitness values being $f_1, f_2, ..., f_n$, probability of selection of individual i is[33]: $p_i = \frac{f_i}{\sum_{j=1}^{n} f_j}$

Since it takes only the fitness value into account, this might result in poor exploration and inability to separate when the good and bad individuals have a small difference in their fitness function.

Rank-Based Selection
The Rank-based selection ranks the population to their fitness values and then computes the selection probabilities based on their rank. This reduces the probability of premature convergence to a local optimum since each individual creates an expected amount of off-springs based on their ranking and not their magnitude. This results in a less biased selection process. There are different rank schemes. For example, Baker defines the selection process in a linear fashion, Yao establishes a stronger non-linear based selection and Michalewicz has an exponential based function .

Tournament Selection
Tournament selection divides the population into subgroups of two or more individuals and the best from each subgroup is chosen to the next generation tournament-style[17]. Here, the selection probability is over the subgroup and not over the whole population, which can be useful for parallel processing.

In addition to the above selection methods, there are many others. Stochastic universal sampling is an extension of the roulette wheel[8] and Boltzmann selection is based on the entropy of the individuals and importance sampling methods in Monte-Carlo simulation[63]. Elitism selection is a supplement to selection methods where the best individual from each generation is brought forward to the next generation. This was introduced to improve the performance of the Roulette wheel.

3.1.3. Crossover Operators

In GA, the crossover operator can be considered the most crucial operator. Chromosome decides how the parent chromosomes are combined to create children. Below methods are utilized for the real-valued populations using interpolation or blending function. Figure 3.2 shows a visual representation of the crossover operators[59].

Single-point Crossover
The point is randomly chosen over the length of the chromosome and genes beyond the point are exchanged between the parents. The crossover point is chosen at random but is uniformly distributed over the length.

Two or k-point Crossover
Here two or more crossover points are selected and the chromosome is divided into segments that are swapped between the parents for off-springs.

Uniform Crossover
The Uniform crossover takes each bit separately and are swapped. In Offspring's genes, each bit has a 50% chance of coming from either of the parents.

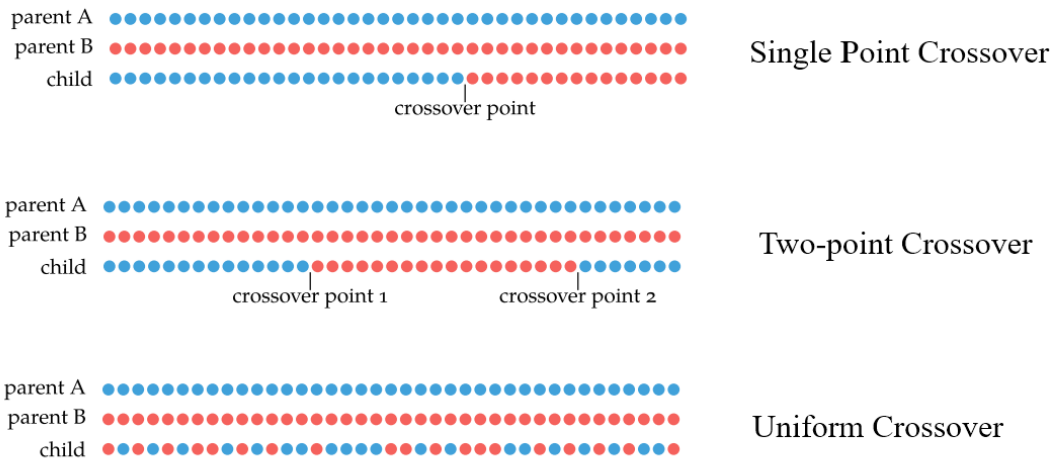

Figure 3.2: GA Crossover Operators[59]

3.1.4. Mutation Operators

Mutation Operators maintain diversity in the population and allows GA to go to the unexplored search space. It also helps bring out new characteristics. For real valued individuals, probability-based distributions are used such as uniform, gaussian or Cauchy. For integer populations, bit-flipping(preferred) or Random bit may be used. Bit-flipping flips the bit between 0 and 1 with a certain probability called mutation rate or mutation probability whereas random bit mutation replaces the bit between 0 and 1 with equal probability; 50%.

Operator		Pros	Cons
Encoding	**Binary**	Ease Implementation Fast Execution	No Support for Inversion
	Octal, Hexadecimal	Easy Implementation	No Support for Inversion
	Permutation	Support Inversion Operator	No Binary Operator Support
	Value	No Value Conversion Required	Requires Specific Crossover Mutation
	Tree	Easy Operator implementation	Difficult to design tree in some cases
Selection	**Roulette Wheel**	Easy implementation Free from Bias	Premature convergence risk Dependence on the variance of fitness function Slow convergence
	Rank	Preserve diversity Free from Bias	Sorting Required Computationally Expensive
	Tournament	Preserve diversity Parallel implementation No Sorting Required	Loss of diversity when size is large
	Boltzmann	Global optimum is achieved	Computationally Expensive
	Elitism	Preserve best individual in population	The best individual can be lost due to crossover and mutation operators
Crossover	**Single Point**	Simple, Easy Implementation	Low Diversity results
	Two or k-point Crossover	Easy to Implement Unbiased Exploration	Applicable on small subsets
	Uniform Crossover	Large subsets operation possible Better recombination potential	Less diverse solutions
Mutation	**Displacement Mutation**	Easy Implementation Applicable on Small Problem Instances	Risk of Premature Convergence
	Simple Inversion Mutation	Easy Implementation	Premature Convergence

Table 3.1: Comparison of GA operators, borrowed from Katoch et.al[55]

3.2. Surrogate Modelling

In complex problems, there is always a battle of efficiency v/s accuracy. The use of high fidelity models gives better results but cost high computational power and time. Surrogate models try to resolve this by creating a "synthetic" mathematical model which is based on the results of a certain number of initial inputs which provide fast results with a feasible accuracy. The approximate results can be used for the prediction in a global optimization problem. The example of Ford motors is provided in the paper by Crombecq et al.. Here the crash simulation of a high fidelity model of a full passenger car takes about 36-160 hours. To run a global optimization on a black-box function like the above problem is not feasible as it takes several hundreds or thousands of iterations to come to a global optimum. Therefore, the use of a surrogate model for such cases are very effective. Sobieszczanski-Sobieski et al. studied different optimization strategies for Multdissciplinary optimizations(MDO) for Aerospace design. The paper describes that the use of Response surface(surrogate model) to remove the obstacles of computation time is a helpful tool in realizing the solution. Surrogate models can be differentiated into global and local models. Global surrogate models are defined on the entire design space whereas local is used in sub-spaces of design space which contains discontinuities/jumps or highly nonlinear behaviour which cannot be realized with a global model. For example, when there is snap-through/bifurcation on a two bar-truss problem. Niutta et al. developed an optimization framework using surrogate modelling which works with such discontinuities for the crashworthiness analysis.

Surrogate models can be formulated using different techniques; for example, polynomial regression, Gaussian regression, Ordinary Kriging model etc. Jin et al. investigates different techniques over various sample sizes and between high and low-order of nonlinearity. It is concluded in the research that the Radial Basis function is generally the best. The performance between different models can be compared using the Tikhonov regularization problem given in Equation **3.1**[99]:

$$\min_{\widehat{f}\in \mathrm{H}} \mathbb{Z}(\hat{f}) = \frac{1}{N_\mathrm{s}} \sum_{i=1}^{N_\mathrm{s}} L\left(f_i - \widehat{f}\left(\mathbf{x}^{(i)}\right)\right) + \lambda \int \left\| D^m \widehat{f} \right\|_\mathrm{H} \mathrm{d}x \tag{3.1}$$

where H is family of surrogate models, $L(x)$ is the loss function, λ is regularization parameter and $D^m \widehat{f}$ is the penalty function. The former term tells the closeness to the data and the latter smoothness of the solution. The loss function can be quadratic, also known as the L_2 norm. L_2 norm is commonly used as it allows estimation of parameters. Other loss functions include linear or Laplace where the magnitude of the error is taken, Huber Loss function where the loss is taken as quadratic when its magnitude is small or else linear and ϵ loss function where its zero if the error is within the margin specified or else linear[84].

3.2.1. Design of Experiment

An effective surrogate model will depend on the number of data points and approximation function used. The data points must be selected in such a way that it provides a good representation of the search space. The study of data points and the parameters associated with optimization experiment in search space are called Design of Experiment(DoE). This is of great importance as the right selection will result in an accurate model and is capable of predicting extreme cases. Liu compared several DOE with different approximation functions, sample size and sample strategies. He concluded that sample size has more impact

than model design on the accuracy of the model. The surrogate model has a trade-off between bias(difference from the true value) and variance(sensitivity of the model to the data set). Both can be improved if the number of sample points is increased. But due to the computation constraint, the maximum number of sample points must be limited. Provost et al. in their study of the progression of sample size concluded that the geometric progression of the sample size is found to be more effective than arithmetic progression.

It is noted that different DoE methods will influence the accuracy of the model. For low bias error, it is prescribed to select the sample points that are distributed uniformly along the design space[84]. Modern Sampling techniques are classified into two: one-shot or static sampling and adaptive sampling. One-shot methods generate all the points at once aiming to fill the design space uniformly. These are easy to implement. The disadvantage is that if the sample points do not meet the design requirements the process will be repeated which takes computational power. Adaptive sampling tries to solve this. It selects a small set of sample points first and sequentially fills up to the desired number by evaluating the earlier sets. Examples of static methods are random, orthogonal and Latin Hypercube Sampling(LHS). Random sampling technique choose points in random within the design space. The random method may cause poor coverage of the space from clustering of points due to the randomness nature. LHS is commonly used and is well-known for selection technique. For a sample size N, each dimension is divided into K bins/grids which create K^N hypercubes. LHS samples the points from each hypercube with the probability of each of the hypercube being selected are the same. This help prevent clustering. However, the selection of bins is still random. Therefore its effectiveness may vary as the visual depiction shows in Figure 3.3. To improve this, optimization algorithms are present to ensure uniformity from sample points[52]. Adaptive Sampling can be divided into 3 categories: single surrogate use, multiple surrogate model combinations and multi-fidelity models. Examples for the single adaptive single model are entropy search, mean square error approach.

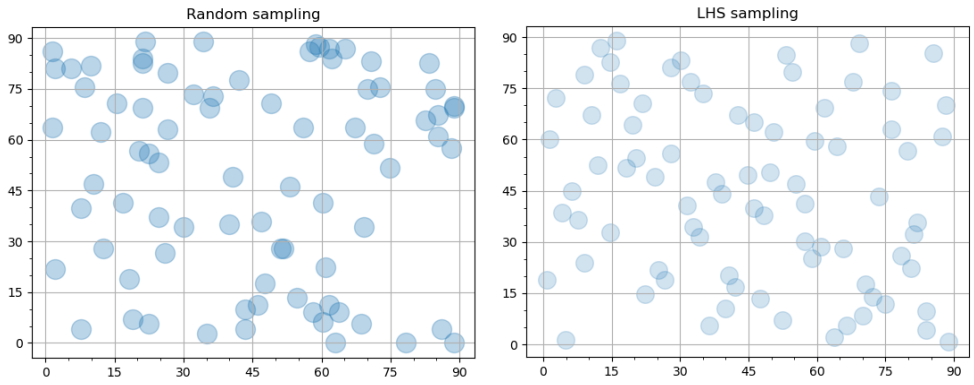

Figure 3.3: Comparison of LHS and random selection criteria

3.2.2. Classical Surrogate models

Polynomial regression model

Polynomial regression model uses a linear polynomial function to determine responses. The coefficients are solved through experimental design. General formulation is repre-

sented by Equation **3.2**:

$$f(x) = \beta_0 + \sum_{j=1}^{m} \beta_i \mathbf{x_j} + \sum_{i=1}^{m} \sum_{j \geq 1}^{m} \beta_{ij} \mathbf{x_i x_j} + \cdots + \epsilon \tag{3.2}$$

where ϵ is the statistical error, $\mathbf{x_i}$ is the i-th component of m-dimensional predictor and β are column parameters with respect to $\mathbf{x}$ to fit the model. Usually, low-order(commonly $2nd$ order) are used due to their flexibility and ease of use[52].

Radial Basis Function(RBF)

RBF uses linear combinations of radially symmetric functions which are based on the euclidean distance between the sample points. RBF model can be expressed as Equation **3.3**.

$$f(\mathbf{x}) = \sum_{i=1}^{n} \beta_i \cdot \phi\left(r^i\right) = \beta^{\mathbf{T}} \phi \tag{3.3}$$

where β are weight coefficients, $\phi(r)$ is the radial function and r represents the euclidean distance between the points $\mathbf{x}$ and $\mathbf{x_i}$. RBF models have good flexibility, are efficient and have a simple structure.

Gaussian Process(GP)

Gaussian process model is a constrained regression model. The GP model creates a joint multivariate Gaussian distribution on the sample points. GP model has some distinct features[52]:

- GP model provides good adaptability; useful when there is a black-box function.
- It can deal with noisy data
- GP passes through all sample points which is crucial for deterministic simulations.
- Suitable for integrating data from different stages.
- GP can generate prediction error at non-test sample points.

GP formulation will be discussed in detail in the next section.

There are many other widely-used models. Support Vector Regression(SVR) and Artificial Neural Network(ANN) are particularly well known. ANN is considered a universal mathematical approximator. It is capable of representing any continuous function[46, 64]. This along with the low computation cost makes it a good option for surrogate models. The limitations of ANN are the high processing power and the likely possibility of over fitting the data. .

3.2.3. Surrogate Model Optimization

Once the Surrogate model is selected and validated, the model can be deemed fit for optimization. The main steps required in this are described below[84]:

- Construct Surrogate model from given data points.
- Estimate function minimizer using Surrogate function.
- Evaluate the true objective for the estimated minima.
- Check convergence. If yes, stop.
- Update Surrogate model with the new data points.

- Repeat till convergence or maximum iterations.

The use of evolutionary-based optimizations and surrogate-based(or "data-driven") optimization has become popular as the world is moving towards quantitative-based choices rather than intuitive [10]. As stated in the book by Elishakoff, in most cases, gathering data from experiments for the sole purpose of collecting data is not feasible as the resource and time taken are far too high to be used for probabilistic analytical models. Therefore, computer simulation is the way to go for exploring the design space. Bisagni and Lanzi has shown that the use of neural networks for post-buckling optimization of composite stiffened panels gave a considerable reduction in computing when compared to Genetic Algorithm. This shows that although the neural network requires large data set for modelling, in this case, the use of data to model and optimize is faster. Likewise, the work of Wagner et al. who optimized composite cylinder stacking for maximum buckling and minimum imperfection sensitivity using decision tree-based machine learning proves the ability of such data-centric methods to turn out high performing results . Similar results can be found where the selected ones are in relation to composite and buckling design[11, 39, 70, 74, 106].

3.3. Bayesian Optimization

Bayesian Optimization(BO) is one such surrogate-based optimization. It relies on the statistical representation of the DoE. BO was first studied in 1964 by Kushner, later popularized by D.R.Jones. BO uses explicit, descriptive statistical models of the objective function. This is an ace in its sleeve as BO performance can be improved by a good objective function description. Bayesian optimization name is formed from the "Bayes Theorem" used in the probability theory. Bayes theorem is given in Equation **3.4** where the posterior probability of the model is calculated where M and E are the events, $P()$ is the probability of a function and $P(A|B)$ is the probability of event A given event B has taken place. .

$$\begin{aligned} P(M|E) &= \frac{P(E|M)P(M)}{P(A)} \\ P(M|E) &\propto P(E|M)P(M) \end{aligned} \tag{3.4}$$

The algorithm finds the maximum likelihood for a solution to occur. From the knowledge perceived from the surrogate model, BO has a sense of which regions in the design space can have an optimum. From the initial samples, BO learns the lows and highs of the objective within the design space and with this, BO will focus on gaining more information on regions it predicts where the optimum is present and further refines the search. The process is repeated till optimum is believed to be found or the upper limit on the number of iterations is reached.

BO has been used in multi-objective, multi-fidelity models[32] and is widely used in hyper-parameter optimization and training deep neural networks[95] but its application is not in plenty in structural optimization. Recent work by Yamaguchi et al. shows BO of ply drop design of laminates for stiffness and failure loads where the results show improved designs in most cases. Bessa and Pellegrino proposes a computational framework for designing non-linear structures, focusing on the design of ultra-thin deployable composite structures. Another work by this author shows the application of BO in metamaterial design resulting in designs that transformed rigid polymers to lightweight and super

compressible metamaterials[12]. Yamawaki et al. uses BO to optimize graphene nanoribbon structures for thermoelectric performances. The BO is based on the linear regression model and shows promising results with the solution. The literature shows that the structural optimization with BO is few and is not studied comprehensively.

BO initiates with collection of an initial data samples which is used to train the surrogate model. The model is tuned from training data and is the essence of predicting the output from new data. The model provides the mean value and variance for the output for a given input which are used by the Acquisition functions in BO to score the inputs. This scores are the interpretation of the acquisition functions of the possibility of the optimum within the inputs. The best score is selected and its true objective is calculated. This is then added to the initial training set and the process is repeated. This allows the algorithm to look through many data sets without having to run each of them individually. This framework is explained as a flowchart in Figure 3.4.

Generally, BO can be divided into two main aspects: Probability model that fits the data; and acquisition function which provides information on which point to be chosen next. Usually, GP regression model is used. GP model defines the objective function $f()$ using normal distribution. With the model created, new sample points are selected. The acquisition function uses the mean and variance predicted from the GP to compare the new points and the likelihood of getting optimum. BO will have to trade-off between exploration and exploitation. Exploitation is the ability of the algorithm to search within the confines of the samples present whereas exploration explores beyond initial samples with the help of the variance information present. There are different acquisition functions each using a combination of mean and variance for its function. The convergence and Acquisition function's prediction over a test case 1-D problem is shown in Figure 3.5[18].

3.3.1. Gaussian Process Regression Model

As described in **Section 3.2**, Gaussian process creates a multivariate Gaussian(normal) distribution between the sample points. GP is specified by its mean function($\mu()$) and covariance function($k()$). For given a given set of inputs $\mathbf{x} = [x_0, x_1 .... x_j]$ which is already analysed and the output is found and $\mathbf{z}$ which is a set of unknown inputs which are to predicted, then the predicted function value is given as:

$$f(\mathbf{z}) \approx GP(\mu_0(\mathbf{z}), k(\mathbf{z}, \mathbf{x}))$$

The mean function μ_0 reflects the expected function value from prior belief, covariance function k gives a correlation between their input values($\mathbf{z}$ and $\mathbf{x}$) and their function values($f(\mathbf{z})$ and $f(\mathbf{x})$). The covariance is more commonly called as kernel functions.

Lizotte in his doctoral thesis, defines Gaussian process regression(GPR) as: "*generalization of least squares linear regression that allows for more complex regression functions and provides information about the uncertainty of the regression model at different domain points*". GPR infers the original expected value $f()$ from the observed value $F()$ which is calculated using the posterior mean and kernel k and has a Gaussian noise inherent in it. When computing the posterior distribution at a new point $z \in \chi$ where χ is the design space, the mean and variance at z is given as Equation **3.5**:

$$\begin{aligned} \mu(F_{\mathbf{z}} \mid F_{\mathbf{x}} = \mathbf{f}) &= \mu_0(\mathbf{z}) + k(\mathbf{z}, \mathbf{x}) \left(k(\mathbf{x}, \mathbf{x}) + \sigma_n^2 \mathrm{I}\right)^{-1} \left(\mathbf{f} - \mu_0(\mathbf{x})\right) \\ \sigma^2(F_{\mathbf{z}} \mid F_{\mathbf{x}} = \mathbf{f}) &= k(\mathbf{z}, \mathbf{z}) - k(\mathbf{z}) \left(k(\mathbf{x}, \mathbf{x}) + \sigma_n^2 \mathrm{I}\right)^{-1} k(\mathbf{x}, \mathbf{z}) \end{aligned} \tag{3.5}$$

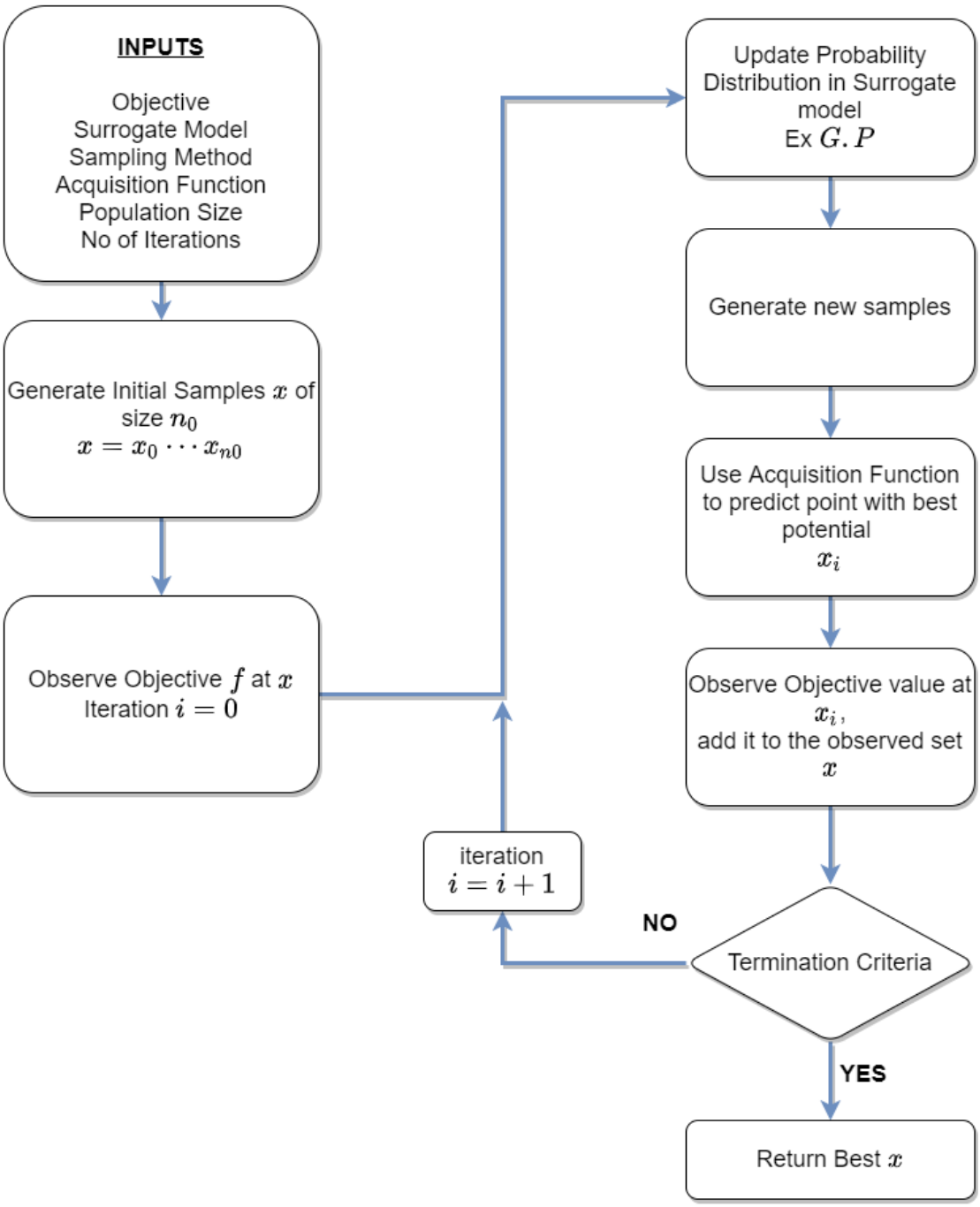

Figure 3.4: Bayesian Optimization Flowchart

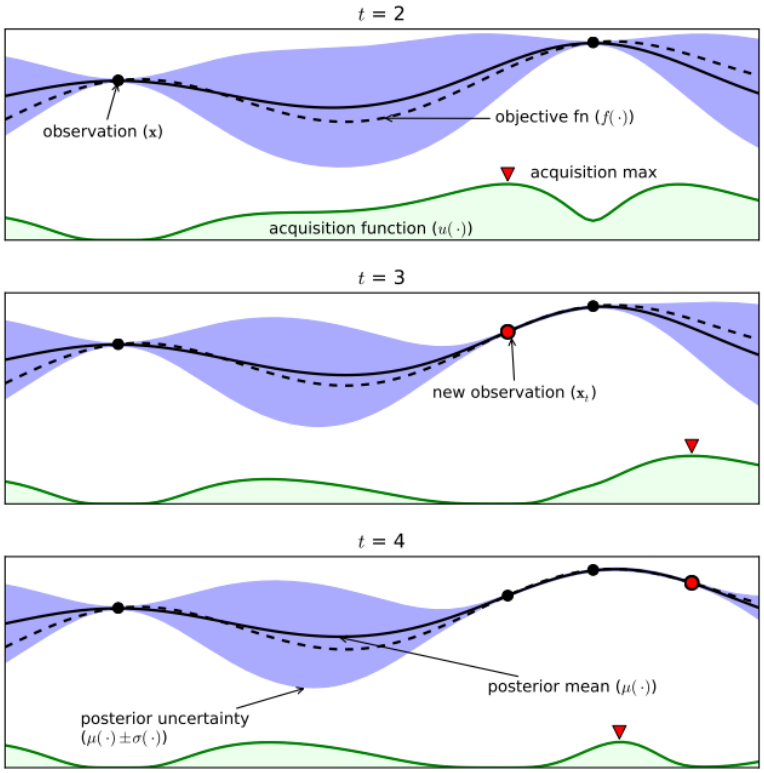

Figure 3.5: Example of Bayesian Optimization on a 1D design problem([18])

where μ_0 is the prior mean, k is the kernel function and σ_n^2 is the noise variance of the GP model.

Kernel Functions

It can be seen that 2^{nd} part of the Equation **3.5** is independent of the new point. This means that second part of the equation can seen as a weighted sum of the kernel function to the mean(for $\mu(F_z \mid F_{\mathbf{x}} = \mathbf{f})$) or kernel(for $\sigma^2(F_z \mid F_{\mathbf{x}} = \mathbf{f})$). This explains that the shape of the GP model is mainly described by the kernel function. Therefore the selection of kernel is of great importance.

Squared Exponential or Radial Basis Function

Squared Exponential(SE) or Radial Basis Function(RBF) is defined in Equation **3.6**

$$k_{SE}(r) = \sigma^2 exp\left(-\frac{r^2}{2l^2}\right) \tag{3.6}$$

where $r = |x - x'|$ and l is characteristic length-scale. Length-scale expresses the movement of the function, it describes length around the point which affects its output. This kernel is infinitely differentiable and hence k_{SE} is very smooth. SE is used universally in GPs if not much information is present on the data.

Periodic

When the model has a repeating behaviour within the same intervals, a periodic kernel can

be used.

$$k_{per}(r) = \sigma^2 exp\left(-\frac{2\sin\left(\pi r/p\right)}{l^2}\right) \tag{3.7}$$

Here in Equation **3.7**, the addition term p is present which determines the distance between its periodicity.

Linear

The linear kernel is non-stationary, i.e. it is dependent on absolute location. Equation **3.8** represents the linear kernel formulation. Offset c determines the point through which all lines in posterior passes(zero variance). The constant variance σ_b determines how far from 0 the height of function will be at zero, it is adding an uncertain offset to the model.

$$k_{\text{Lin}}\left(x, x'\right) = \sigma_b^2 + \sigma_v^2 (x - c)\left(x' - c\right) \tag{3.8}$$

Matern Class

Matern function is defined in Equation **3.9**[98]. ν and ℓ are positive parameters and K_ν is a modified Bessel function[2]. ν is usually varied between $\frac{3}{2}, \frac{5}{2}$ or ∞. Note that when $\nu \to \infty$, the function transforms into SE. The parameter ν can change smoothness of the function.

$$k_{\text{Matern}}(r) = \sigma^2 \frac{2^{1-\nu}}{\Gamma(\nu)} \left(\frac{\sqrt{2\nu} r}{\ell}\right)^{\nu} K_\nu \left(\frac{\sqrt{2\nu} r}{\ell}\right) \tag{3.9}$$

Since Kernel selection and its parameters are problem dependent, it is common to use maximum likelihood for comparison. It uses an empirical Gaussian likelihood function which is given by Equation **3.10**.

$$\log p\left(F_{\mathbf{x}} = \mathbf{f}\right) = -\frac{1}{2}\mathbf{f}^\top k(\mathbf{x},\mathbf{x})^{-1}\mathbf{f} - \frac{1}{2}\log|k(\mathbf{x},\mathbf{x})| - \frac{n}{2}\log 2\pi \tag{3.10}$$

The parameters are selected such that it gives the best likelihood value. The 1st part measures how well the current kernel parameters fit the data, 2nd part is the complexity penalization term and final part is a normalization constant. Therefore Log Marginal likelihood value gives a good representation of the computation power and accuracy of the model.

3.3.2. Acquisition Functions

Once the model is created, there is a general idea of the distribution objective about the design space. Acquisition functions are used to sample new points. Among the sample, a new point is selected on two basis: the point that is most likely to be the optima from prior information and; point selected in order to gain the maximum information about the location. Most acquisition functions use a combination of the two to acquire data.

Maximum probability of improvement(MPI), Expected Improvement(EI) and Lower confidence bound(LCB) are classical acquisition functions . They use only mean, variations data to predict the optimum point. This is proven to work well for most cases. But in some cases, this may cause it to miss the optimum point or prematurely focus on local optima. And as the interest in BO increases, new acquisition functions are proposed to improve the performance or is better for certain cases like parallel processing or optimizing hyperparameters. A few of them are discussed here.

Thomson Sampling(TS) is a sequential optimization process(similar to BO) whose principle can be used as an acquisition function. TS is less explorative than LCB but an addition of an explorative parameter could better the exploration[90].

Entropy-based Acquisition functions are information-based acquisition functions developed by Hennig and Schuler. Two variants are present, Entropy Search(ES) and Predictive Entropy search(PES). Both functions work on the principle of maximizing the information about the global optimizer. The information is calculated using differential entropy of the probability of best input/output. ES works on input and PES on output. These algorithms are weighed down by their complexities and computational power.

Knowledge Gradient(KG) is used when the objective function is not a clear black box and other useful information can be returned. KG assumes the derivative information is present and it uses the additional data further.

Most of the time, the use of single Acquisition function does not provide the best result. It is been observed that iteratively, a set of acquisition functions provides the best points according to Brochu et al. and a meta-criterion is used finally select the next query point. Empirical results show that there is an improvement over EI and LCB but it is also to be noted that this does take more computation. Figure 3.6 shows the comparison shown of BO performance of Acquisition functions over several iterations on a 1-D test problem by Brochu et al..

It is concluded that Bayesian optimization is widely applied in the field of hyperparameter optimization, robotics, environmental monitoring etc.[58, 66, 71]. However, it is observed that the application in structural optimization is few in comparison. The noted ones are the work by Bessa et.al. [10, 12] and Yamawaki et.al[114] which is on the thermoelectrical efficiency of nano-graphene structures. A very recent work by Yamaguchi et al. shows BO in ply drop design of laminates which shows the interest in BO has been ignited. This tells that full potential of BO for structural design is yet to be uncovered. It also has to noted that with the many acquisition functions, sampling techniques and surrogate models it has to develop the framework, it can be tailored for the problem at hand.

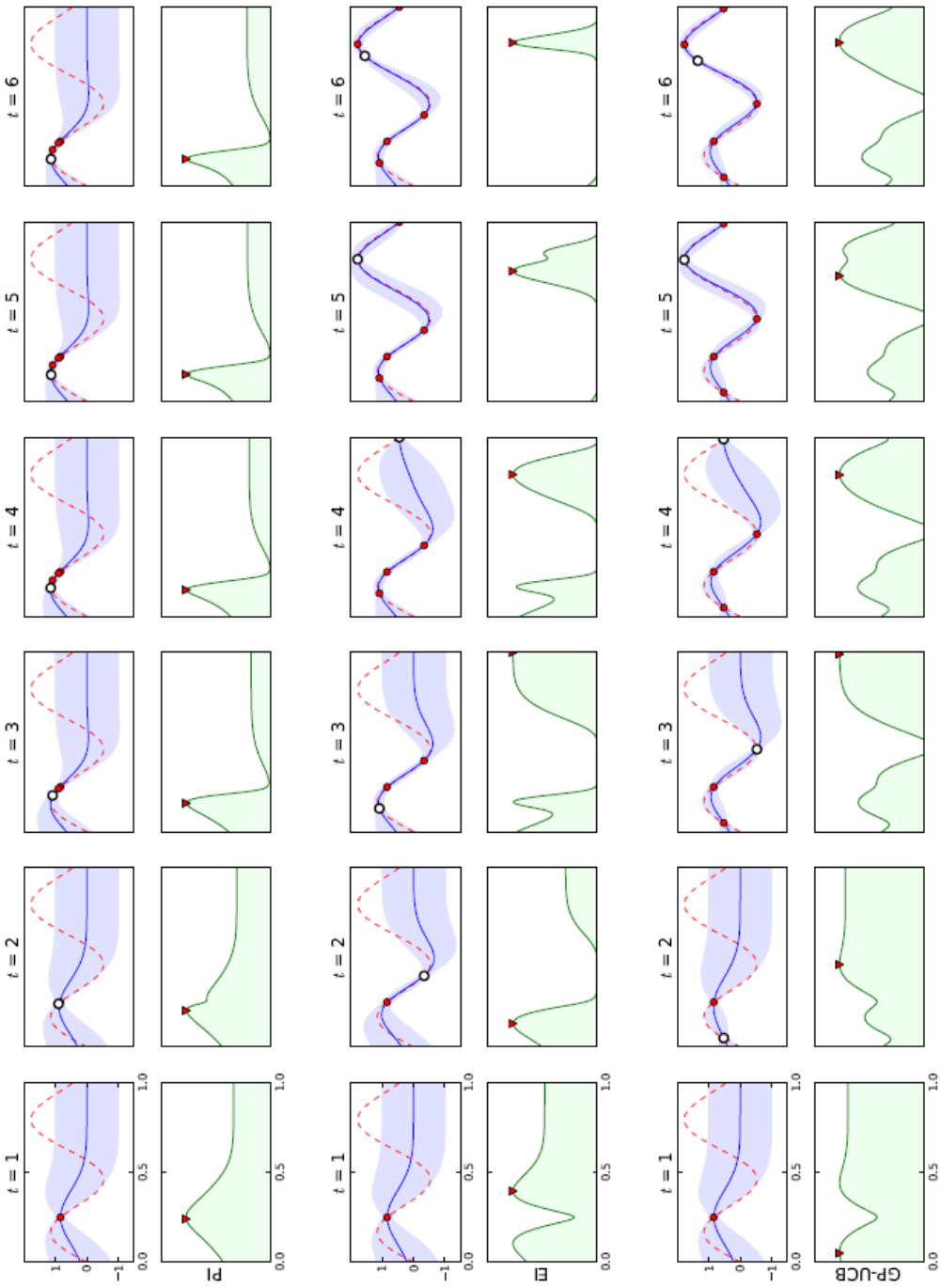

Figure 3.6: Acquisition Function Learning Comparison on a 1D design problem[18]

4

Research Objective

The Literature study reviews the major research in designing and optimizing VS composites and it is evident that a good design of VS composites can outperform conventional composites. The advantages and constraints of the current front runners in manufacturing techniques- Automated Fiber Placement and Continuous Tow Shearing are discussed to provide an idea to the author about manufacturing constraint involved in the numerical simulation and potential experimental validation. The Current scope of the thesis is formulation of the novel BFSC element for the VS cylinder from rectangular plate[27] and optimization of the weight for a given buckling load. BFSC element is selected due to its fundamental advantage from BFS plate element which is easy to implement with the benefit of improved efficiency and convergence rate(**Section 2.2**) due to the added presence of in-plane deformations derivative. This allow for the interpolation of in-plane deformations to be 3^{rd}-order that results in more accurate prediction. Buckling calculation is chosen to be performed linearly(eigen value analysis) as linear buckling provides a good comparison for design studies and its lesser computation time than non-linear analysis. Moreover, priority is given to the SC-BFSC model formulation and optimization. Design methodologies of VS composites produced in recent past are discussed in **Section 2.1**. The important functions for definition of steering of VS composites are Lagrange interpolation function and Lamination Parameters. Although lamination parameters have its advantage being a convex design space and a constant design variables, the thickness being an inherent variable in the lamination parameter formulation makes it hard to choose. Therefore, Lagrange polynomial function is chosen as the beginning point of study. The number of control points and refinement of fiber orientation angle is chosen after a design study.

Optimization of VS composites show lot of work involving gradient based optimizer and genetic algorithm(GA). The studies show that when a black-box function is present, non-deterministic methods are preferred since they require only function value and no gradient information. GA is prioritized due to their robust nature, good success rate seen in previous research. Surrogate model optimization is another non-deterministic method where interest have been booming. Examples of Surrogate model optimization include Bayesian optimization and Artificial neural networks. It is interesting to see that although bayesian optimization has widely used in data-centric optimization and hyperparameter optimization with good results, work on structural optimization are few[10–12, 58, 66, 71, 113]. This is noted in the final remarks in **Chapter 3**. With the difference being in black-box

objective function and its more constrained design space, the likelihood of getting similar improvements in results is a reasonable conclusion. Therefore, it is decided to conduct an optimization study of bayesian optimization against genetic algorithm. The choice of genetic algorithm to compare is due to its robust nature and its proven results in VS design optimization[35].

From the above observations, the thesis was planned into 2 phase: Variable stiffness model and its verfication and; optimization. And the aim or objective of the research is :

> "Develop a framework for lightweight design using Bayesian optimization and apply it to the problem of variable stiffness cylinders, finding the minimum weight for a given geometry and design load levels."

For the purpose of clarity on outcome of the thesis, the objective can be dissolved into the following research questions and sub-questions:

1. How to realize an accurate and yet efficient finite element model for variable stiffness cylindrical shells?
   (a) How to extend existing BFSC element to account for variable stiffness, and to apply the cylindrical shell kinematics?
   (b) How are terms for variable angle function chosen and defined?
   (c) What is the net gain in performance compared to a commercial finite element solution?
2. How to tackle the objective design obstacle?
   (a) How are the control points defined?
   (b) What is the degree of refinement required for orientation angle?
   (c) What are the influence of different design variables?
   (d) How are the constraints defined?
3. What are the performance outcomes from Bayesian Optimization?
   (a) What is the methodology used in selecting the sample size for surrogate model?
   (b) How are the optimization methods compared?
   (c) How does the performance differ with changing number of variables?
   (d) What effect does sample size, population size, number of iterations, kernel and kernel parameters have on the end results?

II

Methodology

5

Single-curvature BFSC Element Definition and Buckling Formulation

5.1. Finite Element formulation

According to Ochoa and Reddy, Finite Element Analysis(FEA) is the most powerful numerical method for solving non-standard solid and structural problems[79]. By splitting the domain into various sub-domains and by applying continuity on the solution at interfaces of elements, FEA is able to assemble the elements and produce an easy approximation function. FEA is based upon the weak form of the engineering problem[9]. Hamilton's principle is applied for the formation of mechanical systems' weak formulation which states that the energy function tends to be stationary for arbitrary possible variations of the system, given the initial and final system configurations are known[62, 85], as shown in Equation **5.1**.

$$\int_{t_1}^{t_2} (\delta U - \delta T - \delta W_{NC})\, dt = 0 \tag{5.1}$$

where δU is the virtual strain energy, δT is the virtual kinetic energy, δW_{NC} is the virtual work done by non-conservative forces and t_1 and t_2 are time at initial and final configuration.

The classical BFS element proposed by Bogner, Fox and Schmit[16] is a popular rectangular plate element and widely utilized for its simplistic implementation. The classical BFS element has 6 Degree of Freedom(DOF) on each node which are the in-plane displacements u and v, out-of-plane displacement w, its first derivatives ($\frac{\delta w}{\delta x}$ or w_x, $\frac{\delta w}{\delta y}$ or w_y) and its cross derivative ($\frac{\delta w}{\delta y \delta y}$ or w_{xy}). However as reviewed in **Section 2.2.1**, the BFS element does not have the ability to solve out-of-plane deflections and in-plane stresses. To remedy this, the classical C_1 element was modified to include higher interpolation terms for the in-plane displacements which is calculated from the cubic hermite functions. The resultant element is termed as BFSC(Bögner-Fox-Schmit-Castro), first proposed by Castro and Jansen [27], introduces in-plane displacement(u, v) and its first derivatives as shown in Equation **5.2**. This creates 10 DOFs per node. The element approximates the in-plane and out-of-plane displacements with 3rd order polynomials enabling an accurate representation of 2^{nd} order displacement fields. The displacement(in-plane and out-of-plane) are approximated using Hermite's Shape functions shown in Equation **5.3** where $S_i^{u,v,w}$ are the

Hermite shape function matrices which are defined in Equation **5.4** and Equation **5.5**[79]. The elements have been proven to work with isotropic plates and composite plates and shows fast convergence on linear buckling analysis[27].

$$u_i^e = \left\{ u^i, u_x^i, u_y^i, v^i, v_x^i, v_y^i, w^i, w_x^i, w_y^i, w_{xy}^i \right\}^T \quad (i = 1,2,3,4) \tag{5.2}$$

$$u, v, w = \sum_{i=1}^{4} S_i^{u,v,w} u_i^e \tag{5.3}$$

5.1.1. Modification to BFSC element

The BFSC element was defined with plates in picture and hence, there was no curvature implemented into the formulation. When applying for the cylindrical shells, the X direction is considered to be axial and Y describes the circumferential surface of the cylinder and Z is the out-of-plane radial displacement. With the cylindrical shells, the curvature characteristic must be added for the circumferential strain calculation. This modification to the BFSC element is termed as 'Single-Curvature BFSC element(SC-BFSC)'[107] . The application of this element for linear buckling analysis is derived in the next section.

$$\begin{aligned} S_i^u &= \left[H_i, H_i^x, H_i^y, 0,0,0,0,0,0 \right] \\ S_i^v &= \left[0,0,0, H_i, H_i^x, H_i^y, 0,0,0 \right] \\ S_i^w &= \left[0,0,0,0,0,0, H_i, H_i^x, H_i^y \right] \end{aligned} \tag{5.4}$$

$$\begin{aligned} H_i &= \frac{1}{16} (\xi + \xi_i)^2 (\xi\xi_i - 2) \left(\eta + \eta_i\right)^2 \left(\eta\eta_i - 2\right) \\ H_i^x &= -\frac{\ell_x}{32} \xi_i (\xi + \xi_i)^2 (\xi\xi_i - 1) \left(\eta + \eta_i\right)^2 \left(\eta\eta_i - 2\right) \\ H_i^y &= -\frac{\ell_y}{32} (\xi + \xi_i)^2 (\xi\xi_i - 2) \eta_i \left(\eta + \eta_i\right)^2 \left(\eta\eta_i - 1\right) \\ H_i^{xy} &= \frac{\ell_x \ell_y}{64} \xi_i (\xi + \xi_i)^2 (\xi\xi_i - 1) \eta_i \left(\eta + \eta_i\right)^2 \left(\eta\eta_i - 1\right) \end{aligned} \tag{5.5}$$

5.2. Buckling formulation for cylinder

The cylinder was modelled with X axis taken as axial direction$(0 \rightarrow L)$, Y circumferential($0 \rightarrow 2\Pi r$) and the radial out-of-plane displacement as Z. An additional boundary condition is applied to the two axial edges as in reality they are one and the same. Therefore, the edges are linked together.

For discretization, the cylindrical plate is divided into n sections along its axis and m along the circumference. The mesh generated are in parallel to the axes which create $m \times n$ rectangular plate elements. Care is taken here such that sides of the elements are of equal ratio for an accurate representation of the deformation characteristics. For the deflection and deformation calculations, the elements must be transformed from a global coordinate system to a local one. The natural coordinates ξ and η which are defined by Equation **5.6**

$$\begin{aligned} \xi &= \frac{2(x - x_c)}{l_x} \qquad (-1 \leq xi \leq 1) \\ \eta &= \frac{2(y - y_c)}{l_y} \qquad (-1 \leq xi \leq 1) \end{aligned} \tag{5.6}$$

where l_x and l_y are the element lengths. This will transform the cartesian co-ordinates into natural co-ordinates with their nodes represented at $(-1,-1),(1,-1),(1,1)$ and$(-1,1)$.

With this, the elements can be assembled. The numerical integration used are gaussian-quadrature. The integration points can vary from 2 with their respective weights accompanying them. Higher integration points result in better displacement but, it also increases the computation. Hence, a number is chosen with good convergence. Applying equivalent single-layer theory which assumes the heterogeneous laminate to be statistically equivalent to a single layer, the total potential energy for a finite element can be defined as Equation **5.7**. $\mathbf{N} = \{N_{xx}, N_{yy}, N_{xy}\}^T$ represents the resultant membrane force and $\mathbf{M} = \{M_{xx}, M_{yy}, M_{xy}\}^T$ are its distributed moments.

$$\Phi = \frac{1}{2}\int_{y=y_1}^{y_4}\int_{x=x_1}^{x_2} (\mathbf{N}\epsilon + \mathbf{M}\kappa)\, dx dy \tag{5.7}$$

The limits of integrals pertain to the element nodes which are: for X between x1 and x2 and; for Y between y1 and y4. The Von-Karman kinematics for thin plates is assumed for strain calculations. This results in Equation **5.8**. Here $(w_{,x})$ represents partial differentiation of w with respect to x. For the cylinder model, the curvature is considered in Y direction and hence, the resultant strain in Y direction will include the curvature factored to w.

$$\begin{aligned} \epsilon &= \begin{Bmatrix} \epsilon_{xx} \\ \epsilon_{yy} \\ \gamma_{xy} \end{Bmatrix} = \begin{Bmatrix} u_{,x} + \frac{1}{2}w_{,x}^2 \\ v_{,y} + \frac{1}{r}w + \frac{1}{2}w_{,y}^2 \\ u_{,y} + v_{,x} + w_{,x}w_{,y} \end{Bmatrix} \\ \boldsymbol{\kappa} &= \begin{Bmatrix} \kappa_{xx} \\ \kappa_{yy} \\ \kappa_{xy} \end{Bmatrix} = \begin{Bmatrix} -w_{,xx} \\ -w_{,yy} \\ -2w_{,xy} \end{Bmatrix} \end{aligned} \tag{5.8}$$

At the load bifurcation point, there exists an equilibrium for the domain of the structure or assembly of finite elements shown in Equation **5.9**. The strain can be calculated from taking partial differentiation of the displacements and their shape functions as shown in Equation **5.10**. The curvature of the cylinder is factored in the circumferential strain from out-of-plane displacements.

$$\delta\Phi = \sum_{e=1}^{n_e}\delta\Phi_e = \sum_{e=1}^{n_e}\int_{\Omega_e}\left(\mathbf{N}^T\delta\epsilon + \mathbf{M}^T\delta\kappa\right)d\Omega_e = 0 \tag{5.9}$$

$$\begin{aligned} \delta\boldsymbol{\varepsilon} &= \begin{bmatrix} \boldsymbol{S}_{,x}^u + w_{,x}\boldsymbol{S}_{,x}^w \\ \boldsymbol{S}_{,y}^v + \frac{1}{r}\boldsymbol{S}^w + w_{,y}\boldsymbol{S}_{,y}^w \\ \boldsymbol{S}_{,y}^u + \boldsymbol{S}_{,x}^v + w_{,x}\boldsymbol{S}_{,y}^w + w_{,y}\boldsymbol{S}_{,x}^w \end{bmatrix}\delta\boldsymbol{u_e} \\ \delta\boldsymbol{\kappa} &= \begin{bmatrix} -\boldsymbol{S}_{,xx}^w \\ -\boldsymbol{S}_{,yy}^w \\ -2\boldsymbol{S}_{,xy}^w \end{bmatrix}\delta\boldsymbol{u_e} \end{aligned} \tag{5.10}$$

The partial differentiation of shape function is realized with the help of Jacobian transformation:

$$\frac{\partial}{\partial x} = \frac{\ell_x}{2}\frac{\partial}{\partial \xi}$$

$$\frac{\partial}{\partial y} = \frac{\ell_y}{2}\frac{\partial}{\partial \eta}$$

The neutral equilibrium criterion also requires that $\delta^2\Phi = 0$ which is shown in Equation **5.11**. The first part of the equation will form the constitutive stiffness matrix and the second part represents the geometric stiffness. In constitutive stiffness matrix, for linear analysis, the non-linear terms when expanded into displacement terms containing w_x, w_y and w_{xy} are ignored. This leads to a matrix of size 40×40. The final expression is shown in Equation **5.12**.

$$\begin{aligned}\delta^2\phi &= \sum_{e=1}^{n_e} \delta^2\phi_e \\ &= \sum_{e=1}^{n_e} \left[\underbrace{\int_{\Omega_e} \left(\delta \boldsymbol{N}^\top \delta\varepsilon + \delta \boldsymbol{M}^\top \delta\boldsymbol{\kappa}\right) d\Omega_e}_{\boldsymbol{K}} + \underbrace{\int_{\Omega_e} \left(\boldsymbol{N}^\top \delta^2\boldsymbol{\varepsilon} + \boldsymbol{M}^\top \delta^2\boldsymbol{\kappa} +\right) d\Omega_e}_{\boldsymbol{K_{G0}}} \right] = 0\end{aligned} \tag{5.11}$$

$$\begin{aligned}\boldsymbol{K_e} = \iint_{xy} &\begin{bmatrix} \boldsymbol{S}^u_{,x} \\ \boldsymbol{S}^v_{,y} + \frac{1}{r}\boldsymbol{S}^w \\ \boldsymbol{S}^u_{,y} + \boldsymbol{S}^v_{,x} \end{bmatrix}^\top \boldsymbol{A} \begin{bmatrix} \boldsymbol{S}^u_{,x} \\ \boldsymbol{S}^v_{,y} + \frac{1}{r}\boldsymbol{S}^w \\ \boldsymbol{S}^u_{,y} + \boldsymbol{S}^v_{,x} \end{bmatrix} \\ &+ \begin{bmatrix} \boldsymbol{S}^u_{,x} \\ \boldsymbol{S}^v_{,y} + \frac{1}{r}\boldsymbol{S}^w \\ \boldsymbol{S}^u_{,y} + \boldsymbol{S}^v_{,x} \end{bmatrix} \boldsymbol{B} \begin{bmatrix} -\boldsymbol{S}^w_{,xx} \\ -\boldsymbol{S}^w_{,yy} \\ -2\boldsymbol{S}^w_{,xy} \end{bmatrix} \\ &+ \begin{bmatrix} -\boldsymbol{S}^w_{,xx} \\ -\boldsymbol{S}^w_{,yy} \\ -2\boldsymbol{S}^w_{xy} \end{bmatrix} \boldsymbol{B} \begin{bmatrix} \boldsymbol{S}^u_{,x} \\ \boldsymbol{S}^v_{,y} + \frac{1}{r}\boldsymbol{S}^w \\ \boldsymbol{S}^u_{,y} + \boldsymbol{S}^v_{v} \end{bmatrix} \\ &+ \begin{bmatrix} -\boldsymbol{S}^w_{,xx} \\ -\boldsymbol{S}^w_{,yy} \\ -2\boldsymbol{S}^\omega_{,xy} \end{bmatrix} \boldsymbol{D} \begin{bmatrix} -\boldsymbol{S}^w_{,xx} \\ -\boldsymbol{S}^w_{yy} \\ -2\boldsymbol{S}^w_{,xy} \end{bmatrix} dxdy\end{aligned} \tag{5.12}$$

The second integral is the geometric stiffness matrix and provides information on the non-linear effects of pre-buckling membrane stress $\mathbf{N}_0$. $\delta^2\kappa$ term is ignored as this becomes very small. This simplifies $\mathbf{K_{G0}}$ into Equation **5.13**.

$$\mathrm{K_{G0e}} = \iint_{xy} \begin{bmatrix} \mathbf{S}^{wT}_{,x} N_{0xx} \mathbf{S}^w_{,x} \\ \mathbf{S}^{wT}_{,y} N_{0yy} \mathbf{S}^w_{,y} \\ \mathbf{S}^{wT}_{,y} N_{0xy} \mathbf{S}^w_{,x} + \mathbf{S}^{wT}_{,x} N_{0xy} \mathbf{S}^w_{,y} \end{bmatrix} dxdy \tag{5.13}$$

The global constitutive stiffness matrix and global geometric stiffness matrix are calculated by combining them element-wise over the structural domain. The pre-buckled stress field of an element is calculated with their nodal displacement $\mathbf{u_{0e}}$. For a balanced laminate, it can be written as in Equation **5.14**. $\mathbf{u_{0e}}$ is calculated from the global displacement vector solved using static analysis given by Equation **5.15**.

$$\mathrm{N_0} = \begin{Bmatrix} N_{0xx} \\ N_{0yy} \\ N_{0xy} \end{Bmatrix} = \mathbf{A} \begin{bmatrix} \mathbf{S^u}_{,x} \\ \mathbf{S^v}_{,y} + \frac{1}{r}\mathbf{S^u}_{,x}\mathbf{S^w} \\ \mathbf{S^u}_{,y} + \mathbf{S^v}_{,x} \end{bmatrix} \mathbf{u_{0e}} \tag{5.14}$$

$$\mathbf{u_0} = \mathbf{K}^{-1}\mathbf{f_0} \tag{5.15}$$

In Equation **5.15**, $\mathbf{f_0}$ is the general pre-buckling load. It is assumed that in bifurcation point, there is a value of internal membrane stresses that satisfies $\mathbf{N} = \lambda\mathbf{N_0}$ such that the condition of neutral equilibrium is achieved. This shifts our focus to finding λ which is given by Equation **5.16**. For the equation to be zero, the determinant of the stiffness part should be zero as shown in Equation **5.17**. This represents the eigen function for a linear buckling problem. The λ are the eigen values and will have the same number of values as solution as total number of DOFs.

$$\delta\mathbf{u}^T(\mathbf{K} + \lambda\mathbf{K_{G0}}) = 0 \tag{5.16}$$

$$\det(\mathbf{K} + \lambda\mathbf{K_{G0}}) = 0 \tag{5.17}$$

Equation **5.17** solves the buckling load and its buckling shape. The bifurcation load is the minimum of the eigenvalue. This can be solved with any general eigen-solvers present.

This gives the formulation of linear buckling analysis for a typical cylinder. For a varible stiffness cylinder, the stiffness varies according to the fibre steering. Hence, the ABD matrix and in-turn stiffness matrix have to be defined locally over each element. This will be discussed in **Chapter 6**.

6

Variable Stiffness Cylinder

6.1. Designing VS cylinder

With fibre steering, the orientation angle of the laminate can vary according to the designer's choice. Applying classical laminate theory, ABD matrix is given by Equation **6.1** where k is the laminate from total lamina N, z_k is the thickness of laminate k and Q_{ij}^k is the material stiffness which is defined by orientation angle θ. This is shown in Equation **6.2**[79].

$$\left(A_{ij}, B_{ij}, D_{ij}\right) = \sum_{k=1}^{N} \int_{z_k}^{z_{k+1}} Q_{ij}^k (1, z, z^2) dz \tag{6.1}$$

$$\begin{aligned}
Q_{11} &= \bar{Q}_{11}\cos^4\theta + 2\left(\bar{Q}_{12} + 2\bar{Q}_{66}\right)\sin^2\theta\cos^2\theta + \bar{Q}_{22}\sin^4\theta \\
Q_{12} &= \left(\bar{Q}_{11} + \bar{Q}_{22} - 4\bar{Q}_{66}\right)\sin^2\theta\cos^2\theta + \bar{Q}_{12}\left(\sin^4\theta + \cos^4\theta\right) \\
Q_{22} &= \bar{Q}_{11}\sin^4\theta + 2\left(\bar{Q}_{12} + 2\bar{Q}_{66}\right)\sin^2\theta\cos^2\theta + \bar{Q}_{22}\cos^4\theta \\
Q_{16} &= \left(\bar{Q}_{11} - \bar{Q}_{12} - 2\bar{Q}_{66}\right)\sin\theta\cos^3\theta + \left(\bar{Q}_{12} - \bar{Q}_{22} + 2\bar{Q}_{66}\right)\sin^3\theta\cos\theta \\
Q_{26} &= \left(\bar{Q}_{11} - \bar{Q}_{12} - 2\bar{Q}_{66}\right)\sin^3\theta\cos\theta + \left(\bar{Q}_{12} - \bar{Q}_{22} + 2\bar{Q}_{66}\right)\sin\theta\cos^3\theta \\
Q_{66} &= \left(\bar{Q}_{11} + \bar{Q}_{22} - 2\bar{Q}_{12} - 2\bar{Q}_{66}\right)\sin^2\theta\cos^2\theta + \bar{Q}_{66}\left(\sin^4\theta + \cos^4\theta\right)
\end{aligned} \tag{6.2}$$

The geometric stiffness matrix is finally calculated with the calculated material stiffness and element dimensions. The material stiffness is calculated at the integration points of each element.This makes sure that the angle and stiffness variation is continuous over the global domain using the interpolation function. The integration point as mentioned in **Chapter 5**, can be chosen in accordance with the designer. As the angle varies, the thickness also locally varies due to bending/ shearing of the tow. The thickness distribution is calculated using the equation which is shown in Equation **6.3**. This will account for the change in the volume of the laminate from fibre steering.

$$h_k(x) = \frac{h_{tow}}{\cos\Delta\theta(x)} \tag{6.3}$$

With the above parameters and design choices made, it is possible to perform the linear buckling analysis of a variable stiffness composite cylinder under axial loading. First, the model is created using the SC-BFSC elements, which is implemented in the 'BFSCCylinder' Python module. The resultant elements are recorded and from the interpolation function and input orientation angles(θ), the stiffness matrix of each element is then calculated according to their axial co-ordinate.

6.2. Model Implementation and Verification

The model is produced entirely on python. With the cylinder model produced and meshed, the stiffness matrix is calculated with the ABD matrix function and geometric stiffness function present in the python library 'composites'[23], which is followed by buckling eigen analysis that is computed using Locally Optimal Block Preconditioned Conjugate Gradient Method (LOBPCG) solver from the 'Scipy' library[104]. With stiffness now defined at the integration point of the element, to give a good distribution of the change in angle θ between its edges, the overall distribution of angle is calculated from interpolation functions and control points defined on the cylindrical domain. It is noted that there may be changes in the choice of integration points, control points and mesh refinement depending on the problem at hand. The verification is performed with a convergence study on cylinders with different diameter to length aspect ratios. For the thesis optimization problem, the diameter is $0.3m$ and height $0.3m$ resulting in a (L/D) ratio of 1 . Excluding this, 2 other cases of different aspect ratios whose results were previously tested are used.

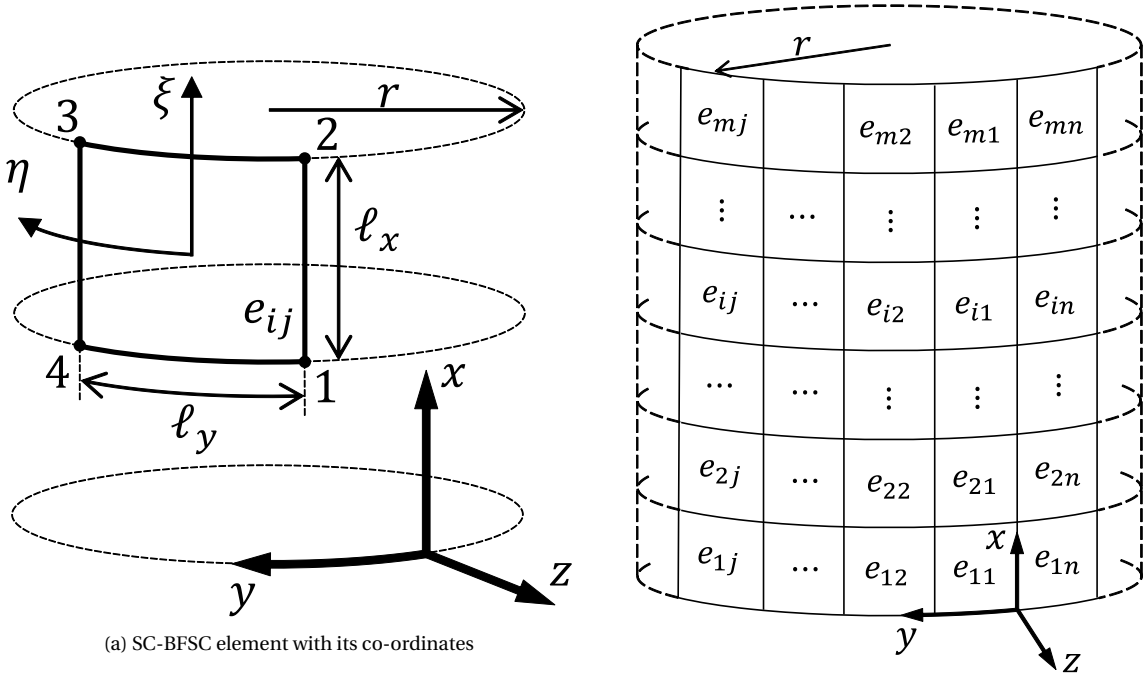

(a) SC-BFSC element with its co-ordinates

(b) SC-BFSC meshed model

Figure 6.1: SC-BFSC element cylindrical model[107]

6.2.1. Interpolation function and control points

For a variable stiffness laminate, the steering angle is not constant. Therefore, we need to define the ABD matrix and in-turn stiffness matrix to each element. This is accomplished with the interpolation function which defines the steering path of the fibre with the help of control points(CP). An interpolation function is defined to vary the angle between these points to measure the rest of the laminates. This can be either linear or non-linear depending on the level of complexity and freedom required by the designer. For this case, interpolation through Lagrange function is considered as given in Equation **6.4**. This equation is a general one with control points on both axial and circumferential axis. If only two

control points are taken on each axis, then the equation becomes bi-linear. As mentioned in **Chapter 2**, the work of Güldü and Kayran proves that for axially compressive loading, the axial variation of tow has a bigger improvement on buckling than circumferential. Therefore, in this study, only axial loading of the cylinder is considered.

$$\theta(x,y) = \Phi_i + \sum_{m=0}^{M-1}\sum_{n=0}^{N-1} T_{mn} \prod_{m\neq i} \frac{x-x_i}{x_m-x_i} \prod_{n\neq j} \frac{y-y_j}{y_n-y_j} \tag{6.4}$$

Here three cases are considered: 3 CPs, 5 CPs and 7CPs. The CPs are defined with symmetry over the mid-plane(along the height). For example, for a cylinder of length L, 5CPs are defined with 3 variables which define the steering orientation at (0,L),(L/4,3L/4) and L/2. Here, the brackets are denoting assignment of same variable. This increases the degree of variation without increasing the computational load. The different CPs and their influence in fibre steering is illustrated in Figure 6.2. It is to be noted that increasing the CPs results in exponential increase in total design space that the optimization has to cover. From the study, it is inferred 5 CPs provides a good degree of flexibility without much penalty in computational time for optimization. Seeing the difference achievable, 5 CPs are taken for final optimization. The equation for the interpolation is given in Equation **6.5**.

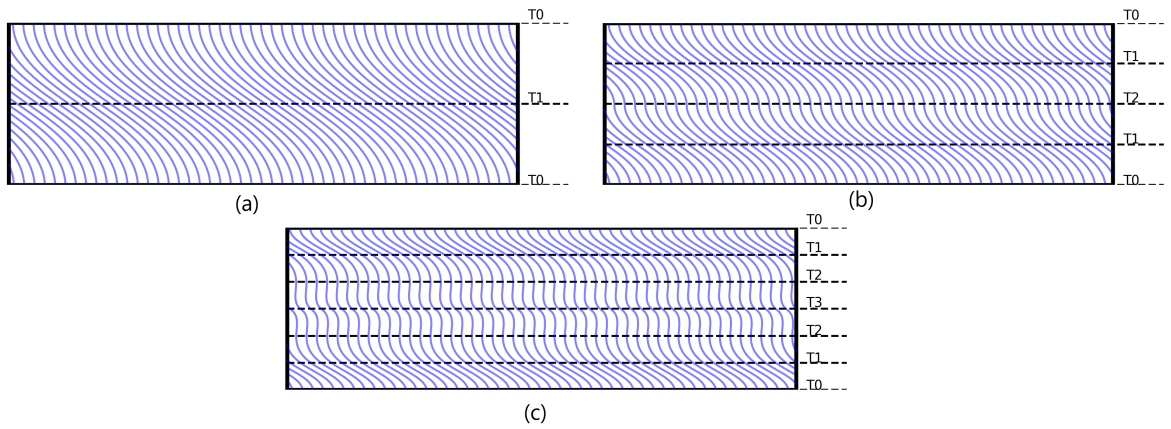

Figure 6.2: Location of control points for different interpolation orders and its fibre steering: (a)-3CP, (b)-5CP, (c)-7CP

$$\theta(x) = \begin{cases} N_1\theta_1^{VP} + N_2\theta_2^{VP} + N_3^L\theta_3^{VP}, & x \leq \frac{L}{2} \\ N_3^R\theta_3^{VP} + N_4\theta_2^{VP} + N_5\theta_1^{VP}, & x > \frac{L}{2} \end{cases} \tag{6.5}$$

where:

$$N_1 = \frac{(x-x_2)(x-x_3)}{(x_1-x_2)(x_1-x_3)}; \quad N_2 = \frac{(x-x_1)(x-x_3)}{(x_2-x_1)(x_2-x_3)}$$
$$N_3^L = \frac{(x-x_1)(x-x_2)}{(x_3-x_1)(x_3-x_2)}; \quad N_3^R = \frac{(x-x_4)(x-x_5)}{(x_3-x_4)(x_3-x_5)}$$
$$N_4 = \frac{(x-x_3)(x-x_5)}{(x_4-x_3)(x_4-x_5)}; \quad N_5 = \frac{(x-x_3)(x-x_4)}{(x_5-x_3)(x_5-x_4)}$$

The effect of number of integration points checked with a convergence analysis are shown in Figure 6.3a and Figure 6.3b. From both cases, it is clear that 4 integration points provide good convergence without a penalty in computation time.

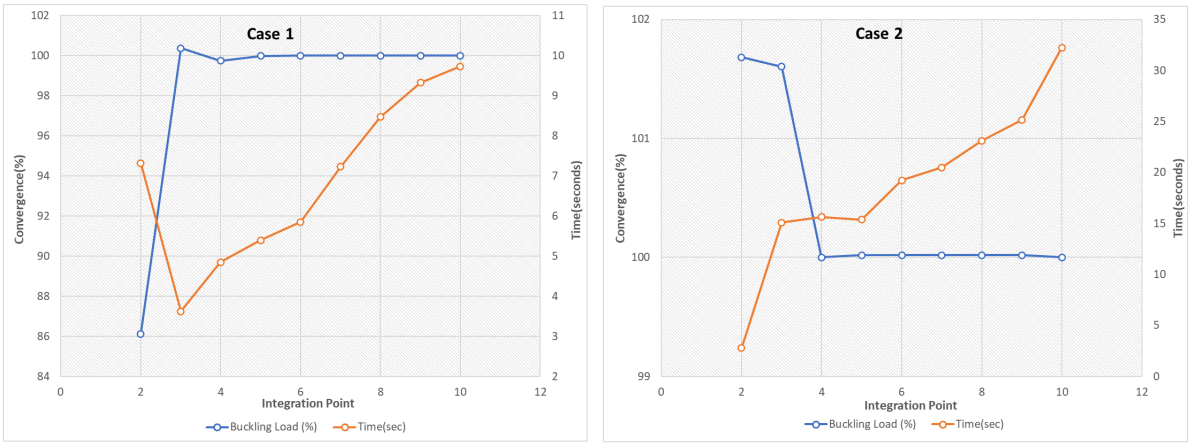

(a) Case 1

(b) Case 2

Figure 6.3: Integration point convergence plot

Table 6.1: Case 1 Properties[61]

Cylinder Dimensions	
L	0.79 m
D	0.6 m
Material Properties	
E_{11}	141 GPa
E_{22}	10.3GPa
ν_{12}	0.3
$G_{12} = G_{13}$	4.5 GPa
G_{23}	4.5 GPa
h_{tow}	0.181×10^{-3}m

Table 6.2: Case 2 Properties[106]

Cylinder Dimensions	
L	0.3 m
D	0.136 m
Material Properties	
E_{11}	90 GPa
E_{22}	7 GPa
ν_{12}	0.32
$G_{12} = G_{13}$	4.4 GPa
G_{23}	1.8 GPa
h_{tow}	$0.4 \times 10^{-3} m$

6.2.2. Mesh Convergence

The mesh convergence is performed with 4 integration point. The convergence rate is calculated as the percentage change in buckling load between 2 consecutive mesh sizes and the said convergence rate v/s number of number of nodes in circumference n_y is plotted. The number along the circumference is chosen as the mesh refinement as the elements are set an aspect ratio of 1. Hence, if n_y is set, then the number of nodes along axial direction is

$$\frac{n_x}{n_y} \simeq \frac{L}{\pi D}$$

$$n_x \simeq n_y \frac{L}{\pi D}$$

The value of n_x is taken as the closest integer to this ratio. n_x is always set to be odd as for the design of variable stiffness, having a node set at the mid-point makes it easier for the control point assignment. For mesh convergence, three classes of fibre steering is looked into as it is observed that the mesh convergence may differ for the same dimensions but with different fibre steering. First being constant stiffness with all the elements having the same fibre orientation, second being variable stiffness with maximum variation between adjacent control points less than 45° and finally variable stiffness with extreme angle varia-

tions which is at the limit of the manufacturing constraint(around 85°). These 3 angles are tested on the 2 cases shown in Figure 6.4a and Figure 6.4b. The convergence rates data are presented in Table **6.3** and Table **6.4** .

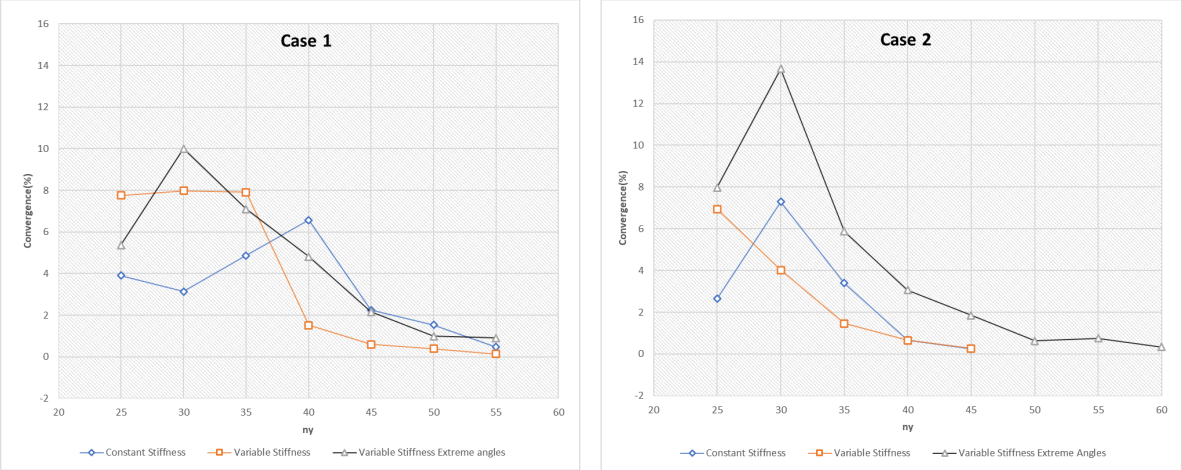

(a) Case 1

(b) Case 2

Figure 6.4: Mesh Convergence plot with respect to Circumference elements

Table 6.3: Mesh Convergence Case 1

Constant Stiffness		**Variable Stiffness**		**Variable Stiffness Extreme orientation**	
n_y	**Convergence**	n_y	**Convergence**	n_y	**Convergence**
25	3.91	25	7.76	25	5.38
30	3.14	30	7.98	30	10.01
35	4.87	35	7.91	35	7.11
40	6.57	40	1.52	40	4.82
45	2.25	45	0.60	45	2.16
50	1.53	50	0.38	50	0.99
55	0.48	55	0.14	55	0.91

Table 6.4: Mesh Convergence Case 2

Constant Stiffness		**Variable Stiffness**		**Variable Stiffness Extreme orientation**	
n_y	**Convergence**	n_y	**Convergence**	n_y	**Convergence**
25	1.76	25	6.945	25	6.934
30	4.86	30	4.025	30	7.106
35	2.27	35	1.468	35	1.661
40	0.417	40	0.661	40	1.230
45	0.106	45	0.353	45	0.400
				50	0.261
				55	0.431
				60	0.107

6.2.3. Verification

Commercial FEA Software ABAQUS is used to verify the results from BFSC results[93]. S4R elements are used for the construction as from literature study show simulation with this element gives good correlation with the experimental loads. For this, two case studies are presented in previous works of Labans and Bisagni and Wang et al. which are showcased as *Case 1* and *Case 2* respectively. In *Case 1*, the variable stiffness is defined with 2 variables and 3 CP and in *case 2*, it is defined with 3 variables and 5 CP are used. Material properties and Geometric properties are given in Table **6.1** and Table **6.2**. Figure 6.5a to Figure 6.8b shows the ABAQUS and SC-BFSC representation of the buckling shape and bifurcation load is seen to match. The S4R results and SC-BFSC results are shown in Table **9.1**. Convergence is based on the two consecutive results difference.

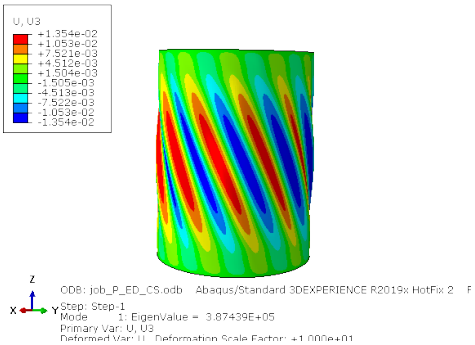

(a) ABAQUS S4R Elements

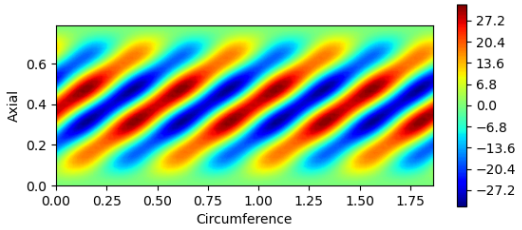

(b) BFSC Elements

Figure 6.5: Verification Case 1- Constant Stiffness

The results show the verification of the cases for the buckling load, thus proving the SC-BFSC element linear buckling analysis. Based on the successful verification of the SC-BFSC model, the optimization of test case can begin. This thesis focused on the applicability of Bayesian Optimization on structural problems. And just as this study of control points, integral points and mesh refinement gave the best solution possible, the same must be done for the optimization parameters. In **Chapter 7**, the optimization problem, its design space and their limiting constraints are discussed and understood to give a better picture for final optimization.

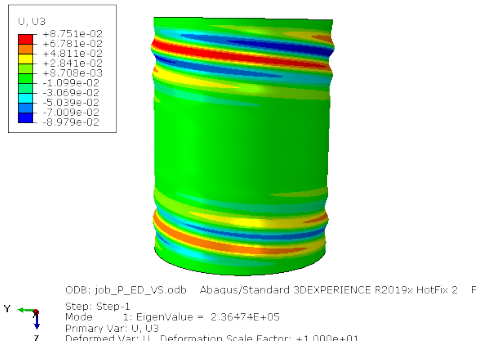

(a) ABAQUS S4R Elements

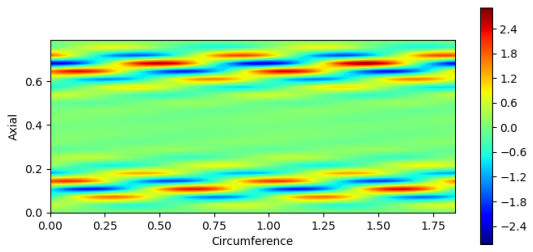

(b) BFSC Elements

Figure 6.6: Verification Case 1 Variable Stiffness

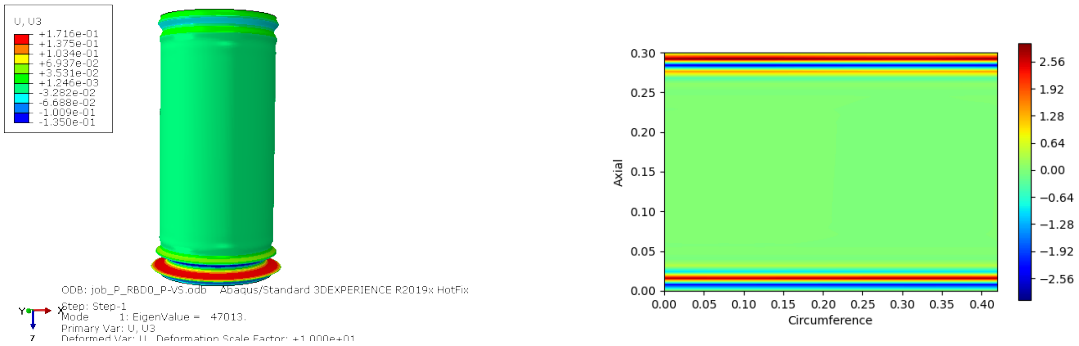

(a) ABAQUS S4R Elements

(b) BFSC Elements

Figure 6.7: Verification Case 2 Variable Stiffness

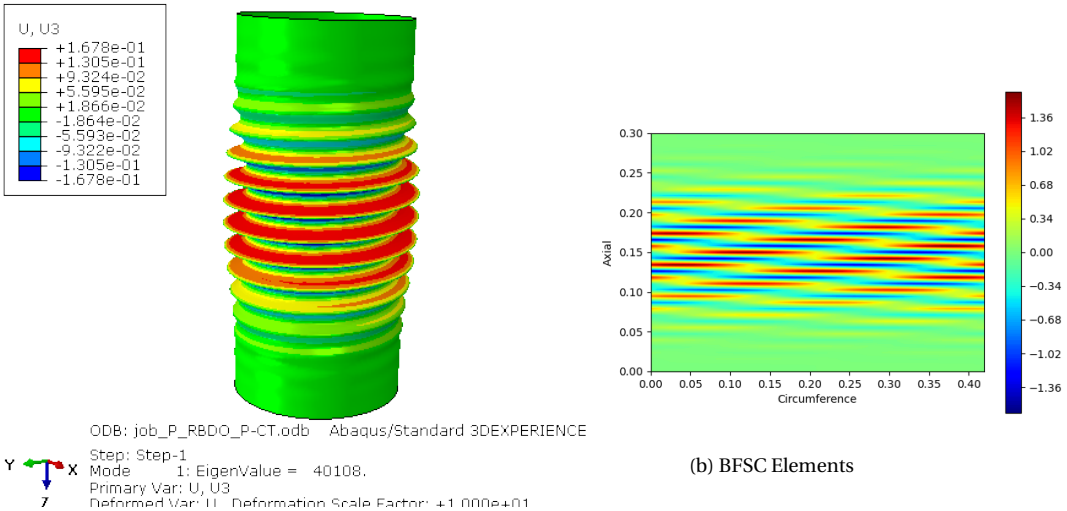

(a) ABAQUS S4R Elements

(b) BFSC Elements

Figure 6.8: Verification Case 2 Variable Stiffness with Constant thickness

Table 6.5: Load verification error on Case 1 and 2

	Published results	**S4R**	**S4R Error**	**BFSC**	**BFSC Error**
Case 1					
CS-$[\pm 45, 0, 90]_s$	420kN	387.439	-7.75%	394.648kN	-6.036%
VS $[[\pm 45], \pm [60, 15]]_s$	260kN	236.470	-9.05%	240.801kN	-7.384%
Case 2					
VS VT$[45.4, 86.5, 85.8]_b$	49.576	47.013	-5.17%	51.1069	3.08%
VS CT$[64.1, 58.4, 57.8]_b$	40.304	40.1	0.5%	42.51	5.47%

7

Optimization Problem

7.1. Objective

Defining the problem objective and its constraints is a crucial aspect of an optimization process. For a lightweight design, the objective inevitably turns to minimization of weight. With the thickness variation of the laminate with respect to fibre steering, the density of the lamina is considered constant. The disadvantage of taking volume as the objective function is that the volume will depend on the geometric dimensions of the cylinder. Therefore, any constraint penalties added to the objective, the effect will vary with volume. Instead, relative volume is employed which is calculated as the ratio of the volume of the laminate to the volume of a constant single-layer laminate.

7.1.1. Constraints

Buckling Load

As previously stated, with weight minimization as the main objective, the design load for buckling must be introduced as limiting constraint. Instead of introducing a constraint function for the objective, a penalty function is used. This reduce the complexity of the objective definition and allow easy implementation between different optimization algorithms without much changes in the objective. The penalty functions are based on the Design Load(***DL***) and Actual Load calculated(P_{cr}). Initially, a quadratic based penalty function was chosen of the form

$$\textbf{PF1} = \begin{cases} 1 & \text{if } P_{cr} \geq \boldsymbol{DL} \\ \left(1 + \left(\frac{\boldsymbol{DL}}{P_{cr}}\right)\right)^2 & \text{if } P_{cr} < \boldsymbol{DL} \end{cases}$$

However, it is observed that at the boundary between feasible and infeasible regions for PF1, there's a sharp drop in the value to 1. As a consequence, the optimizer ignores any value that barely misses the buckling constraint. Penalty functions whose values are continuous about the whole range of the constraint are required since heuristic optimization examines the objective values only. The second penalty function chosen is based on the square-law which is continuous over the feasible region border. This helps keep the information of boundary cases within the optimization loop[38]. Penalty function based on square based law is given below:

$$\textbf{PF2} = max(1, 1/\lambda^2)$$

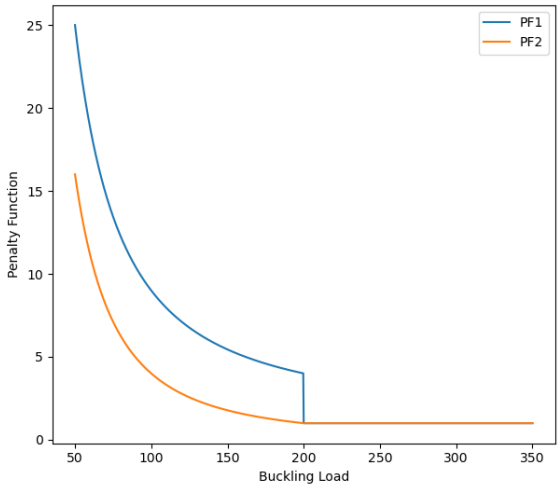

Figure 7.1: Penalty function distribution over the range of buckling load

where

$$\lambda = \frac{0.95 \times P_{cr}}{\boldsymbol{DL}}$$

Figure 7.1 shows the trend of the two penalty functions with 200 kN taken as the design load which shows the sharp jump from **PF1**. A modification is made to **PF2** from the literature which is the inclusion of an additional safety factor of 0.95. This offsets the penalty function increase from slightly before the design load such that the percentage of infeasible designs getting through is reduced. The value of 0.95 is chosen from trial and error.

Maximum Curvature

Manufacturing techniques limit the steering of the tow as excessive steering may cause defects in manufacturing such as wrinkling at the inner edge of the tow(called puckering), twisting or limitation from the machine head for tailoring. The degree of steering is controlled through the constraints posed on the curvature. Curvature is the reciprocal of the radius of curvature of the tow and the maximum curvature depends on the material and tow width being used.

The general form of the equation for radius of curvature between two points is given in Equation **7.1** where the subscript with comma denotes the differentiation with respect to the axis provided .

$$r = \frac{\left[1 + \left(y_{,x}\right)^2\right]^{3/2}}{|y_{,xx}|} \tag{7.1}$$

From the co-ordinate system defined, we can transform $y_{,x} = \tan\theta$ and the equation transforms to

$$y_{,xx} = \frac{1}{\cos^2(\theta)} \frac{\delta\theta}{\delta x}$$

Using Lagrange interpolation function(Equation **6.4**) and differentiating with respect to x

considering only axial variation gives Equation **7.2**.

$$\frac{\delta\theta}{\delta x} = \sum_{m=1}^{M} \theta_M \left(\frac{1}{x_m - x_i} \prod_{i_2=1}^{M} \frac{x - x_{i_2}}{x_m - x_{i_2}} \right) \tag{7.2}$$

In this problem the local steering is being calculated at element level for determining the thickness variation. Therefore, applying curvature globally is not wise as this requires further memory allocation and recalculations of control points for maximum curvature for the same result. Hence, local constraint was introduced which made sure that steering angle of the elements do not go beyond the maximum limit. With local orientation angle θ, the steering angle is the difference between current and previous orientation angle. As a conservative choice, this previous angle is always kept as the minimum of the control points. Therefore, for the design study with 3 CPs and applying the relation $y_{,x} = \tan\theta$, we get Equation **7.3**.

$$\theta_{steer} = |\theta - min(\theta_1, \theta_2, \theta_3)|$$
$$\tan(\theta_{max}) = \frac{R}{w_{tow}} \tag{7.3}$$

The calculation of the maximum steering angle is determined at all integration points individually on each element.

In this optimization VS cylinder, an assumption is made that the width of carbon fibre tow used for this design is $1/4^{th}$ inch, for which the minimum radius of curvature achievable is 1500 mm[94]. The maximum angular difference can be given by Equation **7.3** which is about 87.5° . For the sake of conservation, the maximum change in angle is taken as 80°. When the constraint is violated, the objective returns a non-feasible value like -100 or $1e^6$. This allows for disqualification of such candidates.

7.1.2. Design Space

The design space is explored to understand the problem better and to make the optimization problem as efficient as possible. The problem is defined in such a way that it has the ability to decide the number of layers desired, with only a maximum number of layers given to keep the number of design variables in check. A conscious choice of 4 layers which allows for comparisons of results from the work of Wang et.al[107]. It also allows to check the integrity of the problem without overloading the CPU resources.

Each of the 4 layers will each have 5 control points which are defined by 3 design variables from symmetry i.e. $\theta_1 = \theta_5, \theta_2 = \theta_4$ and θ_3. In addition to this, a boolean variable **S** is added to each layer so as to activate and deactivate each layer individually: **S**=1 means the layer and its variables are used and; **S**=0 means the layer is discarded. Therefore, the problem will have 16 design variables wherein twelve define the steering path and the rest four are boolean variables that switch the layers on or off.

Another **major change in definition which is crucial for the surrogate model** is the loss of points from bad input sets. When creating the data points in the algorithm, as the sampling criterion tries to create points over the whole design space, some part of the variables are taken by inputs with four boolean switch variables off. This result in a null set for the analysis which requires the use of arbitrary high value for objective. This is a major disadvantage because these 'infeasible sets' that get included in the sample space and reduce the density in the 'feasible sets' region of the design space. The biggest drawback from this

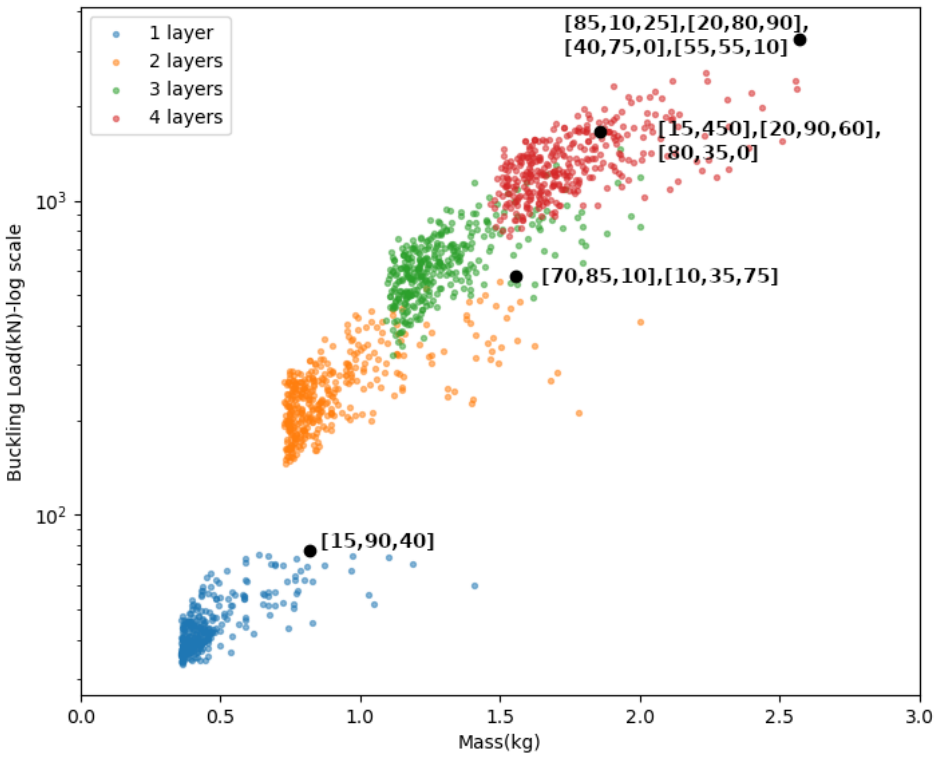

Figure 7.2: Design Space Distribution wrt buckling load and mass

is the degree of increase in points required for the model to start perform sufficiently well. Therefore, the 1st layer in the inputs is always kept active(1) and hence can be omitted from the number of variable reducing the total variables to 15.

For the tow orientation angles, the current fibre layup technology can use full steering angles between $[-90°, 90°]$. For the solver to reach the optimal solution, a balance must be achieved in descretization: it must have fine enough to prevent the global optimum from being overlooked but also limit the number of design points to avoid high computational expense. For instance, with 4 layers, total variables are 16, where the orientation angles variables can be defined between $[-90°, 90°]$. If orientation angles increment is kept 5° and assuming the switch parameters are kept constant at 1(i.e. all 4 layers are on) the total design space size is 6.58×10^{18}. Instead, if given the condition that the laminates are balanced, then the orientation angle limits change to $[0°, 90°]$ and the same discretization of 5° obtain a design space of 2.21×10^{15}. This reduces the design space candidates by a factor of about 3000. Therefore balanced laminates are chosen as the default condition to constrain the design space.

For visualization, buckling load versus mass are compared as shown in Figure 7.2. Each layer points are colour categorized and provide a good representation of the limits of the buckling load each layer can achieve with each additional layer. It is an interesting observation that there is a gap between 1 and 2 layer lamina. This was checked with other aspect ratios as well and the same can be seen for it as well. Possible reason for the gap in the buckling range is possibly because when more than 1 layer is present, the strength can get amplified from multiple layers complementing each other that increase the range of design load. However, this is just a hypothesis and has not been proven to be the case.

Table 7.1: Problem dimensions(Case 3)

Geometric Dimensions	
L	0.3 m
D	0.3 m
Material Properties	
E_{11}	90 GPa
E_{22}	7 GPa
ν_12	0.32
$G_{12} = G_{13}$	4.4 GPa
G_{23}	1.8 GPa
h_{tow}	$0.4 \times 10^{-3} m$

Mathematically, the problem can be written as:

$$minimize \quad \mathbf{Vol}([\theta, \mathbf{S}]_L).\mathbf{PF}(\lambda)$$

where

$$[\theta, \mathbf{S}]_L = [\theta_{1L}, \theta_{2L}, \theta_{3L}, S_L] \qquad L = 1,2,3,4$$

$$\mathbf{PF} = max\left(1, \lambda = \frac{0.95 \times P_{cr}}{DL}\right)$$

s.t. constraint

$$\kappa(\theta_{steer}) \leq \kappa_{max}$$

where the input variables are number of layers in the laminate N_L, and the orientation angle at the control points θ. The chosen design path is with 5 control points with symmetry, angle inputs are 3: $\theta = [\theta_1, \theta_2, \theta_3]$. $\mathbf{PF}(\lambda)$ is the penalty function for the buckling load and the curvature constraint κ which is a function θ_{steer}.

The above study provide necessary outlook into the problem to be optimized. The Objective of lightweight design is defined by minimizing the relative volume. Two constraints are considered which are buckling load which is included into the objective as penalty function and the maximum curvature constraint which is applied locally at an element level. The next step is applying the objective, design space and constraints into the optimization framework to solve. Bayesian optimization(BO) and genetic algorithm(GA) are formulated for the problem. Table **7.1** gives the cylinders properties that is to be optimized. This is taken as the test case as this provides a good comparison between the BO results and GA results which was used in the verification of the Particle Swarm Optimization in the work of Wang.et.al[107](refer **Appendix- B**). **Chapter 8** explains the bayesian optimization process in detail and the an extensive design of experiments provides good understanding for selection of parameters required for optimization.

8

Bayesian Optimization

Bayesian optimization(BO) utilizes the Gaussian process model as the surrogate model to predict the output of points and employ this to locate the minima among the selected random samples. As explained in **Chapter 3**, Bayesian optimization is based on the Bayes theorem of probability where the maximum likelihood of global optimum is calculated for each point with the prior knowledge of design space from the surrogate model. The main advantage of surrogate-based optimization is when each iteration of the analysis is computationally expensive. With a limited number of the initial study of the design space, the data is fit with acceptable deviations for prediction. This produces a notable reduction in the time to solve as with each iteration, the feasibility of many points can be predicted and only the point deemed to be best is evaluated. Another advantage is when data from earlier research is present, the model can be fit from it instead of generating its own data for solving.

BO uses acquisition functions for evaluating the likelihood of the points. The acquisition function uses the mean and variance values provided by the gaussian process regression model and calculate scores based on its Acquisition type. If $[X]$ are the points evaluated and fit to Gaussian model and $[X^*]$ are the new points to be evaluated, then the acquisition function's scores can be given as:

$$\text{Scores} = \text{Acq.func}\left(\mathscr{G}\mathscr{P}\left(\mathbf{X}^*, \mathbf{X}\right)\right)$$

where $\mathscr{G}.\mathscr{P}$ is the Gaussian Process model which outputs the mean and variance for the prediction of output of new points X^* with respect to X.

8.1. Design of Experiments

Design of experiments is the term used for the process of optimizing parameters for the experiment to work best. This is required as an initial study as the problem became more complicated and the parameters present progressively increased. For bayesian optimization to perform well, the design variables definition need modifications to suit the general surrogate model optimization. For example, normalizing is always a good practice to reduce the variations in predictions. The effectiveness of the model can be verified with its performance with various metrics which help provide evidence.

8.1.1. Surrogate Model Verification

Prior to employment, the surrogate model is to be verified against a suitable alternative to assess its performance. This is achieved by predicting for test points when trained on a set of separate "training datasets" wherein deviation between prediction and actual value are used to compare. Use of performance metrics is an effective method to compare the different states of the model and evaluate the best. In this instance, the performance of different parameters is compared using R^2 variance score and Mean Squared Error(MSE). R^2 variance or coefficient of determination is commonly used for validation of regression-based model performance evaluation. It is defined as the ratio between the variance explained by the model to the total variance. Mathematical expression is given by Equation **8.1**[52].

$$R^2 = 1 - \frac{\sum_{i=1}^{N_{test}} \left(y_i - \hat{y}_i\right)^2}{\sum_{i=1}^{N_{test}} \left(y_i - \bar{y}_i\right)^2} \tag{8.1}$$

Here, y_i is the true response, $\hat{y}_i$ is the model prediction for the point, N_{test} is the total number of test samples and $\bar{y}_i$ is the mean of true test values. The value of R^2 may vary between 1 and can go to negative infinity. A good model can be characterized through an R^2 greater than 0.8, between 0.5 and 0.8 score informs the presence of observable error in the model and any score less than 0.5 implies weak model prediction and presence of significant error. Values that go to negative signifies the prediction is worse than the average model and should not be used.

MSE is used to understand the error present in the model. MSE is the mean of overall squared prediction error which is shown in Equation **8.2**.

$$MSE = \frac{1}{N_{test}} \sum_{i=1}^{N_{test}} \left(y_i - \hat{y}_i\right)^2 \tag{8.2}$$

A perfect model will have an MSE of 0 and any good model should have close to zero.

Testing Methods

There are many methods given in the literature on the procedure to test the model[52]. Some of them are Jackknife error, bootstrap error and K-fold cross-validation error. K-fold cross-validation error splits the sample points collected into testing and training data. The sample points are split into k subsets of equal size which is defined by the user. The model is trained with all subsets except one used as test set. The process is repeated till each subsets become the test set. If the samples are able to render a good representation of the design space, then the k-fold test will provide a good average R^2 score with minimum variance. In the current body of work, the verification is performed to a 5-fold cross validation. Figure 8.1 gives the pictoral representation of the test.

8.1.2. Sample size

The selection of sample points must provide an acceptable coverage of the vast design space. This ensures that every region in the design space are accounted for. With a limited number of sample space used in the initial population development and optimization as mentioned in **Section 3.2.1**, a geometrical incrementation strategy is employed to identify the suitable sample size. Since this is very processor intensive work, the points tested are taken from a pool of data points in advance and can be reused. Therefore, 2 data pools

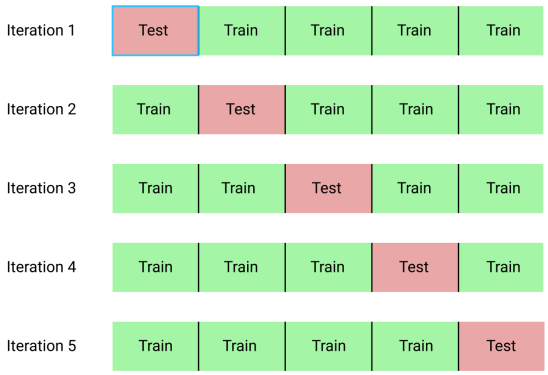

Figure 8.1: K-fold Cross-validation process[92]

of sizes 1000 points and 5000 points are used as reference where the former represents an acceptable low sized reference sample set and latter a large reference set.

The sample size is defined in terms of the number of input variables(IP). An initial sample size of 5 times the IP is taken and iteratively doubled. Since the points are sampled randomly from the data pools provided, to avoid unrepresentative selection of subset for DOE, the 5-fold cross validation is repeated 3 times. This is tested for 2 Design loads: 200kN which is a safe load condition for 2 layers and 500kN which is an extreme case for 3 layers and a lower limit for 4 layers. The total chosen number of sample points are taken such that the training size in the k-fold verification with test train split of 1:4, the training size is equal to the desired number(i.e. n times IP). The test is repeated and the average and variance for R^2, MSE are recorded. And any outputs which violate the manufacturing constraints are reset to a high value(2.5 times the maximum objective value). This ensures that objective values in the design space do not have high discontinuity that are different in the orders of magnitude which is not advisable for fitting. This gives a better representation of the model but is insufficient for prediction.

Table **8.1** shows the different input and output types taken for fitting of model and their performance. It can be observed that, without maximum curvature constraint taken for fitting, the model performs well on 1000 points where as with the constraint, a drastic reduction in performance is observed. It can be concluded that gaussian process model cannot handle buckling penalty function and the maximum curvature constraint behaviour simultaneously as the invalidation of curvature constraint produces a discontinuities in the design space. Hence, the model is fit without the maximum curvature constraint. This is achieved by filtering curvature violating data-points prior to fitting and optimization. It can also be observed that when the absolute X and Y values are used, the model prediction diminishes and does not significantly improve with an increase in training size as tabulated in Table **8.2**. However, when normalized stark difference is observed. This is in line with the previous observations as elaborated in **Section 3.3**. Therefore, the choice is made to normalize the design variables. The input control points angle are converted from [0,90] to [0,1] proportionally. The output objectives values are normalized by dividing it with the maximum value from the training set.

Running the k-fold cross-validation for 1000 data points shows that 40× IP provides accurate results whose average R2 score is 0.89 with a variation of 0.003. It is also seen that 20 × IP also gives adequate results. The same is observed with 5000 data points. However,

Table 8.1: R^2 score, R^2 variance and MSE values for Different Input and Output Variables Types on 1000 Data points pool

	R^2	R^2 var	MSE
Normalized, without manf_cons	0.995	2.5e-6	1.90e-4
Normalized, with manf_cons	0.589	2.5e-2	2.49e-2
Non-Normalized, without manf_cons	0.972	2.3e-5	1.76e+3
Non-Normalized, with manf_cons	0.525	5.6e-3	5.35e+4

Table 8.2: R^2 score and MSE values: 5000 points, 550kN Absolute values

IP times	No	R2 avg	R2var	MSE avg
5	80	0. 098	0.0176	15e3
10	160	0.068	0.11	1.13e3
20	320	0.300	0.011	1.08e4
40	640	0.426	0.0019	9.0e3
80	1280	0.591	1.75e-3	6.0e3
160	2560	0.777	1.73e-3	3.6e3
260(max)	4160	0.868	4.80e-4	2.03e3

as the sample size have increased to 80×IP, a prediction rate of 0.98 is achieved. A minor reduction in the score for a smaller number of training data for 5000 points compared to 1000 points can be attributed to the possible clustering of points over the design space. The initial choice of data points are chosen with Latin Hypercube Sampling(LHS). This ensures that there is a good representation of the whole design space. When the training sample size is taken as a subset of this, there is a chance of overlooking some regions. This idea is shown to be true when we create sample points of training size 20 times Input. The R^2 score can be seen to increase a reasonable level as now chances of missing a wide region has been reduced. The results are tabulated in Table **8.3**,Table **8.7**, Table **8.5** and Table **8.6**.

Table 8.3: R^2 score and MSE values: 1000 points, 550kN Normalized values

IP times	No	R2 avg	R2var	MSE avg	MSE var
5	80	0.287	0.0176	1.8e-7	3.8e-15
10	160	0.568	0.003	1.06e-7	1.36e-1
20	320	0.78	0.003	5.46e-8	1.18e-1
40	640	0.893	0.003	3.22e-8	9.58e-17
50(max)	800	0.921	1.13e-4	2.36e-8	1.24e-17

Table 8.4: R^2 score and MSE values: 1000 points, 200kN Normalized values

IP times	No	R2 avg	R2var	MSE avg	MSE var
5	80	-0.89	5.69	1.6e-5	2.98e-11
10	160	0.57	6.9e-3	3.08e-6	7.98e-13
20	320	0.78	2.89e-3	3.08e-6	7.8e-13
40	640	0.893	7.4e-4	1.83e-6	2.52e-13
50(max)	800	0.91	3.9e-4	1.41e-6	2.95e-14

Table 8.5: R^2 score and MSE values: 5000 points, 550kN Normalized values

IP times	No	R2 avg	R2var	MSE avg	MSE var
5	80	-3.03	24.83	1.11e-7	5.65e-15
10	160	0.680	1.10e-2	5.37e-8	9.20e-17
20	320	0.762	3.58e-3	3.61e-8	9.20e-17
40	640	0.861	7.80e-4	2.09e-8	1.74e–1
80	1280	0.949	7.24e-4	8.49e-9	1.40e-18
160	2560	0.979	5.94e-4	3.48e-9	1.02e-19
250(max)	4000	0.985	1.30e-4	2.31e-9	2.20e-20

Table 8.6: R^2 score and MSE values: 5000 points, 200kN Normalized values

IP times	No	R2 avg	R2var	MSE avg	MSE var
5	80	1.085	21.08	6.16e-6	1.18e-11
10	160	0.603	1.70e-2	3.24e-6	2.57e-12
20	320	0.780	2.15e-3	1.87e-6	6.39e-14
40	640	0.864	2.80e-4	1.17e-6	5.47e-14
80	1280	0.944	8.70e-4	5.15e-7	9.84e-15
160	2560	0.979	4.40e-4	1.32e-6	8.66e-17
250(max)	4000	0.985	2.24e-6	1.35e-7	8.86e-17

Table 8.7: R^2 score and MSE values 20 times Input and 200kN

IP times	No	R2 avg	R2var	MSE avg	MSE var
5	80	0.374	5.69	1.612e-5	4.05e-11
10	160	0.539	0.59	9.433e-6	7.24e-12
20	320	0.861	4e-4	5.200e-6	1.29e-12

8.1.3. Kernel Selection

The choice of the kernel was restricted to RBF, Matern or a combination of constant kernel, RBF, Matern, white and linear. The main choice in kernel selection is the length scale. Length scale defines the neighbouring distance from the point the model will take to predict. The choice of length scale as other parameters depend on the problem. Different combinations were investigated through k-fold cross-validation. The primary metric used to assess performance of the model is the log marginal likelihood(LML) value as shown in equation Equation **3.10**. As mentioned before, LML depicts how well the model predicts taking into account the computational complexity. LML value should be maximized for the set of hyperparameters. The hyperparameters are chosen by analyzing the LML value of the model and confirmed using R^2 variance metrics. It is to be noted that, bayesian optimization itself is a good candidate for hyper-parameter tuning[95] however, since the set of parameters utilized are small and simple, the inherent gradient descent optimizer(Limited Broyden–Fletcher–Goldfarb–Shanno(L-BFGS) algorithm) present in the Gaussian Process model is employed.

With the choice of variables to be normalized, the length-scale bounds are changed between $1e^{-4}$ and $1e1$. Other than length-scale, there are other parameters that are specific to kernels. For example, in matern kernel, another important parameter is ν. If recalled from **Chapter 3** Equation **3.9**, ν is used for dictating the smoothness of the function and the typical values are $\infty, \frac{5}{2}, \frac{3}{2}, \frac{1}{2}$ and 0. This can be visualized as a generalization of the Gaussian RBF kernel as with the choice of ν we can decide between RBF, 1st order exponential and 2nd order. White Kernel is used to learn the distribution of noise that may be present in the outputs and its parameter is the noise level. Table **8.8** shows the different kernels used with their best possible parameters and their corresponding metrics.

From the Table **8.8** it can be gathered that the best kernel for this problem is Matern Kernel with ($\nu = 3/2$) and a dot product of Matern Kernel with ($\nu = 3/2$) and constant kernel. Since Bayesian optimization does not require the exact prediction but only a good estimate, time taken for computing is also to be considered. Taking this into account, the kernel Matern with $\nu = 1.5$ and length scale 1.88 is chosen. It is to be noted that the length scale varies slightly with the different samples as the sample points change. Therefore, an initial optimization is recommended to match the sample points at hand.

8.2. Model Inputs and Outputs

For the surrogate modelling, 2 cases were considered. 1^{st} case is the use of input variables as orientation angles at control points and output as the objective. This is fairly straightforward as the inputs and outputs are already tested and tried. In the 2^{nd} case, the inputs remain the same but the output used for modelling is changed to buckling load from objective function. The reason behind this is that this will give a direct correlation between the design variables and the buckling and the complexity of using penalty functions and manufacturing constraints are removed. The predicted buckling load is used to calculate the penalty function which is multiplied with relative volume to obtain the predicted objective.

With the help of K-fold cross-validation with R^2 and MSE scores, it is observed that in 1^{st} case, even though a more complex objective is used, it is very efficient and the GP model is able to predict with good accuracy. It is important to note that the prediction is

Table 8.8: Kernel parameters and its performance metrics

Kernel with its optimized parameters	**Log Marginal Likelihood(LML)**	R^2 **score**	R^2 **variance**	**Time(seconds)**
RBF($l = 1.06$)	-2362.97	0.949	$4.04\ 10^{-05}$	15.90
Constant($l = 0.85$) . **RBF**($l = 1$)	-1772.16	0.95	$2.96\ 10^{-05}$	18.30
Matern($l = 1.88, \nu = 1.5$)	116.54	0.96	$1.62\ 10^{-05}$	19.225
Constant($l = 1.4$) . **Matern**($l = 2.51, \nu = 1.5$)	153	0.96	$1.86\ 10^{-05}$	22.05
Matern($l = 1.49, \nu = 2.5$)	38.15	0.960	$4.5\ 10^{-05}$	29.46
Matern($l = 5.02, \nu = 0.5$)	-394.28	0.95	$3.9\ 10^{-05}$	21.34
Matern($l = 1.33, \nu = 2.5$)**+ White(noise=0.0195)**	-0.05	0.957	$2.36\ 10^{-05}$	29.77

quite the same between reduced switch variable and normal(15 vs 16, refer **Section 7.1.2**) even though there is a reduction in input variables. We can surmise that the GP model is able to interpret the boolean switch variables effectively. Interestingly, 2^{nd} case is the slowest in the optimization process and the GP model predicting is lower than Case 1. This is attributed to post-processing of the predicted buckling loads leading to larger errors and the slower nature can be attributed to the secondary calculation of relative volume and objective function which even though minor, added up when the data points increase.

8.3. Acquisition functions

The acquisition function utilizes the information from the GP model about the input variables and translates them into scores. The highest score points are chosen for running the actual test as this has the highest chance to be the optimal point or a point from an unexplored region. 3 acquisition functions are focused on here: Probability of improvement(PI), Expected Improvement(EI) and Lower Confidence bound(LCB). The focus is on static state of acquisition function in this thesis.

Probability of Improvement

Probability of Improvement(PI) was first introduced by Kushner[60]. The function measures the maximum probability of a point to improve over its current best-known value. The function is purely exploitative in nature which is a drawback since, this may cause it to ignore points that have good value but high uncertainty. To reduce this effect, a trade-off parameter ξ is introduced in the function. It is formulated as Equation **8.3**. $\Phi()$ is the normal cumulative distribution function. In simple terms, cumulative distributive function(CDF) provides the probability of a function to yield a lower or equal result than that

provided.

$$\begin{aligned} \mathrm{PI}(x,\xi) &= P\left[F_x \geq \mu_{\max} + \xi\right] \\ &= 1 - \Phi\left(\frac{\mu(x) - \left(\mu_{\max} + \xi\right)}{\sigma(x)}\right) \\ &\equiv \left(\frac{\mu(x) - \left(\mu_{\max} + \xi\right)}{\sigma(x)}\right) \end{aligned} \tag{8.3}$$

Expected Improvement

Although PI introduced the parameter ξ, it still is poor in selecting points with a high chance for improvement. Expected Improvement(EI) was proposed to mitigate this[30, 75]. Equation **8.4** measure the expectation of improvement over the model.

$$\mathrm{EI}(\mathbf{x}) = \begin{cases} \left(\mu(\mathbf{x}) - \mu_{\max} - \xi\right)\Phi(Z) + \sigma(\mathbf{x})\phi(Z) & \text{if } \sigma(\mathbf{x}) > 0 \\ 0 & \text{if } \sigma(\mathbf{x}) = 0 \end{cases} \tag{8.4}$$

where

$$Z = \begin{cases} \frac{\mu(\mathbf{x}) - \mu_{\max} - \xi}{\sigma(\mathbf{x})} & \text{if } \sigma(\mathbf{x}) > 0 \\ 0 & \text{if } \sigma(\mathbf{x}) = 0 \end{cases}$$

The first term is the exploitation term and 2nd is the exploration term. Φ and ϕ are cumulative distribution function(CDF) and probability density function(PDF) respectively. Probability density gives the likelihood of function to be near the specific value. ξ is introduced as an exploration weight parameter. The recommended value is about 0.01. Value can be increased to explore further but beyond a certain limit, it transforms to random selection.

Lower/Upper Confidence Bound:

Lower/ Upper confidence bound(LCB or UCB) are used for minimization/maximization problems. It tries to manage exploration-exploitation by being optimistic when faced with uncertainty. Equation **8.5** gives the formulation for LCB which is quite simple in nature. LCBs tend to require fewer iterations to get to the global optima[5, 6].

$$\mathrm{LCB}(x) = \mu_x - \xi\sigma(x) \tag{8.5}$$

8.4. Optimization framework

Bayesian optimization begins with an initial population size which is selected with the LHS sampling criterion. The maximin criterion is chosen in LHS selection criterion where this maximizes the minimum euclidean distance between points. This ensures that the initial population which is used for training possesses a good picture of the design space as the points are spread in the design space. These initial data points and their corresponding calculated objectives are used to fit in the Gaussian regression model. From the design of experiments, the parameters found for the Matern32 kernel(Matern Kernel with $\nu = 3/2$) is used as a starting point. The Gaussian regression fit model is capable of predicting the objective values for the new points with good accuracy and thus the optimization process can be utilized. A specified size of the population is generated using either random or LHS. The acquisition functions take the points and with the help of the GP model, it assess the

points from predicted mean and variance provides scores to each point. The best scored point is evaluated and its actual objective value is then added to the training population of inputs and outputs to be fit. The buckling constraint is present in the objective value as penalty function and the maximum curvature constraint is applied externally and if it is not met, then the point is not considered for the Acquisition function scores. This way, the algorithm does not spend time on infeasible sets. This process is repeated until a maximum number of generations or when the predicted solution has converged over a certain number of generations. The framework is illustrated as a flowchart in Figure 8.2.

For finding the best parameters, the use of pseudo-random sets is considered. With it, the numbers although generated randomly is repeatable with a seed value given to the random function. This helps replicate results that are used to compare the performance when parameters are changed. This is mainly useful for comparision of the acquisition functions. The performance of the acquisition functions is measured by monitoring its convergence to the minimum and the ability to find the best optima among the selected.

With the focus of study on the acquisition functions, the design space for the initial population is kept very coarse and the initial population size is kept at 10 times the inputs which is found to be the minimum requirement for the model to make an adequate prediction. Along with this, as mentioned above, the use of pseudo-random points with the use of random seed value help make generation to generation comparison. Each Acquisition function with varying weights is tested with 50kN and 1000kN design loads. The rate of convergence and the final global optimum are studied. The use of Maximum probability of Improvement(MPI) as the equation suggests, leans only on the mean value to provide. This limits the function to only exploit among the points gathered and does not factor in exploration whereas Expected improvement(EI) and Lower confidence bound have exploration weight factor which can be altered as needed. Figure 8.3 shows the case for EI with 50kN design load. Along with the final objective value and the convergence plot, the relative distance between 2 consecutive input values selected are also shown. When the value gets close to 0, this means the selected value is very close to the previous point. This lets the user know if the solver has found a region in the design space it believes the optimum is present. In this case, since the design space is large, the probability of adjacent iterations lying close to each other is less. The rest of the plots are in **Appendix- A** and data found from them are tabulated in Table **8.9**. The convergence column provides the iteration in which the final objective value is reached. This shows that there is no one best performing Acquisition function with specific weight but it is more dependent on the design load. For example, for a design load of 50kN which is a safe load for 1 laminate solution, the EI and LCB prefer exploitation with EI 0.025 weight and LCB 0.3. Whereas for 1000 kN, which is on the upper limit of the 3 layer lamina, the acquisition functions prefer exploration more with EI weight= 0.1 and LCB =0.4. Therefore, the weights should be considered with the design load in mind.

Since each acquisition function prioritizes different points, the idea proposed by Brochu et.al. is considered which uses all 3 sets of Acquisition function and select the best point from this set[19]. The disadvantage is that this increases the actual calculation by a factor of 3(if all 3 MPI, EI and LCB are considered) which will increase the total time taken considerably. Instead, the use of the acquisition function on a rotation based is attempted. This uses a combination of LCB, EI and PI which is changed with each iteration. Interestingly, this results in a much lower optimum for the 50 kN case but not for the 1000kN case.

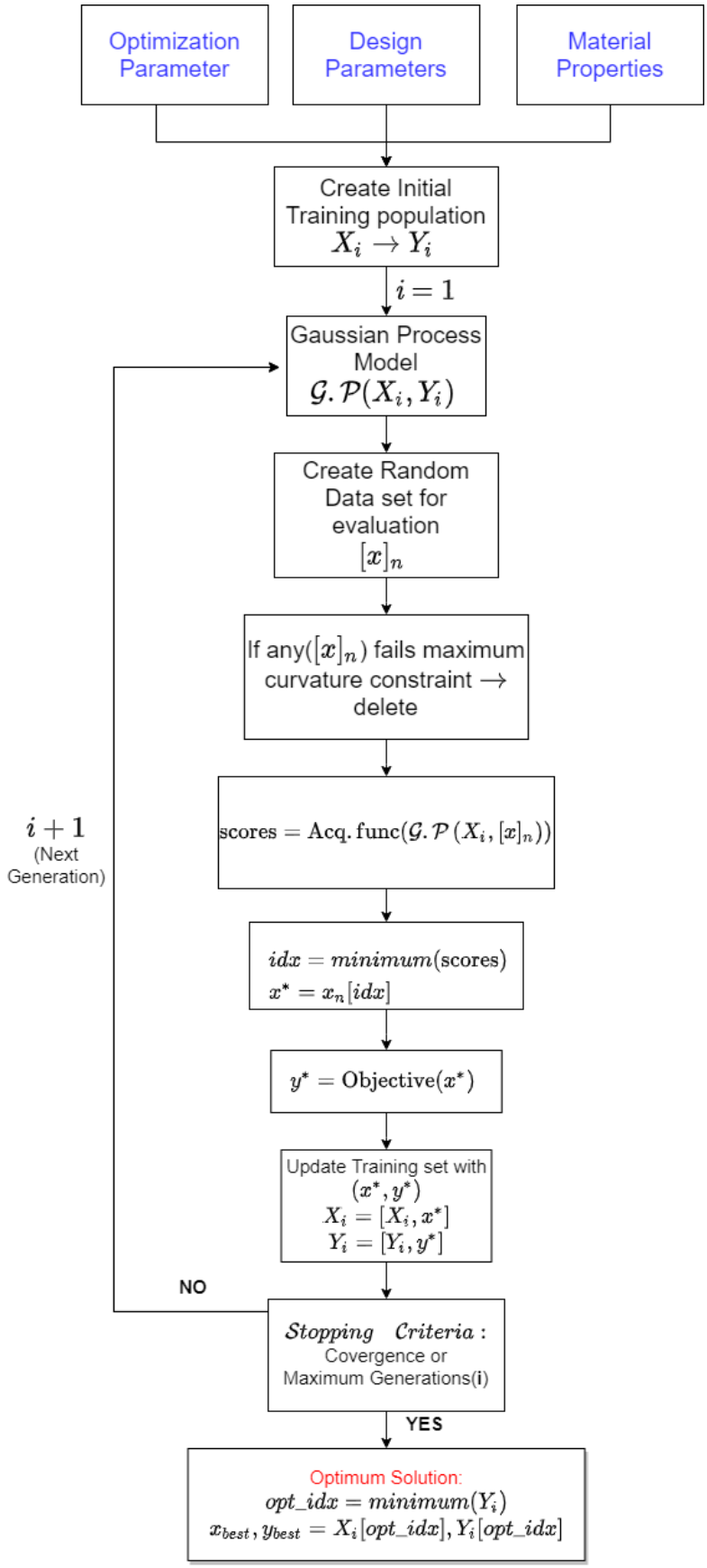

Figure 8.2: Bayesian Optimization Framework

Table 8.9: Acquisition function performance with different weight factors

Acquisition function	Weight	50 kN		1000 kN	
		Objective	Convergence	Objective	Convergence
MPI	-	0.16622	240	0.00397	150
LCB	0.1	0.15602	360	0.00372	155
	0.2	0.15880	325	0.00397	148
	0.3	0.15581	320	0.00389	350
	0.4	0.16325	310	0.00384	290
	0.6	0.16112	310	0.00389	240
	0.8	0.16720	340	0.00389	240
EI	0.01	0.16290	355	0.00406	295
	0.025	0.15601	360	0.00410	310
	0.05	0.16278	380	0.00383	105
	0.1	0.16286	365	0.00372	155
Combo(LCB, PI, EI)	-	0.15410	245	0.00395	380

Table 8.10: Bayesian Optimization Parameters

Parameter	Value
Initial Sample Size	10 times the Input variables
Angle Increment	0.5
Total iterations	400
Tolarance	1e-3
Population size	50
Acquisition function	Combination of EI, LCB and PI
Exploration Weight	EI=0.025,LCB=0.3, PI=NA

This increase and decrease of the objective are attributed to the change in points learnt by the model which affects the prediction. However, as checked over the entire design loads, there is a slight improvement in the final solution overall and hence is selected for the final optimization. Therefore, after all consideration the rotation strategy with acquisition functions with EI(weight = 0.025), LCB(weight = 0.3) and PI is chosen. The resulting optimization results are tabulated in Table **9.2** and further discussed in **Chapter 9**.

8.4.1. Bayesian Optimization Setup

The current framework is created in python BO framework and the acquisition functions are defined in the standalone python script. Other than the standard libraries, "Scikit-Learn(sklearn)" module is used for the GP model fit[21] and "Scikit-Optimize(skopt)" is employed for LHS sampling technique[45].

8.5. Verification with Genetic Algorithm

The genetic algorithm(GA) is a robust optimization tool that has a proven track record of identifying the optimum. As mentioned in **Chapter 3**, GA's robust nature and ability to find the optimum has proven to work well in the variable stiffness design and therefore, is regarded for comparison of results from the BO results. A simple Genetic Algorithm is used

Acquisition function	Weight	Final objective	Plot
EI	**0.1**	**50kN =** Objective= 0.16286 Weight: 0.4160	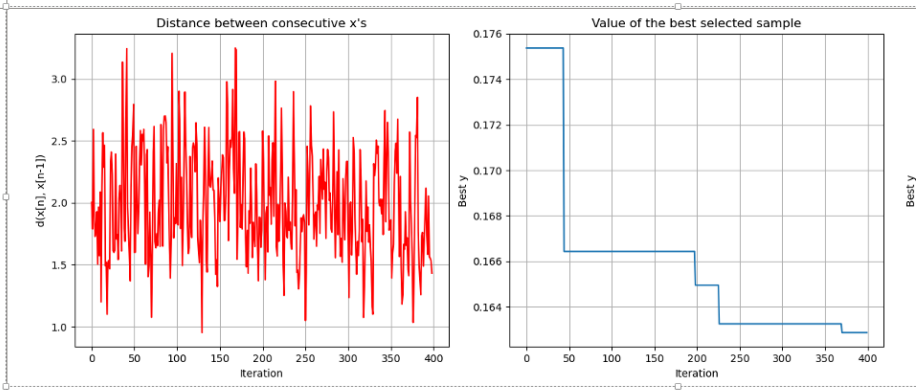
		1000kN= Objective= 0.00372 Weight: 1.37107	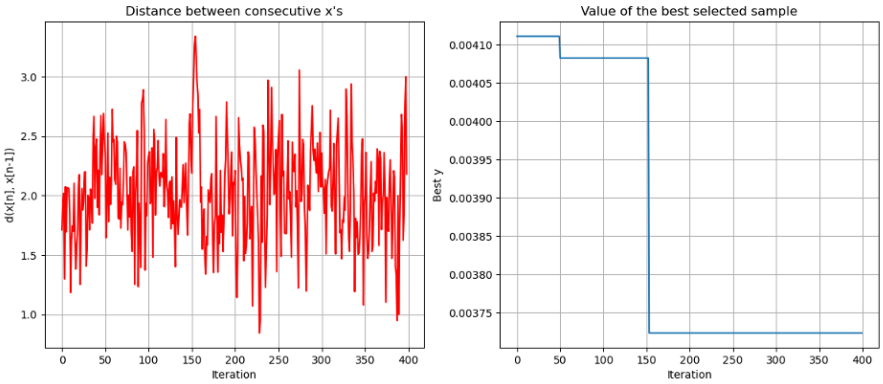
EI	**0.05**	**50kN =** Objective= 0.16278 Weight: 0.4158	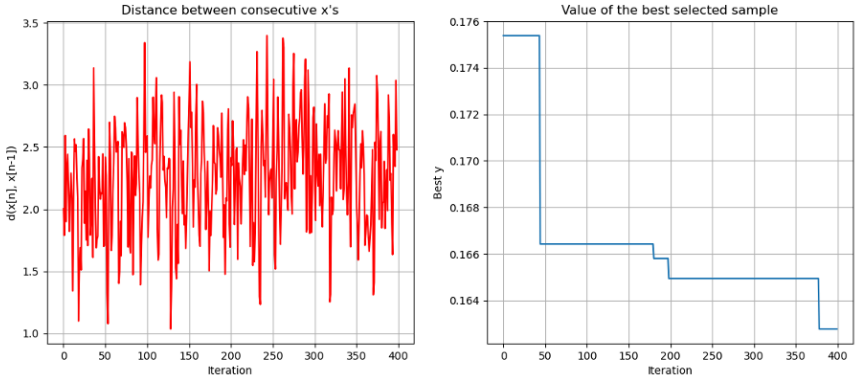
		1000kN= Objective= 0.00383 Weight: 1.4105	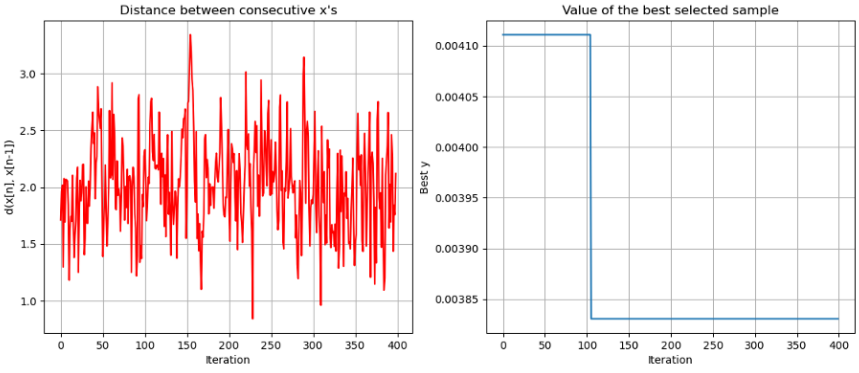

Acquisition function	Weight	Final objective	Plot
EI	**0.025**	**50kN =** Objective= 0.15601 Weight: 0.3972	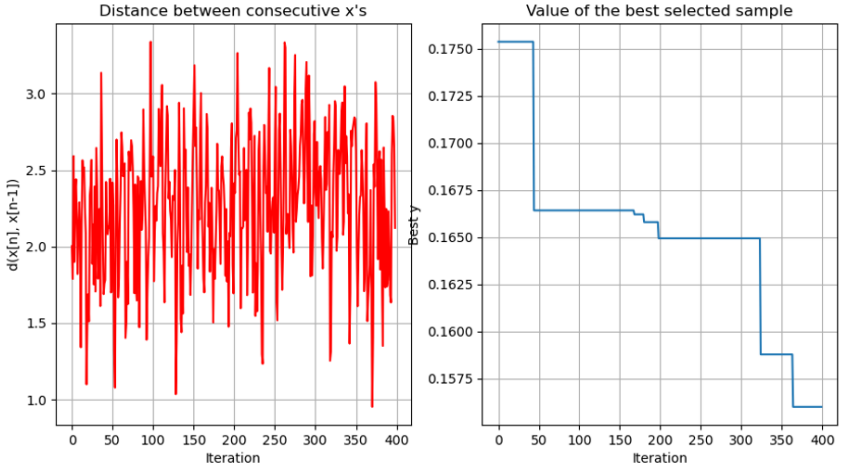
		1000kN= Objective= 0.00410 Weight: 1.5086	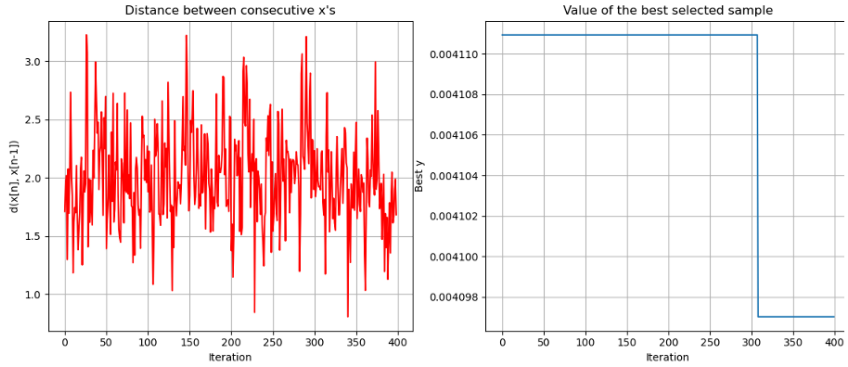
EI	**0.01**	**50kN=** Objective= 0.16290 Weight: 0.3987	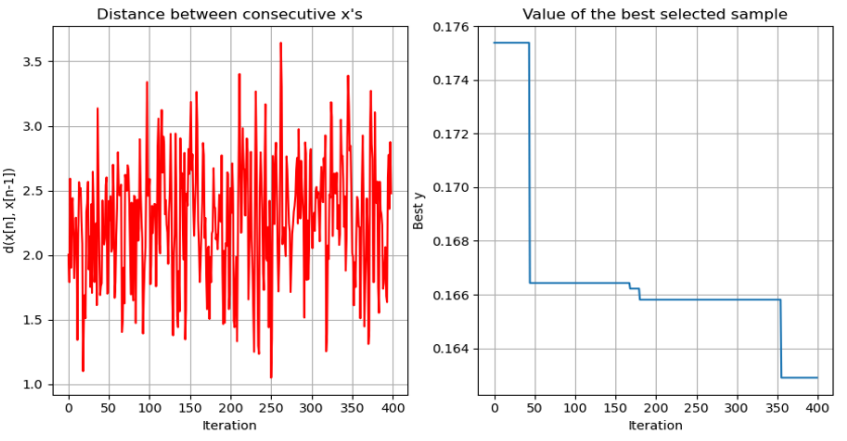
		1000kN= Objective= 0.00406 Weight: 1.4961	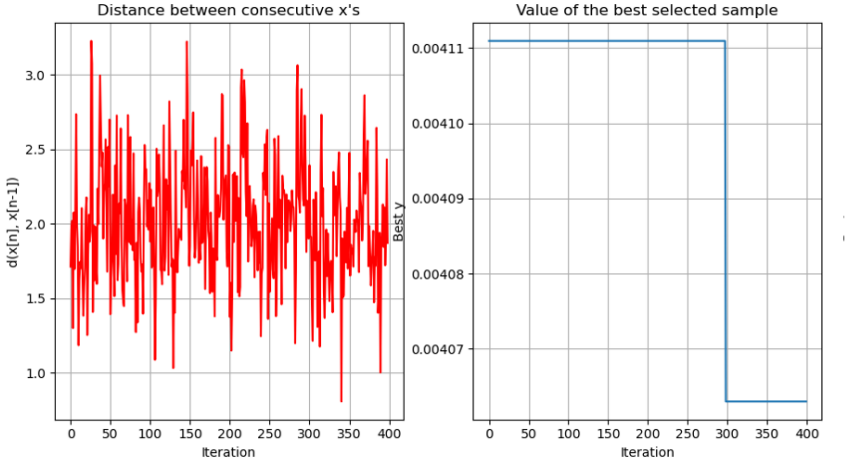

Figure 8.3: Expected improvement performance with different exploration weights

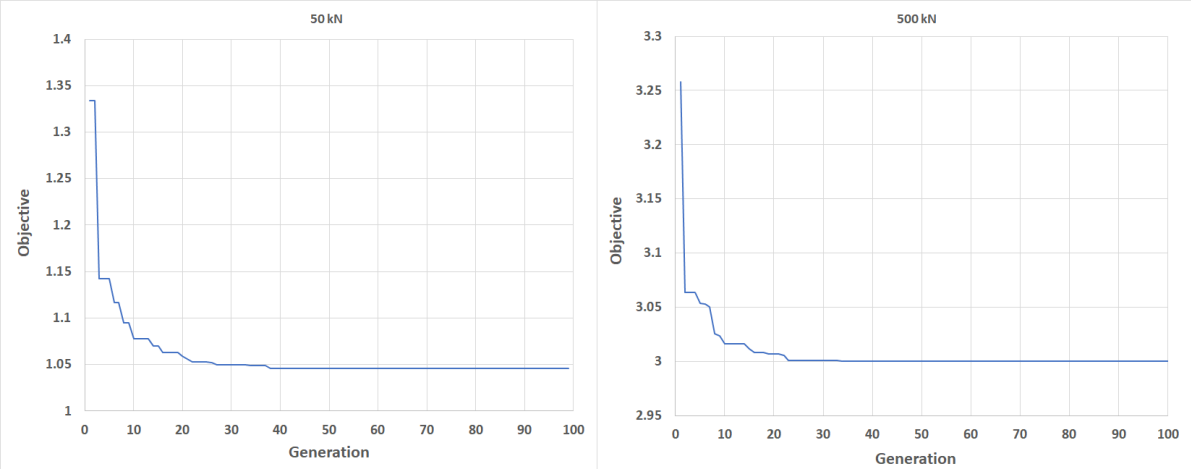

Figure 8.4: GA Convergence to the optimum solution

Table 8.11: Genetic Algorithm Parameters used

Parameters	**Value**
Maximum generation	80
bits size	7
Mutation rate P_m	0.02
Crossover rate P_c	0.1
Elitism	True

here which is implemented in the python module OpenMDAO [37]. As described in the literature study, the decision on the parameter values should be defined according to the current problem.

Discretization: In GA, discretization of the design space of each variable is performed by defining the bits. In this algorithm, design space is divided in the order of binary numbers(2^n). Here, the bit size is taken as 7 for all the steering angle variables. Therefore, the design space is divided into 128(2^7) parts with increments of 0.71 deg.

Population Size: Recommended value for population size is 4 times the bit size. After trial and error with different sizes, 4 times the bit size is found to perform the best.

Mutation rate: The default value for mutation is 0.01. This is increased to 0.02 which resulted in better results. The possible reason for the improvement is the higher number of mutated children which are available which results in better exploration.

Maximum Generations: The convergence is tested with two loading cases: 50kN which is a very safe value for layer 1 and 500kN which is in on the upper limit of 2 layers and lower limit of 3 layers. This means that the minimum weight option is the 2 layer case which is a tricky case for the optimizer. This will help show the versatility of the solver in finding both a straightforward design load and a tricky one. Figure 8.4 shows the convergence to the optimum solution which tells that the convergence occurs about 70 Generations in which is found to be similar for the rest of the load cases. Therefore, a maximum generation of 80 can be taken as the limit.

The whole set of parameters used are given in Table **8.11**.

The results of Bayesian with final chosen acquisition function combo and genetic algorithm and their comparisons are provided in the **Chapter 9**.

9

Results

9.1. SC-BFSC Element Verification

For verification, two cases from the literature were studied and the buckling loads calculated were benchmarked against them. The two case study models were created in SC-BFSC element in python and the model is replicated with the S4R element in ABAQUS. The buckling load was verified with the results in the literature and both S4R and SC-BFSC models were compared in terms of the buckling performance, minimum refinement required, and the computation times. All the models created were meshed with an equal aspect ratio between the 2 directions which also helped compare the results with the number of elements along one side. In this work, n_y, the number of elements along circumference, was taken as the reference as explained in **Section 6.2.2**. Table **9.1** shows the loads calculated from the S4R and SC-BFSC models and the corresponding error percentages with respect to the literature results.

Case 1: Results from SC-BFSC elements showed an error of about -6.036% for CS layup and -7.32% for VS layup. This was even larger in the case of ABAQUS results which was -7.75% for CS layup and -9.05% for the VS layup. The convergence of S4R elements occurred with 102550 elements(n_y=350) and the buckling load was verified with total elements ranging up to 209500(n_y = 500) whereas the SC-BFSC element converged with 1100 elements(n_y = 50) and was tested up to 1755(n_y = 65). It was also observed that the results from S4R elements and SC-BFSC elements were comparable. The slightly higher values in the literature could be attributed to insufficient mesh refinements and the influence of the aspect ratio. Specifically, for S4R elements linear buckling analysis, it was seen that convergence occurs at about 102550 elements which comes to a mesh size of 5.4 mm whereas,

Table 9.1: Load verification error on Case 1 and 2

	Published results	**S4R**	**S4R Error**	**BFSC**	**BFSC Error**
Case 1					
CS-$[\pm 45, 0, 90]_s$	420kN	387.44kN	-7.75%	394.648kN	-6.036 %
VS $[[\pm 45], \pm[60, 15]]_s$	260 kN	236.47kN	-9.05 %	240.97kN	-7.32%
Case 2					
VS VT$[45.4, 86.5, 85.8]_b$	49.576kN	47.013kN	-5.17%	51.1069kN	3.08%
VS CT$[64.1, 58.4, 57.8]_b$	40.304kN	40.1kN	0.5%	42.51kN	5.47%

in the literature, it was stated as 10mm. A higher difference in the variable stiffness for the ABAQUS elements could be attributed to defining the orientation angle of the lamina which was split into constant stiffness regions instead of an element-wise distribution. It must be noted that these results were closer to the non-linear analysis and the experimental results(303kN for CS and 208kN for VS) confirmed that the model implementation was compatible.

Case 2: A similar trend of lower element requirements for SC-BFSC was observed here as well. The convergence for S4R element occurred at 85750(n_y = 350) and was tested up to 212850(n_y = 550). SC-BFSC took 2925 elements(n_y=65) to converge and was tested up to 3975(n_y=75) elements. Case 2 showed closer values to the results from the research with a maximum error of 5.17% in ABAQUS with variable thickness(VS-VT) case and 5.47% in BFSC elements for constant thickness(VS-CT).

Computation time: The total time for an eigen value analysis with BFSC element took an average of 12.1 seconds(for case 1 n_y= 55 and case 2 n_y=65) whereas, with ABAQUS S4R elements it took approximately 900 seconds(case 1 n_y= 350 and case 2 n_y=500). This difference is amplified in the case of large-scale analysis. In reality, with multi-processing available in the ABAQUS software, the computation of S4R can be reduced to about 120 seconds, which is still slower than SC-BFSC models by a factor of 10. However, since the python code used a single core, the comparison is made in the same manner. This showed the distinct advantage of SC-BFSC elements over S4R elements. For SC-BFSC models, the integration points were also studied. As seen in **Chapter 6**, 4 integration points provided sufficient information from the element and any additional number of integration points increased the computation without enhancing results.

9.2. Optimization

9.2.1. Genetic Algorithm

The optimization problem was run for 5 design load cases which were 50kN, 100kN, 200kN, 500kN, and 1000kN. These loads were considered so as to allow for validation against the results obtained by Wang et al.. The results are tabulated in Table **9.3** and the mode shapes predicted by both BFSC and ABAQUS analysis are illustrated in Figure 9.2. The results showed that 100 and 200 kN loads provided a similar weight. This could be attributed to the gap present in design space as explained in the investigation of design space in **Section 7.1.2**.

9.2.2. Bayesian Optimization

The Bayesian optimization problem was first studied and a Design of Experiments was conducted in **Chapter 8** where different kernels, hyperparameters, and the acquisition functions were examined. For the current problem, the optimum settings comprised of Matern32 with a length scale of 1.88 as the kernel chosen for the Gaussian process regression model. The initial population size was 10 times the input variables and a total of 400 iterations were chosen. From the various acquisition functions and their combinations, it was decided that the combination acquisition function which iteratively changes from PI, EI, LCB would give the best blend between convergence rate and computational power. The exploration weights for EI and LCB were 0.025 and 0.3 respectively. The resulting opti-

Table 9.2: Bayesian Optimization results

Design Load	Lamina Design Parameters	Weight(kg)	Buckling Load(kN)
50 kN	[37.58 65.27 57.36]	0.3968	48.147
100 kN	[7.91 1.98 1.98] [5.93 7.91 11.87]	0.7296	162.313
200 kN	[15.82 23.73 27.69] [31.64 35.6 39.56]	0.7336	262.254
500 kN	[23.73 0. 15.82] [47.47 31.64 35.6] [55.38 43.51 43.51]	1.1009	560.725
1000 kN	[35.6 19.78 47.47] [63.29 83.07 47.47] [0. 59.33 47.47]	1.3943	1113.12

Table 9.3: GA results

Design Load	Lamina Design Parameters	Weight(kg)	Buckling Load(kN)
50 kN	[41.8,68.0,49.9]	0.3888	49.99
100 kN	[22.9,22.9,21.4] [40.0,40.0,40.0]	0.7238	288.15
200 kN	[28.3,28.3,27.6] [40.0,40.0,40.0]	0.7238	242.83
500 kN	[49.6,48.9,48.2] [59.8,65.7,63.7] [39.0,39.0,45.4]	1.0861	659.80
1000 kN	[21.7,40.6,36.4] [44.1,83.4,84.1] [24.5,50.5,54.0]	1.2313	1045.76

mum solutions are tabulated in Table **9.2**. The buckling mode shapes of the BO results are shown in Figure 9.1.

9.2.3. Results Comparison

The results show that the BO final optimum solutions were very similar to the results produced by GA. The results and their percentage difference is tabulated in Table **9.4**. Most of the results show that GA provided a better result with every result varying only within 2% except for 1000kN which was about 13% which showed the inherent advantage of GA. However, upon closer inspection, it was seen that with different penalty function factors in the objective function and exploration-exploitation weight in acquisition functions, the results could be much closer. In this case, with rotational acquisition functions and higher population size, close to 80% of total iterations resulted in a solution for 1000kN with a weight of 1.357 kg which is 10.21% greater than that of GA. This shows that further improvement can be found but as it's a heuristic process, the optimum cannot be guaranteed in this case. In the case of GA's, the mutation from the best results allowed the algorithm to proceed in the direction of the global optimum. On the other hand, the sampling criterion chosen here

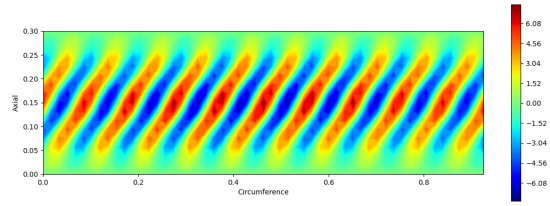

(a) 50kN

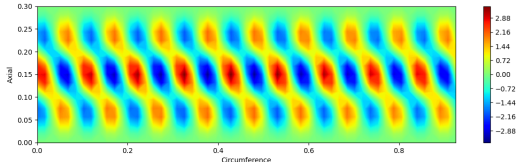

(b) 100kN

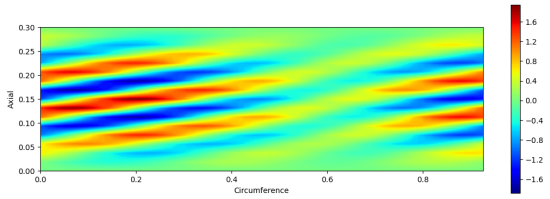

(c) 200kN

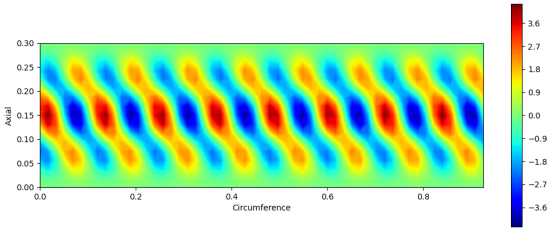

(d) 500kN

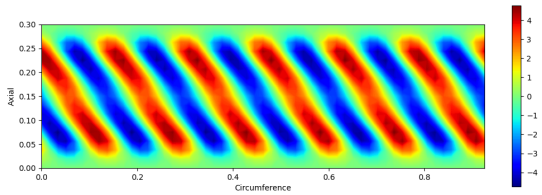

(e) 1000kN

Figure 9.1: BO results mode shapes

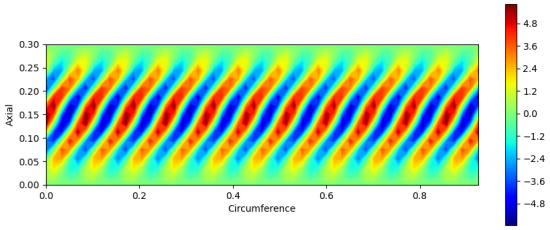

(a) GA result mode shape: 50kN

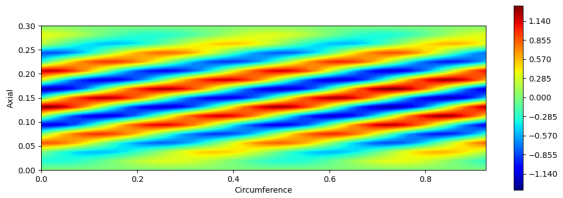

(b) GA result mode shape: 100kN

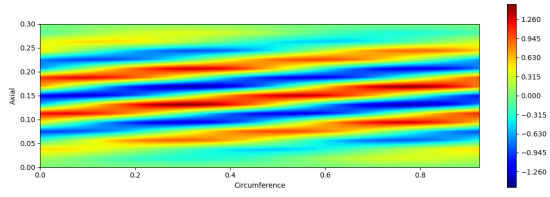

(c) GA result mode shape: 200kN

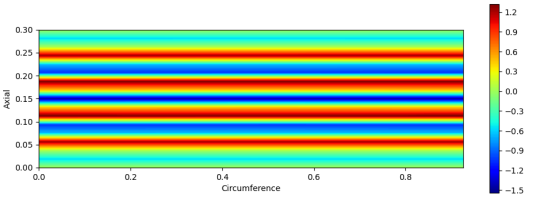

(d) GA result mode shape: 500kN

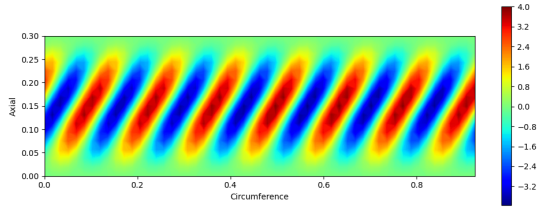

(e) GA result mode shape: 1000kN

Figure 9.2: GA Results mode shape

was static in nature which did not adapt to the previously chosen points and best known points. This is the limitation of the BO in its current state.

On the other hand, the computational time paints a different picture. The GA process required on average 8 hours of computation. A comparable solution to BO is achieved at around 40 generations which took about 4 hours to compute whereas BO took an average of 1.8 hours. In terms of number of runs, GA took 2268 to reach the optimum whereas BO only required 560 which was a reduction by a factor of 4. This is a major advantage in the processing power and time required for the calculation and underlines the capability of BO over GA.

Table 9.4: BO and GA results

Design Load (kN)	**Weight(kg)**		**Percentage Difference (%)**
	BO Total Evaluations=560	**GA Total Evaluations=2268**	
50	0.3968	0.3888	2.06
100	0.7296	0.7238	0.80
200	0.7336	0.7238	1.35
500	1.1009	1.0861	1.36
1000	1.3943	1.2313	13.23

10

Conclusion

Essentially, all models are wrong, some are useful

George Box,1976

This thesis provided an opportunity to journey through the field of design of variable stiffness cylinders and realize a methodology to solve the weight minimization problem with the application of Bayesian optimization. This was initiated with a literature survey on variable stiffness plates and cylinders followed by the creation of the finite element formulation of the single-curvature BFSC element for cylindrical shells with variable stiffness and culminated in the framework for Bayesian optimization of variable stiffness (VS) cylinders. The thesis was split into 2 phases: **i)** Model formulation and implementation of the single-curvature-BFSC model for variable stiffness cylinders; **ii)** the Bayesian optimization framework. And as the quote from George Box, the results tells that even though the models are approximations of the real world solution, it has been very useful and efficient for optimization of the VS cylinder designs.

The foundation of this thesis is formulated by the initially posed research objective that is repeated here for the sake of convenience:

> "Develop a framework for a lightweight design using Bayesian optimization and apply it to the problem of variable stiffness cylinders, finding the minimum weight for a given geometry and design load levels."

To achieve this objective, a set of research questions were formulated and were sequentially explored to satisfaction.

10.0.1. How to realize an accurate and yet efficient finite element model for variable stiffness cylindrical shells?

To improve the computational efficiency, a finite element based on 'Bögner-Fox-Schmit-Castro(BFSC)' [27] was developed. The finite element is modified to introduce variable stiffness and the kinematics due to the cylindrical shell curvature and is referred to as **Single Curvature-BFSC(SC-BFSC)** element. The implementation is made available as a

Python module called "BFSCCylinder". The variable stiffness is applied with control points defined along the cylinder surface. The variation of stiffness is limited to the axial direction mainly due to manufacturing constraints, and it is clear from previous research that the most improvement of the load distribution is achieved through axial variation. The linear buckling constraint that is used in the optimization is then successfully calculated using eigen value analysis of the assembled model.

The SC-BFSC model was verified against 2 case studies where the convergence and the accuracy were tested against models based on Abaqus general-purpose shell elements S4R, with linear displacement interpolation and reduced integration. Case 1 is the buckling and vibration analysis of VS composite cylinder by Bisagni and Labans[61], who modeled and experimentally validated the linear and nonlinear buckling behavior. Although there is a noticeable difference in the linear buckling analysis, the likely cause for this is the different mesh convergence strategies employed. While the convergence study within this thesis yielded for an equal aspect ratio element of size 5.4 mm, the literature presented the mesh convergence at 10 mm. However, the element ratio and laminate theory used in the research were unclear. Additionally, the results showed conformity with the nonlinear behavior and experimental results. A higher difference in the case of VS laminate can be seen which can be attributed to the region-wise assignment of orientation rather than individual definition at each integration point and interpolating over the element.

Case 2 is the research by Z.Wang et.al.[106] which used reliability-based design optimization (RBDO) for variable stiffness. The results between the S4R and SC-BFSC models against the literature showed a difference in results being about 5% for the mesh refinement adopted in the RBDO scheme.

The computation time taken for the result is also observed. It is found that the SC-BFSC finite element model performs faster than ABAQUS by a factor of 50, using a single processor for both the SC-BFSC model and ABAQUS. Enabling ABAQUS-multi-processing reduced the efficiency gain of the SC-BFSC to a factor of 10. These studies showed the superiority of the SC-BFSC element to accurately represent the variable stiffness and shell kinematics of the investigated cylindrical shells and also showcases the potential for improvement available if multi-processing is applied to the SC-BFSC formulation. Therefore, the two cases verify the SC-BFSC model formulation and therefore justify its utilization within the Bayesian optimization framework.

10.0.2. How to tackle the objective design obstacle?

After examining different fibre steering paths with control points distributed along the cylinder axis, it was decided to employ 5 control points with symmetry about axial mid cross-section. This number of control points provides a good balance between high tailoring potential and limited number of design variables, specifically 3 steering variables per layer in this case.

From the study, balanced laminate designs were assumed. The fibre orientation at the control points was limited between 0° and 90° degrees and allowed to change in steps of 0.5° degrees. The thickness variation and maximum curvature constraints are two factors that must be considered when designing VS laminates. The thickness variation is calculated based on the local steering angle. The maximum curvature, or minimum steering angle constraint, is applied element-wise locally, by transforming the curvature constraint into a maximum steering angle that is treated as a local constraint to the model.

The optimizations provided data for a greater understanding of the design space by mapping how the mass changes for different buckling loads. A gap in the design space was observed between 1 and 2 layers, even with cylinders of different aspect ratios. A possible reason for the gap can be due to 2 laminates complementing each other resulting in the higher upper limit of the design .

With the design objective being the weight minimization for given design buckling loads, the buckling load limit constraint is introduced by means of penalty functions in addition to the objective. The penalty function is based on the square-law which provides a continuous function over the design load boundary. An additional factor is added to enhance the sensitivity towards infeasible loads.

10.0.3. What are the performance outcomes from Bayesian optimization?

For an efficient general problem, it is desired that the optimizer should have the ability to choose the number of required layers for a given design load, meaning that the optimizer should simultaneously decide on the number of layers as well as the variable stiffness orientation of each layer, controlled by 3 fibre orientation angle variables located at the control points. To achieve this in the Bayesian optimization framework, Boolean design variables were introduced alongside the fibre orientation angle variables, allowing the optimizer to switch each layer on (1) or off (0) as it pleases.

The Bayesian optimization (BO) framework is created and implemented in Python. Three different inputs and outputs for the problem definitions were considered. After testing them, it was found that the use of 15 input variables ($[\theta_{11},\theta_{12},\theta_{13}]$, $[\theta_{21},\theta_{22},\theta_{23},S_2]$, $[\theta_{31},\theta_{32},\theta_{33},S_3]$, $[\theta_{41},\theta_{42},\theta_{33},S_4]$) and the objective function as the output was the choice that showed the best results. An interesting observation was a reduction in the performance when the buckling load was used as the output for the Gaussian process (GP) model and the predicted load was used to calculate the objective. This was the consequence of additional calculations required to reach the predicted objective value from the buckling load prediction, which caused higher computation time with each iteration. An exhaustive Design of Experiments study on the GP model and hyper-parameters of the Bayesian optimization were conducted, including the investigation of different kernels for the GP model and their respective parameters, initial sample space and population size. Two test data of sizes 1000 and 5000 were used for this. The selection of kernels was based on the maximum Log-likelihood value and the total computational time. Upon investigation, the Matern32 kernel was found to be best suited for the problem at hand. The selection of the initial sample size was based on the accuracy required by the GP model. The accuracy and error calculation was looked into with the help of R^2 variance score and Mean Squared Error (MSE). These two metrics provide a good representation of how the model performs. The sample size was defined as a factor of input variables that would help with a more generic representation of the parameters for future use. With both the test data, it was seen that 10 times the input provides a good prediction accuracy.

With the GP model and initial sample size decided, 3 acquisition functions were studied: Probability of improvement; Expected Improvement and; Lower Confidence Bound. Each function's characteristics and exploration-exploitation weights were studied. Individually, LCB was found to be the most efficient. However, an overall improvement is found when the acquisition functions are used on a rotational basis with each iteration. The convergence is not consistent with BO as with GA. This is due to the fact that although the

sample points selection has a good distribution over the design space, it is random in nature. But with 400 generations, it is seen to reach an optimum value or a value close to the optimum. This is with an initial sample size of 10 times the input variables which amounts to 160. Therefore, the total number of linear buckling calculations performed is 560.

The genetic algorithm (GA) optimization was achieved with the Python module "OpenMDAO", which employs the simple GA algorithm. The parameters for the GA solver were selected through trial and error and a convergence analysis showed that the solution converged to an optimum within 80 generations, amounting to a total number of 2800 individual evaluations.

When comparing both the results, the BO provided a solution heavier than the GA solution with a larger maximum deflection of 2% for all the cases except 1000kN. For the 1000kN case, the result showed that BO provides an optimum which is 13% heavier than the GA solution. With a population size increase, this can be reduced to 10%. This showcased the narrow difference in the final solution obtained by the two optimization strategies. It shows that GA's mutation of the best samples allowed it to explore further in the case of 1000 kN, which has proved to be advantageous. The results showed that BO can compete with GA and can provide proximate results apart from few extreme cases,where the parameters have to be tuned to match the specific case. The superiority of the weight can be attributed to the exploitation ability of GA with the mutation. However, the computation time required to converge to the optimum solution is significantly larger. Since the GA required the calculation of a larger number of linear buckling analysis, the average time was about 9 hours. Whereas BO required an average of 2 hours to complete the same optimization. It was noted that a portion of time was taken up by the GP model fit function and as the data points increase, fit and prediction time increases by a small amount.

With the above results, it can be concluded that BO is a very simple yet capable optimization tool that can be used in the field of lightweight structural design and optimization. As the world is moving towards data-centric analyses, the use of previous data to obtain faster results proves to be an exceedingly efficient method to solve complex problems. BO with the help of the surrogate model achieves this with its stochastic approach to the problem and therefore can be highly effective. Thus, the second phase of the thesis has yielded a promising scope for further exploration.

10.1. Recommendations

The two goals of the thesis: creating the framework for Bayesian optimization and using SC-BFSC element for VS cylinder model have been successfully completed. However, the examination of the results illuminate the limitations of the same methods. These limitations can be explored through future works in line with a set of recommendations based on the observations during the course of this thesis.

The Bayesian optimization is seen to perform very well with the current linear buckling analysis and weight minimization. However, as with all optimizations, its performance changes from problem to problem. Therefore the feasibility must be looked into when nonlinear analysis is implemented.

The use of adaptive sampling: a modern sampling criterion which selects points based on the partly selected set of points may bring significant improvement on the effectiveness

of BO depending on the problem. Additionally, some points found in the training data are repeated into the test population. This may lead the optimizer to select the same point due to zero variance, which is obviously inefficient. A filtering process can be introduced to avoid such points.

Currently, the SC-BFSC model is utilized only for linear buckling constraints. Although linear buckling can provide the fundamental solution, nonlinear analysis and introduction of geometric imperfections to the cylinder would be the next step in this regard of assessing stability, aiming to obtain designs that also tailor the post-buckling response. The successful formulation herein demonstrated can be extended to develop the SC-BFSC element further, for example to include initial post-buckling analysis using a displacement-based Koiter's method [27], which could then be compared with a Newton-Raphson-based nonlinear post buckling analysis. The expected outcome from introduction of geometric imperfections are to find out whether the geometric sensitivity of the cylinder can be reduced with variable angle tow and by what measure. Moreover, strength-related failure modes, such as those calculated using Hashin's failure criteria should be included, especially when entering the post-buckling regime. Such expanded scope would further promote and support the manufacturing and testing of compelling variable stiffness designs.

With successful verification, the linear buckling model can be extended to bending and/or circumferential loading. This will require the fibre variation in circumferential direction as well. This naturally increases the design variables and hence, the effectiveness of the model should be investigated further.

A

Appendix-A

Tabulation and plot for the different Acquisition functions and their final optimum

Acquisition function	Weight	Final objective	Plot
EI	**0.1**	**50kN =** Objective=0.16286 Weight: 0.4160	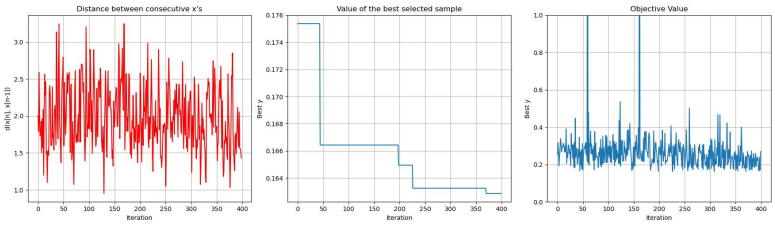
		1000kN= Objective=0.00372 Weight: 1.37107	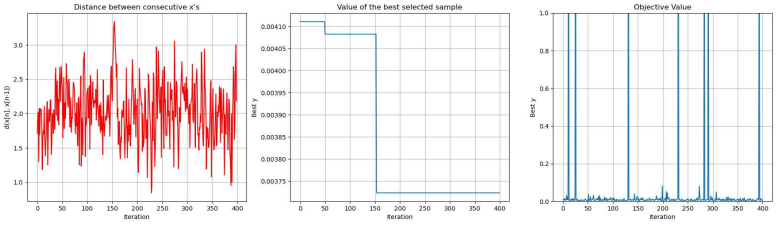
EI	**0.05**	**50kN =** Objective=0.16278 Weight: 0.4158	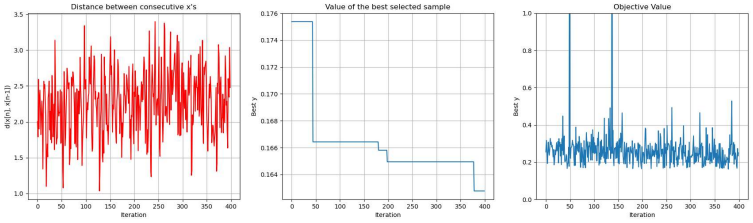
		1000kN= Objective=0.00383 Weight: 1.4105	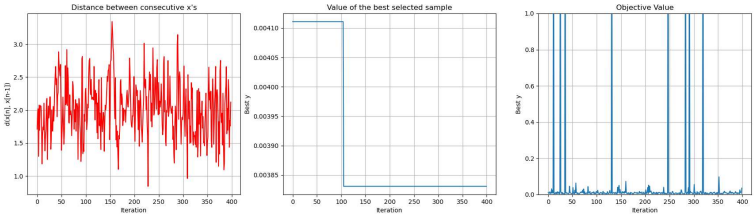

EI	**0.025**	**50kN =** Objective=0.15601 Weight: 0.3972	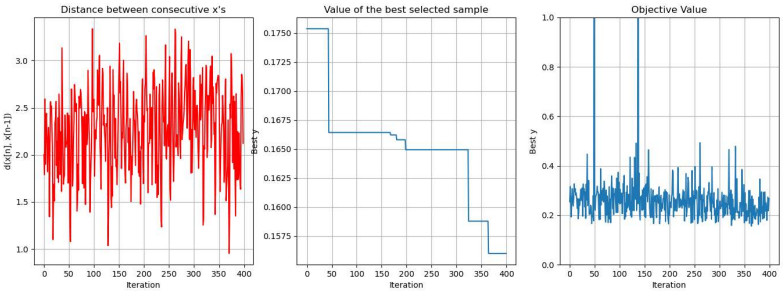
		1000kN= Objective=0.00410 Weight: 1.5086	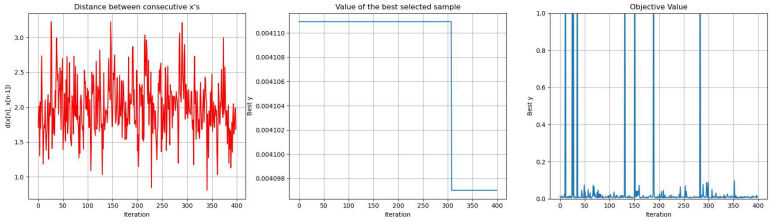
EI	**0.01**	**50kN=** Objective=0.16290 Weight: 0.3987	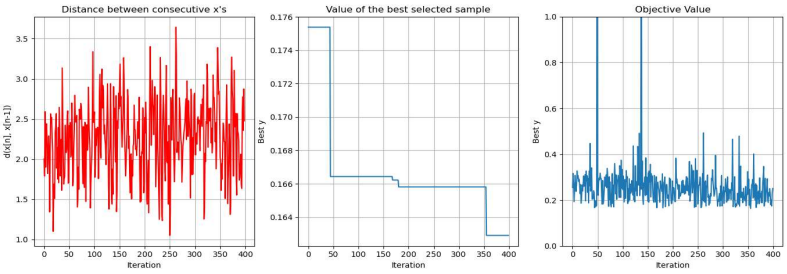
		1000kN= Objective=0.00406 Weight: 1.4961	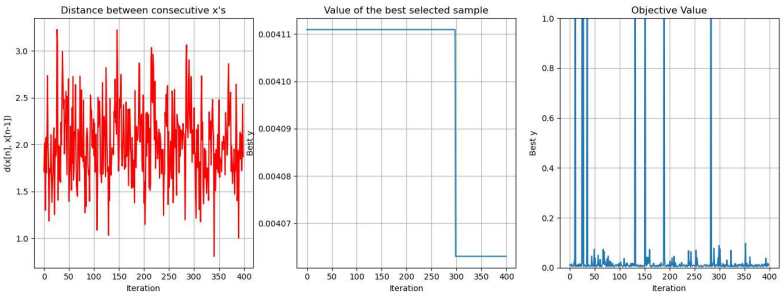

LCB	**0.05**	**50kN=** Objective=0.16019 Weight: 0.4092 **1000kN=** Objective=0.00397 Weight: 1.3675	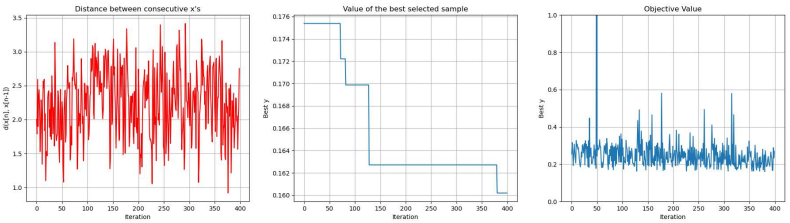 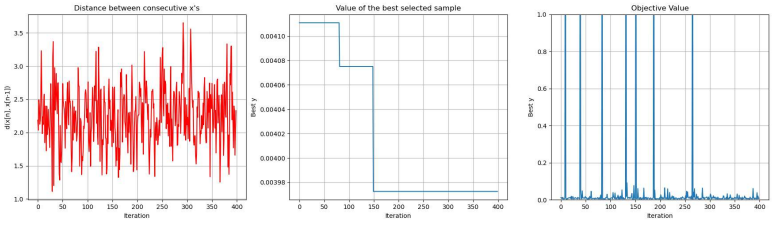
LCB	**0.1**	**50kN=** Objective=0.15602 Weight: 0.3973 **1000kN=** Objective=0.00372 Weight: 1.371	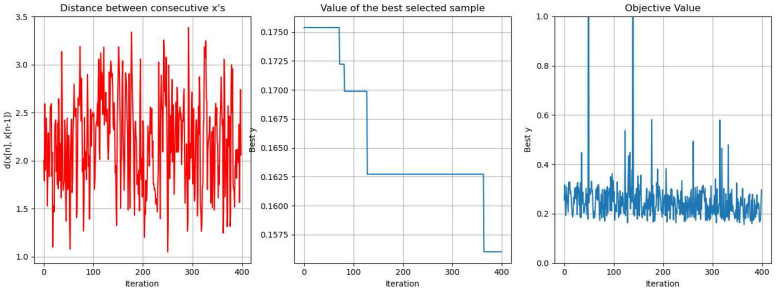 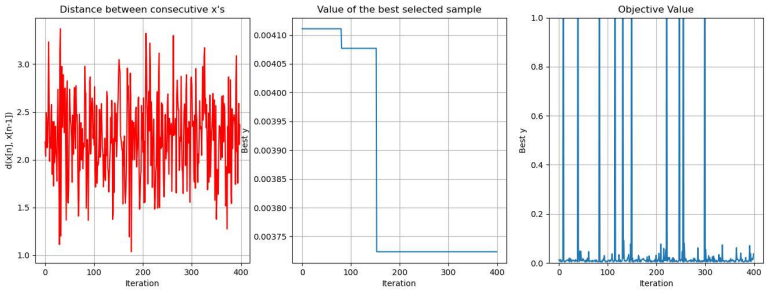

	0.2	**50kN=** Objective=0.15880 Weight: 0.4008	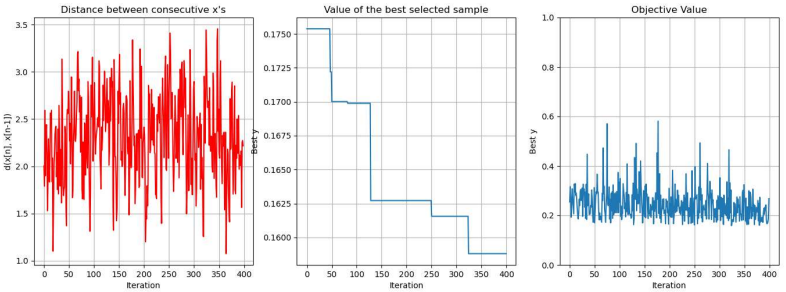
		1000kN= Objective=0.00397 Weight: 1.3675	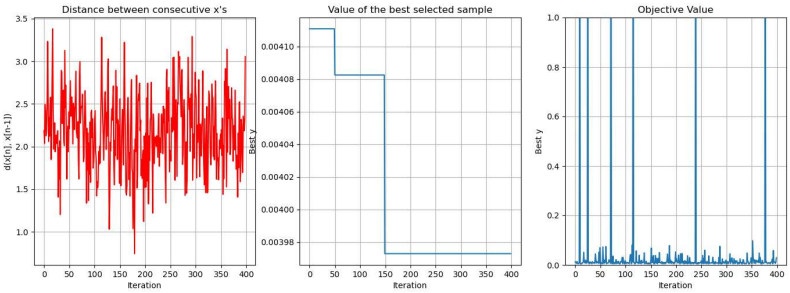
	0.3	**50kN=** Objective=0.15881 Weight: 0.4008	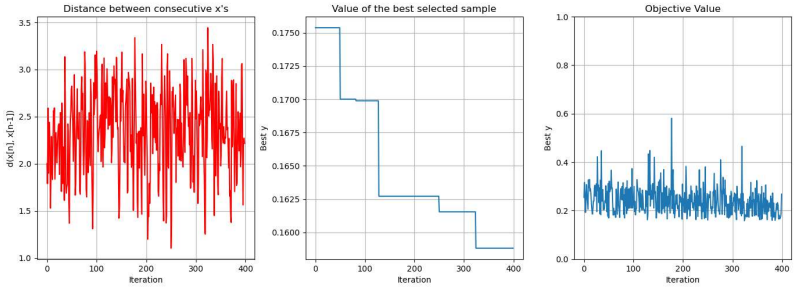
		1000kN= Objective=0.00389 Weight: 1.4293	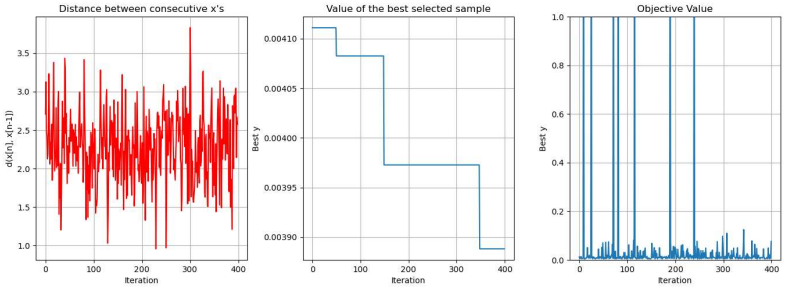

	0.4	**50kN=** Objective=0.16325 Weight: 0.4171	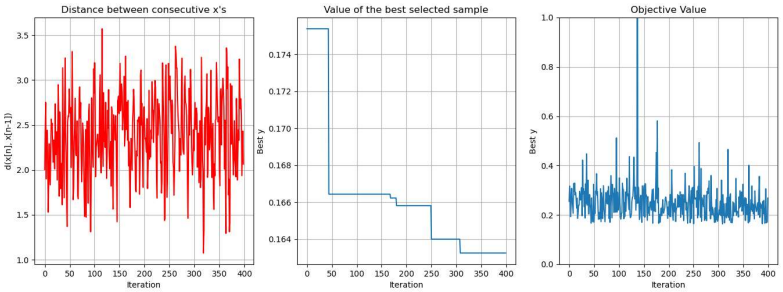
		1000kN= Objective=0.00384 Weight: 1.4145	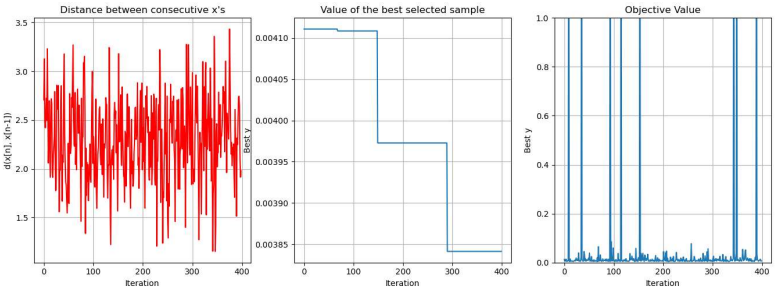
	0.8	**50kN=** Objective=0.16720 Weight: 0.4271	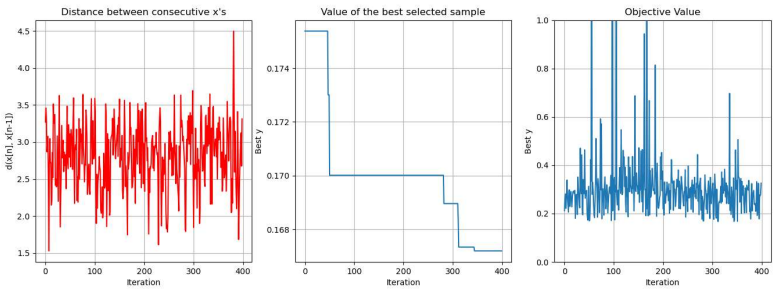
		1000kN= Objective=0.00389 Weight: 1.4201	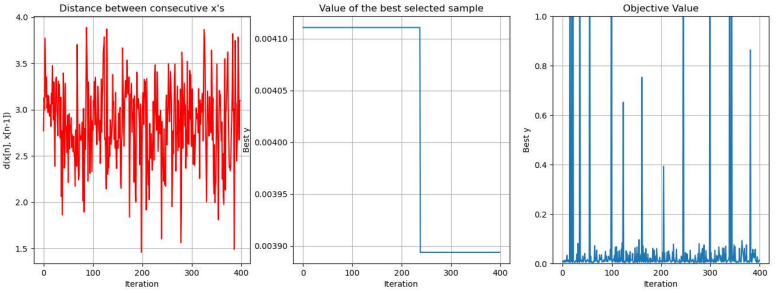

	0.6	**50kN=** Objective=0.16112 Weight: 0.4116 **1000kN=** Objective=0.00389 Weight: 1.4201	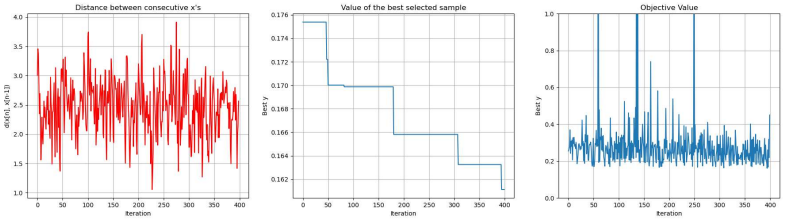 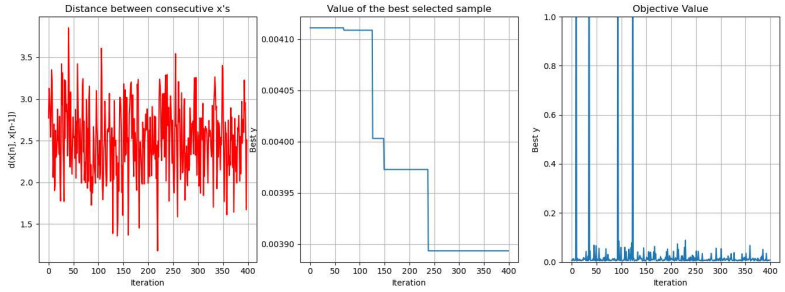
MPI		**50kN=** Objective=0.16622 Weight: 0.4246 **1000kN=** Objective=0.00397 Weight: 1.3675	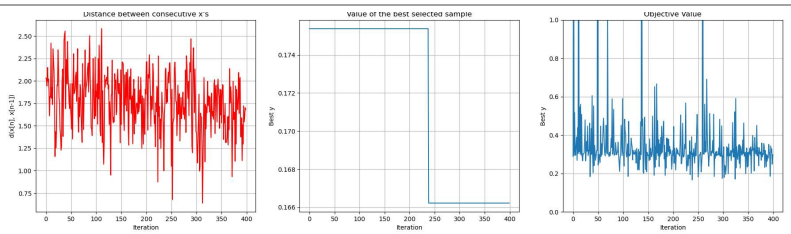 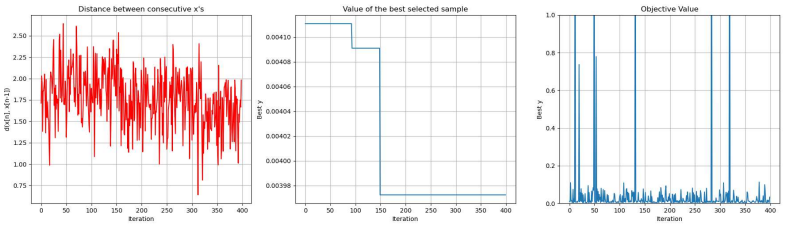

Combo-(LCB, EI, MPI,EI,LCB) n times		**50kN=** Objective=0.16286 Weight: 0.4161 **1000kN=** Objective=0.00397 Weight: 1.3675	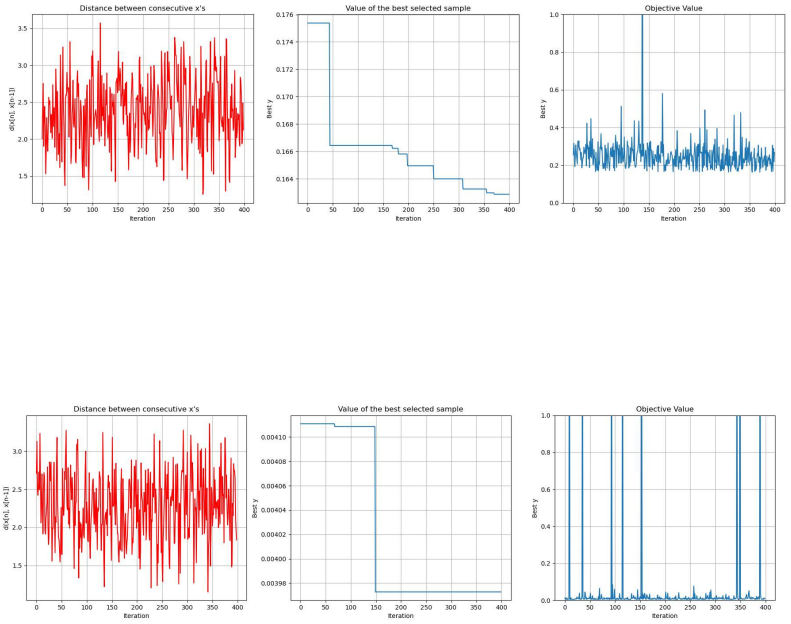
Combo (LCB, MPI, EI) n times		**50kN=** Objective=0.00397 Weight: 1.3675 **1000kN=** Objective=0.16112 Weight: 0.4116	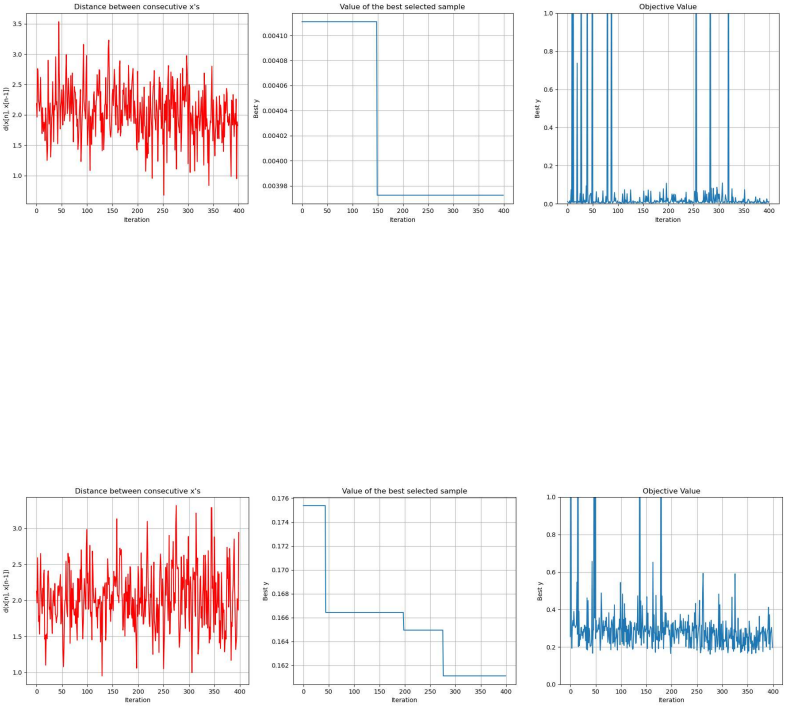

B

Appendix-B

Structural and Multidisciplinary Optimization manuscript No.
(will be inserted by the editor)

Lightweight design of variable-angle filament-wound cylinders combining Kriging-based metamodels with particle swarm optimization

Zhihua Wang* · **José Humberto S. Almeida Jr.*‡** · **Aravind Ashok** · **Zhonglai Wang‡** · **Saullo G. P. Castro*‡**

Submitted: 22 April 2021
Re-submitted after first review: 16 September 2021

Abstract Variable-angle filament-wound (VAFW) cylinders are herein optimized for minimum mass under manufacturing constraints, and for various design loads. A design parameterization based on a second-order polynomial variation of the tow winding angle along the axial direction of the cylinders is utilized to explore the nonlinear steering-thickness dependency in VAFW structures, whereby the thickness becomes a function of the filament steering angle. Particle swarm optimization coupled with three Kriging-based metamodels is used to find the optimum designs. A single-curvature Bogner-Fox-Schmit-Castro finite element is formulated to accurately and efficiently represent the variable-stiffness properties of the shells, and verifications are performed using a general-purpose plate element. Alongside the main optimization studies, a vast analysis of the design space is performed using the metamodels, showing a gap in the design space for the buckling strength that is confirmed by genetic algorithm optimizations. Extreme lightweight whilst buckling-resistant designs are reached, along with non-conventional optimum layouts thanks to the high degree of thickness build-up tailoring.

Keywords Design · lightweight · Mass minimization · Metamodeling · Variable stiffness · variable-angle · filament winding · buckling

* Equal contribution
‡ Corresponding authors
Zhihua Wang
Faculty of Aerospace Engineering, Delft University of Technology, Delft, The Netherlands & School of Mechanical and Electrical Engineering, University of Electronic Science and Technology of China, Chengdu, China & Chengdu Aircraft Industrial Group Co. Ltd, Chengdu, China
ORCID: 0000-0001-8930-4817
E-mail: zhwanglbb@gmail.com

José Humberto S. Almeida Jr.
Department of Mechanical Engineering, Aalto University, Espoo, Finland &
Advanced Composites Research Group, School of Mechanical and Aerospace Engineering, Queen's University Belfast, UK
ORCID: 0000-0002-9408-7674
E-mail: humberto.almeida@aalto.fi

Aravind Ashok
Faculty of Aerospace Engineering, Delft University of Technology, Delft, The Netherlands
ORCID: 0000-0002-6587-3107
E-mail: A.Ashok-2@student.tudelft.nl

Zhonglai Wang
School of Mechanical and Electrical Engineering, University of Electronic Science and Technology of China, Chengdu, China
ORCID: 0000-0002-1708-4197
E-mail: wzhonglai@uestc.edu.cn

Saullo G. P. Castro
Faculty of Aerospace Engineering, Delft University of Technology, Delft, The Netherlands
ORCID: 0000-0001-9711-0991
E-mail: S.G.P.Castro@tudelft.nl

1 Introduction

The development of new concepts for lightweight structures has been overwhelmingly exploited in several fields, mainly in aeronautical and aerospace structures, to comply with Green Aviation for enhancing fuel efficiency and decrease aviation emissions towards reaching carbon-neutral air transportation. A practical and direct manner to improve the energy efficiency and reduce the fuel consumption of an aircraft is by reducing the mass of its components [1], achieving carbon footprint reduction and better flight performance. Both aeronautical and space industries have been continuously develop-

Bibliography

[1] Mostafa M Abdalla and I Introduction. Optimization of Variable-Stiffness Panels for Maximum Buckling Load Using Lamination Parameters. 48(1), 2010. doi: 10.2514/1.42490.

[2] Milton Abramowitz and Irene Stegun. *Handbook of Mathematical Functions*. Dover Publications, 1965.

[3] Patrick B. Stickler Adriana W. Blom and Zafer Gürdal. Optimization of a composite cylinder under bending by tailoring stiffness properties in circumferential direction, March 2010.

[4] Mazen Albazzan, Ramy Harik, Brian Tatting, Zafer Gurdal, Adriana Blom-Schieber, Mostafa Rassaian, and Steven P. Wanthal. Optimization of cylinders with holes under bending using nonconventional laminates. In *2018 AIAA/ASCE/AHS/ASC Structures, Structural Dynamics, and Materials Conference*. American Institute of Aeronautics and Astronautics, January 2018. doi: 10.2514/6.2018-1377.

[5] Francesco Archetti and Antonio Candelieri. *Bayesian Optimization and Data Science*. Springer International Publishing, 2019. doi: 10.1007/978-3-030-24494-1. URL https://doi.org/10.1007%2F978-3-030-24494-1.

[6] Peter Auer. Using confidence bounds for exploitation-exploration trade-offs. *J. Mach. Learn. Res.*, 3(null):397–422, March 2003. ISSN 1532-4435.

[7] J. E. Baker. Adaptive selection methods for genetic algorithms. In *ICGA*, 1985.

[8] J.E. Baker. Reducing bias and inefficiency in the selection algorithm. Hillsdale, N.J. : L. Erlhaum Associates, 1987., Jan 1987. URL https://agris.fao.org/agris-search/search.do?recordID=US201301782152.

[9] TED BELYTSCHKO. The finite element method: Linear static and dynamic finite element analysis: Thomas j. r. hughes. *Computer-Aided Civil and Infrastructure Engineering*, 4(3):245–246, 1989. doi: https://doi.org/10.1111/j.1467-8667.1989.tb00025.x. URL https://onlinelibrary.wiley.com/doi/abs/10.1111/j.1467-8667.1989.tb00025.x.

[10] M. A. Bessa and S. Pellegrino. Design of ultra-thin shell structures in the stochastic post-buckling range using bayesian machine learning and optimization. *International Journal of Solids and Structures*, pages 174–188, 2018. ISSN 00207683. doi: 10.1016/j.ijsolstr.2018.01.035.

[11] Miguel A Bessa and Sergio Pellegrino. Design of ultra-thin composite deployable shell structures through machine learning. *Proceedings of IASS Annual Symposia*, (16):1–8, 2017. ISSN 2518-6582. URL https://www.ingentaconnect.com/content/iass/piass/2017/00002017/00000016/art00006.

[12] Miguel A. Bessa, Piotr Glowacki, and Michael Houlder. Bayesian machine learning in metamaterial design: Fragile becomes supercompressible. *Advanced Materials*, 31 (48):1904845. doi: https://doi.org/10.1002/adma.201904845.

[13] Sherrill B. Biggers and Sundar Srinivasan. Compression buckling response of tailored rectangular composite plates. *AIAA Journal*, 31(3):590–596, March 1993. doi: 10.2514/3.61543.

[14] C. Bisagni and L. Lanzi. Post-buckling optimisation of composite stiffened panels using neural networks. *Composite Structures*, 58(2):237–247, 2002. ISSN 0263-8223. doi: https://doi.org/10.1016/S0263-8223(02)00053-3.

[15] C. Guus E. Boender and H. Edwin Romeijn. Stochastic methods. In *Nonconvex Optimization and Its Applications*, pages 829–869. Springer US, 1995. doi: 10.1007/978-1-4615-2025-2_15.

[16] F K Bogner, R L Fox, and L A Schmit. The generation of inter-element-compatible stiffness and mass matrices by the use of interpolation formulas(Generation of interelement compatible stiffness and mass matrices by use of interpolation formulas), 1966.

[17] Anne Brindle. *Genetic algorithms for function optimization*. PhD thesis, Jan 1980. URL https://era.library.ualberta.ca/items/58923fb3-9557-448f-aedb-a82e95d1067e.

[18] Eric Brochu, Vlad M. Cora, and Nando de Freitas. A Tutorial on Bayesian Optimization of Expensive Cost Functions, with Application to Active User Modeling and Hierarchical Reinforcement Learning. 2010. URL http://arxiv.org/abs/1012.2599.

[19] Eric Brochu, Matthew W. Hoffman, and Nando de Freitas. Portfolio allocation for bayesian optimization, 2011.

[20] M. L. Bucalem and K. J. Bathe. Finite element analysis of shell structures. *Archives of Computational Methods in Engineering*, 4(1):3–61, 03 1997. ISSN 1886-1784. doi: 10.1007/BF02818930.

[21] Lars Buitinck, Gilles Louppe, Mathieu Blondel, Fabian Pedregosa, Andreas Mueller, Olivier Grisel, Vlad Niculae, Peter Prettenhofer, Alexandre Gramfort, Jaques Grobler, Robert Layton, Jake VanderPlas, Arnaud Joly, Brian Holt, and Gaël Varoquaux. API design for machine learning software: experiences from the scikit-learn project. In *ECML PKDD Workshop: Languages for Data Mining and Machine Learning*, pages 108–122, 2013.

[22] David Bushnell. Buckling of shells-pitfall for designers. *AIAA Journal*, 19(9):1183–1226, 1981. doi: 10.2514/3.60058.

[23] Saullo Castro. GitHub Repository- Composites: Useful functions to calculate composite material properties. URL https://github.com/saullocastro/composites.

[24] Saullo G P Castro. Semi-analytical tools for the analysis of laminated composite cylindrical and conical imperfect shells under various loading and boundary conditions. (October):199, 2014. doi: 10.21268/20150210-154320. URL https://dokumente.ub.tu-clausthal.de/receive/clausthal_mods_00000094.

[25] Saullo G.P. Castro, Christian Mittelstedt, Francisco A.C. Monteiro, Mariano A. Arbelo, Gerhard Ziegmann, and Richard Degenhardt. Linear buckling predictions of unstiffened laminated composite cylinders and cones under various loading and boundary conditions using semi-analytical models. *Composite Structures*, 118:303–315, 2014. ISSN 0263-8223. doi: https://doi.org/10.1016/j.compstruct.2014.07.037.

[26] Saullo G.P. Castro, Maurício V. Donadon, and Thiago A.M. Guimarães. ES-PIM applied to buckling of variable angle tow laminates. *Composite Structures*, 209(June 2018):67–78, 2019. ISSN 02638223. doi: 10.1016/j.compstruct.2018.10.058.

[27] S.G.P. Castro and E.L. Jansen. Displacement-based formulation of koiter's method: Application to multi-modal post-buckling finite element analysis of plates. *Thin-Walled Structures*, Nov 2020. URL https://www.sciencedirect.com/science/article/pii/S0263823120310892#bib33.

[28] K. Crombecq, E. Laermans, and T. Dhaene. Efficient space-filling and non-collapsing sequential design strategies for simulation-based modeling. *European Journal of Operational Research*, 214(3):683–696, 2011. ISSN 0377-2217. doi: https://doi.org/10.1016/j.ejor.2011.05.032.

[29] Kenneth Alan De Jong. *An Analysis of the Behavior of a Class of Genetic Adaptive Systems*. PhD thesis, USA, 1975. AAI7609381.

[30] W.J.Welch D.R.Jones, M.Schonlau. Efficient global optimization of expensive black-box functions. *Journal of Global Optimization*, 13:455–492, 1998.

[31] Isaac Elishakoff. *Resolution of the Twentieth Century Conundrum in Elastic Stability*. WORLD SCIENTIFIC, 2014. doi: 10.1142/9086.

[32] Peter I. Frazier. A tutorial on bayesian optimization. *arXiv*, (Section 5):1–22, 2018. ISSN 23318422.

[33] Vladimir Gantovnik. An improved genetic algorithm for the optimization of composite structures. In *DAC 2006*, 2006.

[34] Hossein Ghiasi, Damiano Pasini, and Larry Lessard. Optimum stacking sequence design of composite materials part i: Constant stiffness design. *Composite Structures*, 90, 2009. doi: 10.1016/j.compstruct.2009.01.006.

[35] Hossein Ghiasi, Kazem Fayazbakhsh, Damiano Pasini, and Larry Lessard. Optimum stacking sequence design of composite materials Part II: Variable stiffness design. *Composite Structures*, 93(1):1–13, 2010. ISSN 02638223. doi: 10.1016/j.compstruct.2010.06.001.

[36] David E. Goldberg. *Genetic Algorithms in Search, Optimization and Machine Learning*. Addison-Wesley Longman Publishing Co., Inc., USA, 1st edition, 1989. ISBN 0201157675.

[37] Justin S. Gray, John T. Hwang, Joaquim R. R. A. Martins, Kenneth T. Moore, and Bret A. Naylor. OpenMDAO: An Open-Source Framework for Multidisciplinary Design, Analysis, and Optimization. *Structural and Multidisciplinary Optimization*, 59: 1075–1104, 2019. doi: 10.1007/s00158-019-02211-z.

[38] R. M.J. Groh and P. M. Weaver. Mass optimization of variable angle tow, variable thickness panels with static failure and buckling constraints. *56th AIAA/ASCE/AHS/ASC Structures, Structural Dynamics, and Materials Conference*, (January):5–9, 2015. doi: 10.2514/6.2015-0452.

[39] Grace X. Gu, Chun-Teh Chen, and Markus J. Buehler. De novo composite design based on machine learning algorithm. *Extreme Mechanics Letters*, 18:19–28, 2018. ISSN 2352-4316. doi: https://doi.org/10.1016/j.eml.2017.10.001.

[40] Thiago A. Guimaraes, Saullo G. Castro, Domingos A. Rade, and Carlos E. Cesnik. *Panel Flutter Analysis and Optimization of Composite Tow Steered Plates*. 2017. doi: 10.2514/6.2017-1118.

[41] Sedat Güldü and Altan Kayran. Maximizing buckling load factors of fiber-placed composite cylindrical shells by particle swarm optimization. *56th AIAA/ASCE/AHS/ASC Structures, Structural Dynamics, and Materials Conference*, (January):1–25, 2015. doi: 10.2514/6.2015-0449.

[42] Z. Gürdal, B.F. Tatting, and C.K. Wu. Variable stiffness composite panels: Effects of stiffness variation on the in-plane and buckling response. *Composites Part A: Applied Science and Manufacturing*, 39(5):911–922, 2008. ISSN 1359-835X. doi: https://doi.org/10.1016/j.compositesa.2007.11.015.

[43] Zafer Gürdal, Raphael Haftka, and Prabhat Hajela. *Design and Optimization of Laminated Composite Materials*. Wiley-Interscience, 1 edition, 1999.

[44] Hong Hahn and Stephen Tsai. *Introduction to Composite Materials*. Technomic Publishing Co, Inc., 1 edition, 1980.

[45] Tim Head, Manoj Kumar, Holger Nahrstaedt, Gilles Louppe, and Iaroslav Shcherbatyi. scikit-optimize/scikit-optimize, October 2021. URL https://doi.org/10.5281/zenodo.5565057.

[46] R. Hecht-Nielsen. Kolmogorov"s mapping neural network existence theorem. 1987.

[47] Philipp Hennig and Christian J. Schuler. Entropy search for information-efficient global optimization, 2011.

[48] John H. Holland. *Adaptation in Natural and Artificial Systems: An Introductory Analysis with Applications to Biology, Control and Artificial Intelligence*. MIT Press, Cambridge, MA, USA, 1992. ISBN 0262082136.

[49] M. W. Hyer and R. F. Charette. Use of curvilinear fiber format in composite structure design. *AIAA Journal*, 29(6):1011–1015, June 1991. doi: 10.2514/3.10697.

[50] M.W. Hyer and H.H. Lee. The use of curvilinear fiber format to improve buckling resistance of composite plates with central circular holes. *Composite Structures*, 18 (3):239–261, January 1991. doi: 10.1016/0263-8223(91)90035-w.

[51] Samuel Tsunduka Ijsselmuiden. *Stellingen Optimal Design of Variable Stiffness Composite Structures Using Lamination Parameters*. ISBN 9789461130327.

[52] Ping Jiang, Qi Zhou, and Xinyu Shao. *Surrogate-Model-Based Design and Optimization*. 2020. ISBN 9789811507304. doi: 10.1007/978-981-15-0731-1_7.

[53] R. Jin, W. Chen, and T.W. Simpson. Comparative studies of metamodelling techniques under multiple modelling criteria. *Structural and Multidisciplinary Optimization*, 23(1):1–13, 2001. doi: 10.1007/s00158-001-0160-4.

[54] Robert Millard Jones. *Buckling of Bars, Plates, and Shells*. Van Haren Publishing, Zaltbommel, Netherlands, 2006.

[55] Sourabh Katoch, Sumit Singh Chauhan, and Vijay Kumar. *A review on genetic algorithm: past, present, and future*, volume 80. Multimedia Tools and Applications, 2020. doi: 10.1007/s11042-020-10139-6.

[56] Byung Chul Kim, Kevin Potter, and Paul M. Weaver. Continuous tow shearing for manufacturing variable angle tow composites. *Composites Part A: Applied Science and Manufacturing*, 43(8):1347–1356, 2012. ISSN 1359-835X. doi: https://doi.org/10.1016/j.compositesa.2012.02.024.

[57] Byung Chul Kim, Paul M. Weaver, and Kevin Potter. Manufacturing characteristics of the continuous tow shearing method for manufacturing of variable angle tow composites. *Composites Part A: Applied Science and Manufacturing*, 61:141–151, 2014. ISSN 1359-835X. doi: https://doi.org/10.1016/j.compositesa.2014.02.019.

[58] Aaron Klein, Stefan Falkner, Simon Bartels, Philipp Hennig, and Frank Hutter. Fast bayesian optimization of machine learning hyperparameters on large datasets, 2017.

[59] Mykel Kochenderfer and Tim Wheeler. *Algorithms for Optimization (The MIT Press)*. The MIT Press, illustrated edition, 2019.

[60] H. Kushner. A new method of locating the maximum point of an arbitrary multipeak curve in the presence of noise. *Journal of Basic Engineering*, 86:97–106, 1964.

[61] Edgars Labans and Chiara Bisagni. Buckling and free vibration study of variable and constant-stiffness cylindrical shells. *Composite Structures*, 210(November 2018):446–457, 2019. ISSN 02638223. doi: 10.1016/j.compstruct.2018.11.061.

[62] Cornelius. Lanczos. *The variational principles of mechanics*. University of Toronto Press, Toronto SE - XXX, 418 p. ; .. cm., 4th ed. edition, 1974. ISBN 0802017436 9780802017437. URL https://tudelft.on.worldcat.org/oclc/898775508.

[63] Chang-Yong Lee. Entropy-boltzmann selection in the genetic algorithms. *IEEE transactions on systems, man, and cybernetics. Part B, Cybernetics : a publication of the IEEE Systems, Man, and Cybernetics Society*, 33 1:138–49, 2003.

[64] Moshe Leshno, Vladimir Ya. Lin, Allan Pinkus, and Shimon Schocken. Multilayer feedforward networks with a nonpolynomial activation function can approximate any function. *Neural Networks*, 6(6):861–867, 1993. ISSN 0893-6080. doi: https://doi.org/10.1016/S0893-6080(05)80131-5.

[65] Longjun Liu. Could enough samples be more important than better designs for computer experiments? In *38th Annual Simulation Symposium*, pages 107–115, 2005. doi: 10.1109/ANSS.2005.17.

[66] Daniel Lizotte, Tao Wang, Michael Bowling, and Dale Schuurmans. Automatic gait optimization with gaussian process regression. In *Proceedings of the 20th International Joint Conference on Artifical Intelligence*, IJCAI'07, page 944–949. Morgan Kaufmann Publishers Inc., 2007.

[67] Daniel James Lizotte. Practical Bayesian Optimization. page 177, 2008.

[68] C.S. Lopes, Z. Gürdal, and P.P. Camanho. Variable-stiffness composite panels: Buckling and first-ply failure improvements over straight-fibre laminates. *Computers & Structures*, 86(9):897–907, 2008. ISSN 0045-7949. doi: https://doi.org/10.1016/j.compstruc.2007.04.016. Composites.

[69] Vijini Mallawaarachchi. How to define a Fitness Function in a Genetic Algorithm?, 2017. URL https://bit.ly/2TsqgsL.

[70] Upendra K. Mallela and Akhil Upadhyay. Buckling load prediction of laminated composite stiffened panels subjected to in-plane shear using artificial neural networks. *Thin-Walled Structures*, 102:158–164, 2016. ISSN 0263-8231. doi: https://doi.org/10.1016/j.tws.2016.01.025.

[71] Roman Marchant and Fabio Ramos. Bayesian optimisation for intelligent environmental monitoring. In *2012 IEEE/RSJ International Conference on Intelligent Robots and Systems*, pages 2242–2249, 2012. doi: 10.1109/IROS.2012.6385653.

[72] Zbigniew Michalewicz. Genetic algorithms + data structures = evolution programs, 1996. URL https://www.springer.com/gp/book/9783540606765.

[73] R. D. Mindlin. Influence of Rotatory Inertia and Shear on Flexural Motions of Isotropic, Elastic Plates. *Journal of Applied Mechanics*, 18(1):31–38, 04 2021. ISSN 0021-8936. doi: 10.1115/1.4010217.

[74] Bharat. Bhushan. Mishra, Ajay. Kumar, Pijush. Samui, and Roshni Thendiyath. Buckling of laminated composite skew plate using FEM and machine learning methods | Emerald Insight, 10 2020. URL https://www.emerald.com/insight/content/doi/10.1108/EC-08-2019-0346/full/html.

[75] Jonas Mockus, Vytautas Tiesis, and Antanas Zilinskas. The application of Bayesian methods for seeking the extremum. *Towards Global Optimization*, 2(117-129):2, 1978.

[76] S Nagendra, Srinivas Kodiyalam, Jonathan Davis, and V Parthasarathy. *Optimization of tow fiber paths for composite design*. AIAA, 1995. doi: 10.2514/6.1995-1275. URL https://arc.aiaa.org/doi/abs/10.2514/6.1995-1275.

[77] Michael Chun-Yung. Niu. *Composite airframe structures: practical design information and data*. Hong Kong Conmilit Press, 2010.

[78] C.Boursier Niutta, E. J.Wehrle, and G.Belingardi F. Duddeck. Surrogate modeling in design optimization of structures with discontinuous responses. *Structural and Multidisciplinary Optimization*, 57, 01 2018. doi: 10.1007/s00158-018-1958-7.

[79] O. O. Ochoa and J. N. Reddy. *Finite Element Analysis of Composite Laminates*, pages 37–109. Springer Netherlands, Dordrecht, 1992. ISBN 978-94-015-7995-7. doi: 10.1007/978-94-015-7995-7_3.

[80] V. Oliveri and A. Milazzo. A rayleigh-ritz approach for postbuckling analysis of variable angle tow composite stiffened panels. *Computers & Structures*, 196:263–276, 2018. ISSN 0045-7949. doi: https://doi.org/10.1016/j.compstruc.2017.10.009. URL https://www.sciencedirect.com/science/article/pii/S004579491730768X.

[81] Reynaldo Olmedo and Zafer Gurdal. Buckling response of laminates with spatially varying fiber orientations. *Collection of Technical Papers - AIAA/ASME Structures, Structural Dynamics and Materials Conference*, (pt 4):2261–2269, 1993.

[82] Eugenio Oñate. *Structural analysis with the finite element method: linear statics: v.1: Basis and solids*, volume 47. 2010. ISBN 9781402087424. doi: 10.5860/choice.47-4446.

[83] Foster Provost, David Jensen, and Tim Oates. Efficient progressive sampling. *Proc fifth ACM SIGKDD Int Conf Knowl Discov data Min*, 04 2000. doi: 10.1145/312129.312188.

[84] Nestor V. Queipo, Raphael T. Haftka, Wei Shyy, Tushar Goel, Rajkumar Vaidyanathan, and P. Kevin Tucker. Surrogate-based analysis and optimization. *Progress in Aerospace Sciences*, 41(1):1–28, 2005. ISSN 03760421. doi: 10.1016/j.paerosci.2005.02.001.

[85] Douglas Quintanilha. *The aeroelastic behavior of laminated composite panels undergoing progressive damage in supersonic flow*. PhD thesis, Instituto Tecnologico de Aeronautica, 2019.

[86] G. F. Raggett. Numerical optimization of computer models, hans-paul schwefel, wiley, chichester, 1981. price: £12.50. *Optimal Control Applications and Methods*, 3(1):97–97, 1982. doi: https://doi.org/10.1002/oca.4660030109.

[87] I. Rechenberg, B.F. Toms, and Royal Aircraft Establishment. *Cybernetic Solution Path of an Experimental Problem:*. Library translation / Royal Aircraft Establishment. Ministry of Aviation, 1965. URL https://books.google.nl/books?id=FaWrtAEACAAJ.

[88] J. N. Reddy. A Simple Higher-Order Theory for Laminated Composite Plates. *Journal of Applied Mechanics*, 51(4):745–752, 12 1984. ISSN 0021-8936. doi: 10.1115/1.3167719.

[89] Eric Reissner. The Effect of Transverse Shear Deformation on the Bending of Elastic Plates. *Journal of Applied Mechanics*, 12(2):A69–A77, 03 2021. ISSN 0021-8936. doi: 10.1115/1.4009435.

[90] Daniel Russo, Benjamin Van Roy, Abbas Kazerouni, Ian Osband, and Zheng Wen. A tutorial on thompson sampling, 2017.

[91] Shahriar Setoodeh, Mostafa M. Abdalla, and Zafer Gürdal. Design of variable–stiffness laminates using lamination parameters. *Composites Part B: Engineering*, 37(4):301–309, 2006. ISSN 1359-8368. doi: https://doi.org/10.1016/j.compositesb.2005.12.001.

[92] Rahil Shaikh. Cross Validation Explained: Evaluating estimator performance., 11 2018. URL https://towardsdatascience.com/cross-validation-explained-evaluating-estimator-performance-e51e5430ff85.

[93] Michael Smith. *ABAQUS/Standard User's Manual, Version 2019*. Dassault Systèmes Simulia Corp, United States, 2019.

[94] RP Smith, Z Qureshi, RJ Scaife, and HM El-Dessouky. Limitations of processing carbon fibre reinforced plastic/polymer material using automated fibre placement technology. *Journal of Reinforced Plastics and Composites*, 35(21):1527–1542, 2016. doi: 10.1177/0731684416659544.

[95] Jasper Snoek, Hugo Larochelle, and Ryan P. Adams. Practical bayesian optimization of machine learning algorithms, 2012.

[96] L. H. Sobel and S. Z. Newman. Plastic buckling of cylindrical shells under axial compression. *Journal of Pressure Vessel Technology*, 102(1):40–44, 02 1980. ISSN 0094-9930. doi: 10.1115/1.3263299.

[97] Sobieszczanski-Sobieski, Jaroslaw, and Raphael Haftka. Multidisciplinary aerospace design optimization: Survey of recent developments. *Structural Optimization*, 14:1–23, 08 1997. doi: 10.1007/BF01197554.

[98] Michael L. Stein. *Interpolation of Spatial Data*. Springer New York, 1999. doi: 10.1007/978-1-4612-1494-6. URL https://doi.org/10.1007%2F978-1-4612-1494-6.

[99] Andre-I Nikolaevich Tikhonov. *Solutions of Ill Posed Problems (Scripta series in mathematics)*. Vh Winston, 1977.

[100] S. Tsai, N. Pagano, and AIR FORCE MATERIALS LAB WRIGHT-PATTERSON AFB OH WRIGHT-PATTERSON AFB". INVARIANT PROPERTIES OF COMPOSITE MATERIALS, 03 1968. URL https://apps.dtic.mil/sti/citations/AD0668761.

[101] J. M. J. F. Van Campen. *Optimum lay-up design of variable stiffness composite structures*. 2011. ISBN 9789090264264. URL http://repository.tudelft.nl/view/ir/uuid:148c69e4-50a3-4990-bc2b-0e76a2e16bdf/.

[102] Julien M.J.F. van Campen, Christos Kassapoglou, and Zafer Gürdal. Generating realistic laminate fiber angle distributions for optimal variable stiffness laminates. *Composites Part B: Engineering*, 43(2):354–360, 2012. ISSN 1359-8368. doi: https://doi.org/10.1016/j.compositesb.2011.10.014.

[103] L. Vertonghen and S.G.P. Castro. Modelling of fibre steered plates with coupled thickness variation from overlapping continuous tows. *Composite Structures*, 268:113933, 2021. ISSN 0263-8223. doi: https://doi.org/10.1016/j.compstruct.2021.113933.

[104] Pauli Virtanen, Ralf Gommers, Travis E. Oliphant, and et al. SciPy 1.0: Fundamental Algorithms for Scientific Computing in Python, 2020.

[105] H.N.R. Wagner, H. Köke, S. Dähne, S. Niemann, C. Hühne, and R. Khakimova. Decision tree-based machine learning to optimize the laminate stacking of composite cylinders for maximum buckling load and minimum imperfection sensitivity. *Composite Structures*, 220:45–63, 2019. ISSN 0263-8223. doi: https://doi.org/10.1016/j.compstruct.2019.02.103.

[106] Zhihua Wang, José Humberto S. Almeida Jr., Luc St-Pierre, Zhonglai Wang, and Saullo G.P. Castro. Reliability-based buckling optimization with an accelerated kriging metamodel for filament-wound variable angle tow composite cylinders. *Composite Structures*, 254:112821, 2020. ISSN 0263-8223. doi: https://doi.org/10.1016/j.compstruct.2020.112821.

[107] Zhihua Wang, Jr. Almeida, José H S, Aravind Ashok, Zhonglai Wang, and Saullo G P Castro. Lightweight design of variable-angle filament-wound cylinders combining kriging-based metamodels with particle swarm optimization, May 2021.

[108] Roudy Wehbe, Brian Tatting, Sreehari Rajan, Ramy Harik, Michael Sutton, and Zafer Gürdal. Geometrical modeling of tow wrinkles in automated fiber placement. *Composite Structures*, 246:112394, 2020. ISSN 0263-8223. doi: https://doi.org/10.1016/j.compstruct.2020.112394.

[109] Simon C. White, Paul M. Weaver, and K. Chauncey Wu. Post-buckling analyses of variable-stiffness composite cylinders in axial compression. *Composite Structures*, 123:190–203, 2015. ISSN 0263-8223. doi: https://doi.org/10.1016/j.compstruct.2014.12.013.

[110] J. M. Whitney and N. J. Pagano. Shear Deformation in Heterogeneous Anisotropic Plates. *Journal of Applied Mechanics*, 37(4):1031–1036, 12 1970. ISSN 0021-8936. doi: 10.1115/1.3408654. URL https://doi.org/10.1115/1.3408654.

[111] Zhangming Wu, Paul M. Weaver, Gangadharan Raju, and Byung Chul Kim. Buckling analysis and optimisation of variable angle tow composite plates. *Thin-Walled Structures*, 60:163–172, 2012. ISSN 02638231. doi: 10.1016/j.tws.2012.07.008.

[112] Zhangming Wu, Gangadharan Raju, and Paul M Weaver. Optimization of postbuckling behaviour of variable thickness composite panels with variable angle tows: Towards "buckle-free" design concept. *International Journal of Solids and Structures*, 132-133:66–79, 2018. ISSN 0020-7683. doi: https://doi.org/10.1016/j.ijsolstr.2017.08.037.

[113] Koshiro Yamaguchi, Sean E. Phenisee, Zhisong Chen, Marco Salviato, and Jinkyu Yang. Ply-drop design of non-conventional laminated composites using bayesian optimization. *Composites Part A: Applied Science and Manufacturing*, 139:106136, 2020. ISSN 1359-835X. doi: https://doi.org/10.1016/j.compositesa.2020.106136. URL https://www.sciencedirect.com/science/article/pii/S1359835X20303729.

[114] Masaki Yamawaki, Masato Ohnishi, Shenghong Ju, and Junichiro Shiomi. Multifunctional structural design of graphene thermoelectrics by bayesian optimization. *Science Advances*, 4(6):eaar4192, 2018. doi: 10.1126/sciadv.aar4192.

[115] Henry T. Y. Yang, S. Saigal, A. Masud, and R. K. Kapania. A survey of recent shell finite elements. *International Journal for Numerical Methods in Engineering*, 47(1-3):101–127, 2000. doi: https://doi.org/10.1002/(SICI)1097-0207(20000110/30)47:1/3<101::AID-NME763>3.0.CO;2-C.

[116] Xin Yao. An empirical study of genetic operators in genetic algorithms. *Microprocessing and Microprogramming*, 38(1):707–714, 1993. ISSN 0165-6074. doi: https://doi.org/10.1016/0165-6074(93)90215-7. Proceedings Euromicro 93 Open System Design: Hardware, Software and Applications.

[117] Shangyou Zhang. On the full C1-Qk finite element spaces on rectangles and cuboids. *Advances in Applied Mathematics and Mechanics*, 2(6):701–721, 2010. ISSN 20700733. doi: 10.4208/aamm.09-m0993.